CONFIDENTIAL

NACA

RESEARCH MEMORANDUM

STATIC LATERAL STABILITY CHARACTERISTICS OF AN AIRPLANE MODEL HAVING A 47.7° SWEPTBACK WING OF ASPECT RATIO 6 AND THE CONTRIBUTION OF VARIOUS MODEL COMPONENTS AT A REYNOLDS NUMBER OF 4.45×10^6

By Roland F. Griner

Langley Aeronautical Laboratory
Langley Field, Va.

NATIONAL ADVISORY COMMITTEE
FOR AERONAUTICS

WASHINGTON

September 1, 1953

CONFIDENTIAL

NACA RM L53G09 CONFIDENTIAL

NATIONAL ADVISORY COMMITTEE FOR AERONAUTICS

RESEARCH MEMORANDUM

STATIC LATERAL STABILITY CHARACTERISTICS OF AN AIRPLANE MODEL HAVING A 47.7° SWEPTBACK WING OF ASPECT RATIO 6 AND THE CONTRIBUTION OF VARIOUS MODEL COMPONENTS AT A REYNOLDS NUMBER OF 4.45×10^6

By Roland F. Griner

SUMMARY

An investigation was made at a Reynolds number of 4.45×10^6 to determine the low-speed yaw characteristics of an airplane model having a 47.7° sweptback wing of aspect ratio 6 and to determine the lateral stability contributions of the various model components and the associated mutual interference. Particular reference is made to the vertical-tail effectiveness. The wing had NACA 64-210 airfoil sections and taper ratio of 0.313.

The complete airplane model was directionally stable through the yaw-angle range (0° to 28.7°) for angles of attack up to approximately 23°. In the higher angle-of-attack range, the airplane model with or without the leading-edge flaps, fences, and double slotted flaps was directionally unstable for yaw angles below approximately 10° even though a high degree of directional stability existed at higher yaw angles.

At low angles of yaw (-5° to 5°) for all wing-fuselage model configurations investigated (with or without flaps), 60 to 80 percent of the loss in the directional stability between 0° and 26° angle of attack was due to the change in yawing-moment contribution of the vertical tail.

A reduction of the vertical-tail length by 20 percent caused a 25 percent reduction (at 0° angle of attack) of the directional-stability-parameter contribution of the vertical tail at low yaw angles (-5° to 5°). At high angles of attack, the reduction in tail length located the vertical tail in a more favorable flow field, whereby the vertical-tail-effectiveness parameter had less variation with yaw angle and indicated a more stabilizing contribution of the vertical tail.

No appreciable scale effects on the directional stability parameter of any of the configurations investigated were indicated when the Reynolds number was varied from 4.45×10^6 to 1.2×10^6.

INTRODUCTION

As pointed out in reference 1, estimations of the yaw characteristics of a complete airplane should be based, for the most part, on experimental data because of the inadequacy of the present theory for predicting the large interference effects between various airplane components and the large variations of the static stability derivatives with angle of attack which result from flow separation. Investigations made by the National Advisory Committee for Aeronautics on the yaw characteristics of swept wings such as references 2 to 8 provide low-speed data for wing and wing-fuselage configurations. Low-speed static lateral stability derivatives of more complete models are presented at high Reynolds number in references 9 and 10 and at low Reynolds number in references 11 to 15. These data have dealt with wings having an aspect ratio 4 or less with the exception of one of the thirty wing models of reference 8.

In order to provide information on a wing of higher aspect ratio, an investigation of an airplane configuration having a 47.7° swept wing of aspect ratio 6 was conducted in the Langley 19-foot pressure tunnel at a Reynolds number of 4.45×10^6 for the purpose of determining (1) the static lateral stability characteristics of a complete airplane model having a swept wing of relatively high aspect ratio, and (2) the lateral stability contributions of the main airplane components (wing, fuselage, vertical and horizontal tail) and the associated mutual interference effects. Particular reference is made to the vertical-tail effectiveness. In addition to determining the contributions of the main airplane components, the effects of leading-edge flaps, trailing-edge flaps, and fences on the lateral stability characteristics were investigated. Brief studies of the effects of fuselage length and Reynolds number were also made.

SYMBOLS

Unless otherwise noted, the data presented for each model configuration are referred to the stability system of axes with the origin at a point corresponding to the quarter-chord point of the wing mean aerodynamic chord projected to the plane of symmetry. The positive directions of the forces, moments, and angular displacements are shown in figure 1.

C_L lift coefficient, $\frac{\text{Lift}}{qS_W}$

C_D drag coefficient, $\frac{\text{Drag}}{qS_W}$

C_X longitudinal-force coefficient, $\frac{X}{qS_W}$, $\left(\text{at } \psi = 0^\circ, \ C_X = -C_D\right)$

C_Y lateral-force coefficient, $\frac{Y}{qS_W}$

C_l rolling-moment coefficient, $\frac{L}{qS_W b_W}$

C_m pitching-moment coefficient, $\frac{M}{qS_W \bar{c}_W}$

C_n yawing-moment coefficient, $\frac{N}{qS_W b_W}$

D drag force, lb

X longitudinal force (at $\psi = 0$, $X = -D$), lb

Y lateral force

L rolling moment

M pitching moment

N yawing moment

q dynamic pressure, $\frac{\rho}{2} V^2$, lb/sq ft

q_V/q ratio of local dynamic pressure at vertical tail to free-stream dynamic pressure

ρ mass density of air, slug/cu ft

μ coefficient of viscosity of air, slug/ft sec

V free-stream velocity, ft/sec

R Reynolds number, $\frac{\rho V \bar{c}_W}{\mu}$

M Mach number, $\frac{V}{\text{Velocity of sound}}$

b	span measured perpendicular to fuselage center line, ft
A	aspect ratio, $\frac{b^2}{S}$
S	area, sq ft
c	local chord measured parallel to fuselage center line
c'	local wing chord measured normal to the 0.286 chord line
$\bar{c}$	mean aerodynamic chord, $\frac{2}{S}\int_0^{b/2} c^2 dy$, ft
d	maximum diameter of fuselage, ft
g	longitudinal distance from fuselage nose to origin of stability system of axes, ft
h'	height above wing-chord plane (in Y,Z plane), percent mean aerodynamic chord of wing
l_B	length of fuselage measured parallel to fuselage center line, ft
l_V	distance from quarter-chord point of wing mean aerodynamic chord to quarter-chord point of vertical-tail mean aerodynamic chord (measured parallel to wing-chord plane), ft
l_S	longitudinal distance from quarter-chord point of wing mean aerodynamic chord to plane of air-flow survey (parallel to horizontal data plane or tunnel center line), ft
y	spanwise coordinate
Z	vertical coordinate
α	angle of attack of wing measured from wing-chord plane, deg
α_B	angle of attack of fuselage, $\alpha - 2^\circ$, deg
α'_V	vertical-tail effective angle of attack measured in the plane perpendicular to the vertical-tail axis of rotation, deg
ψ	angle of yaw, $-\beta^\circ$, deg
σ	sidewash angle (angle between direction of air flow and tunnel center line measured in the X,Y plane), negative when angle of attack of vertical tail is increased, deg

i_V vertical-tail incidence measured from the fuselage center line to the vertical-tail plane of symmetry (in the plane perpendicular to the vertical-tail axis of rotation), deg

i_H incidence of horizontal tail measured from horizontal-tail plane of symmetry to wing-chord plane (positive when tail leading edge is below X,Y plane), deg

C_{Y_ψ} lateral-force parameter, $\left(\frac{\partial C_Y}{\partial \psi}\right)_{\psi=0^\circ}$, per degree

C_{n_ψ} directional-stability parameter, $\left(\frac{\partial C_n}{\partial \psi}\right)_{\psi=0^\circ}$, per degree

C_{l_ψ} effective-dihedral parameter, $\left(\frac{\partial C_l}{\partial \psi}\right)_{\psi=0^\circ}$, per degree

$\left.\begin{matrix}\Delta_1 C_{Y_\psi} \\ \Delta_1 C_{n_\psi} \\ \Delta_1 C_{l_\psi}\end{matrix}\right\}$ increments of lateral-stability parameter caused by wing-fuselage interference

$C_{n_{i_V}} = \frac{\partial C_n}{\partial i_V}$ rate of change of yawing moment with vertical-tail incidence i_V

$\left(C_{L_\alpha}\right)_{V_{is}} = \left[\frac{\partial (C_L)_V}{\partial \alpha}\right]$ theoretical lift-curve slope of vertical tail where $(C_L)_V$ is based on the total projected area of vertical tail (to the fuselage center line)

η vertical-tail efficiency factor (based on yawing-moment data)

γ_N vertical-tail effectiveness parameter based on yawing-moment data

Model designations:

W wing

B_1	fuselage (l_B = 185.98 in.)
B_2	fuselage (l_B = 203.32 in.)
B_3	fuselage (l_B = 125.34 in.)
B_4	fuselage (l_B = 108.00 in.)
V	vertical tail
H	horizontal tail ($i_H = -14^\circ$)
F	leading-edge flaps (located 0.481 wing semispan)
D	double slotted flaps (located 0.462 wing semispan)
f_1	wing fences (located 0.232 wing semispan)
f_2	wing fences (located 0.544 wing semispan)
f_3	wing fences (located 0.700 wing semispan)

Subscripts:

W	wing
B	fuselage
V	vertical tail
H	horizontal tail
e	effective
is	isolated

MODEL, APPARATUS, AND TESTS

MODEL

The model investigated was a midwing airplane configuration having a sweptback wing, sweptback vertical and horizontal tail surfaces, and a fuselage of circular cross section.

The wing (refs. 16 and 17) had a 47.7° sweptback leading edge, NACA 64-210 airfoil sections normal to the 0.286 chord line, a taper ratio of 0.313, and an aspect ratio of 6.0. The wing dihedral angle was zero and the uniform twist about the 0.286 wing-chord line produced 1.72° of washout at the wing tips (see fig. 2).

The leading-edge and double slotted flaps and their respective spans were selected as a result of the investigation presented in references 17 and 18. The leading-edge flaps (fig. 3) had a span of 0.481 wing semispan and a constant chord of 3.05 inches measured normal to the wing leading edge and were deflected down 45° from the wing-chord plane (measured normal to the leading edge). The outboard ends of the leading-edge flaps were located 0.975 wing semispan from the plane of symmetry.

The double slotted flap (fig. 3) was comprised of a 0.25c' main flap and a 0.075c' vane. The vane and main flap of the double slotted flap were deflected down 25° and 50°, respectively, measured normal to 0.286c line. A more complete description and also the ordinates of the vane, main flap, and flap well of the double slotted flap may be found in reference 19. The outboard and inboard ends were located 0.462 and 0.061 semispans, respectively, from the plane of symmetry.

The wing fences and the spanwise locations used in the present investigation are shown in figure 3. The height of a fence was constant over the wing chordwise length of the fence as shown in figure 3.

The fuselage B_1 of fineness ratio 11.07 had circular cross sections with a constant diameter of 16.8 inches over the midsections and tapered to approximately pointed ends (see figs. 2 and 4). Ordinates of fuselage B_1 are presented in reference 20. A section (having a constant diameter of 16.8 inches) was added to fuselage B_1 to form fuselage B_2 having a fineness ratio 12.10. The fuselages designated B_3 and B_4 were formed by removing the afterportion (pointed) from fuselages B_2 and B_1, respectively. Fuselages B_3 and B_4 have fineness ratios of 7.46 and 6.43, respectively. The incidence of the wing with the fuselage was 2° and no fillets or fairings were used at the junctures.

The vertical tail had the quarter-chord line swept back 45°, a taper ratio of 0.588, a total projected area (to fuselage center line) of 0.1515 wing area, and a corresponding aspect ratio of 1.545. The vertical tail was constructed of laminated mahogany with a steel spar and had an NACA 65A008 airfoil parallel to the free airstream. The vertical-tail incidence i_V was varied from 0° to 4° by means of a steel wedge positioned with dowels and the axis of rotation was the vertical-tail axis

which is normal to and located at 0.826 theoretical root chord (parallel to fuselage center line) of the tail. The tail length l_V was varied by changing the fuselage length B_2 to B_1 and is measured parallel to the wing-chord plane as shown in figure 4. No fillets were used at the juncture of the vertical tail with the fuselage.

The horizontal tail had a 42.05° sweptback leading edge, a taper ratio of 0.625, an aspect ratio of 4.01, and NACA 0012-64 airfoil sections parallel to the plane of symmetry. The incidence of the horizontal tail is referred to the wing-chord plane and is changed by rotating the tail about the $0.25\bar{c}_H$ of the tail. The horizontal-tail height is 0.0305 wing semispan below the wing-chord plane.

APPARATUS

The model was mounted on the yaw support system in the Langley 19-foot pressure-tunnel test section, as shown in figures 5, 6, and 7. The yaw support permitted either or both the angle of attack and yaw angle of the model to be varied. A small fairing to cover the wing yaw support fitting was necessary for the wing-alone investigation (see fig. 7).

A six-tube survey rake (fig. 8) was employed to measure the local dynamic pressure and sidewash angle.

TESTS

The tests were conducted in the Langley 19-foot pressure tunnel. For the majority of the tests, the air in the tunnel was compressed to approximately 33 pounds per square inch absolute, and the dynamic pressure was approximately 40 pounds per square foot. For these conditions, the Reynolds number was 4.45×10^6 and the Mach number was 0.122. Some tests were conducted when the tunnel atmosphere was at atmospheric pressure and the dynamic pressure was approximately 7 pounds per square foot. For these latter conditions, the Reynolds number and Mach number were 1.23×10^6 and 0.065, respectively.

The static lateral stability characteristics of the model were measured by a simultaneously recording, six-component balance system. The stalling characteristics of the model in yaw were determined from visual observations and from movies of wool tufts placed on the surface of the model.

The local air-flow characteristics behind the model in the vicinity of the vertical tail (fig. 9 and table I) were obtained with the six-tube survey rake. During the air-flow surveys, sidewash angles were encountered which exceeded the calibration of the survey rake. Linear extrapolations of the calibration data were made in order to provide a few of the values of local sidewash and dynamic pressure for some of the model configurations at approximately 21° angle of attack. Any inaccuracies that might be introduce by extrapolating are believed to be very small.

In general, the yaw characteristics of the model were obtained through the yaw-angle range from -10° to 28.7° for four selected constant angles of attack.

The static lateral stability characteristics of the model were obtained from force and moment data for angles of attack of -2° to 30° when the yaw angle was 0° and ±5°.

CORRECTION OF DATA

The jet-boundary corrections, calculated as in reference 21, have been applied to the angle-of-attack, longitudinal-force, and pitching-moment data presented herein with the exception of the fuselage-alone data. No jet-boundary corrections were applied to the yawing-moment, lateral-force, and rolling-moment coefficients.

The data were corrected for airstream misalinement and blockage effects ($\psi = 0$) but not for support tare and interference effects.

The jet-boundary corrections applied to the airstream survey data amounted to a downward displacement of the flow field with respect to the vertical location in the plane of survey.

METHOD OF ANALYSIS

CONTRIBUTION AND INTERFERENCE EFFECT OF AIRPLANE PARTS

The static-lateral-stability derivatives of a complete airplane at any angle of attack are expressed as follows (for the unflapped configuration as the example):

$$C_{Y_\psi} = \left(C_{Y_\psi}\right)_B + \left(C_{Y_\psi}\right)_W + \Delta_1 C_{Y_\psi} + \left(C_{Y_\psi}\right)_{V+H} \qquad (1)$$

$$C_{n_\psi} = \left(C_{n_\psi}\right)_B + \left(C_{n_\psi}\right)_W + \Delta_1 C_{n_\psi} + \left(C_{n_\psi}\right)_{V+H} \tag{2}$$

$$C_{l_\psi} = \left(C_{l_\psi}\right)_B + \left(C_{l_\psi}\right)_W + \Delta_1 C_{l_\psi} + \left(C_{l_\psi}\right)_{V+H} \tag{3}$$

The subscripts B and W refer to the derivatives of the isolated fuselage and of the isolated wing, respectively. For flapped configurations, the subscript W may be replaced by W + F or W + F + D where F is the subscript for the given leading-edge flaps and D is the subscript of the given double slotted flaps of this investigation.

The increments $\Delta_1 C_{Y_\psi}$, $\Delta_1 C_{n_\psi}$, and $\Delta_1 C_{l_\psi}$ are the lateral-stability-parameter increments caused by wing-fuselage interference and are obtained as follows (for the unflapped configuration as the example):

$$\Delta_1 C_{Y_\psi} = \left(C_{Y_\psi}\right)_{W+B} - \left(C_{Y_\psi}\right)_W - \left(C_{Y_\psi}\right)_B \tag{4}$$

$$\Delta_1 C_{n_\psi} = \left(C_{n_\psi}\right)_{W+B} - \left(C_{n_\psi}\right)_W - \left(C_{n_\psi}\right)_B \tag{5}$$

$$\Delta_1 C_{l_\psi} = \left(C_{l_\psi}\right)_{W+B} - \left(C_{l_\psi}\right)_W - \left(C_{l_\psi}\right)_B \tag{6}$$

The contribution of the vertical and the horizontal tail to the static lateral stability of the complete airplane at any angle of attack is obtained from the experimental data as follows (for the unflapped configuration as the example):

$$\left(C_{Y_\psi}\right)_{V+H} = \left(C_{Y_\psi}\right)_{W+B+V+H} - \left(C_{Y_\psi}\right)_{W+B} \tag{7}$$

$$\left(C_{n_\psi}\right)_{V+H} = \left(C_{n_\psi}\right)_{W+B+V+H} - \left(C_{n_\psi}\right)_{W+B} \tag{8}$$

$$\left(C_{l_\psi}\right)_{V+H} = \left(C_{l_\psi}\right)_{W+B+V+H} - \left(C_{l_\psi}\right)_{W+B} \tag{9}$$

The derivatives with subscript $V + H$ include the effectiveness of the isolated vertical tail, the fuselage-vertical tail interference, the wing and wing-fuselage interferences on the vertical tail, and the effect of the horizontal tail (see ref. 22). If the subscript $V + H$ is replaced by V, then equations (7) to (9) and (1) to (3) will include the same effects as the derivatives having $V + H$ subscripts with the exception of the horizontal-tail effect.

The contribution of the vertical tail to the characteristics of the fuselage-alone configuration is expressed in a form similar to equations (7) to (9); that is,

$$\left(C_{Y_\psi}\right)_V = \left(C_{Y_\psi}\right)_{B+V} - \left(C_{Y_\psi}\right)_B \tag{10}$$

$$\left(C_{n_\psi}\right)_V = \left(C_{n_\psi}\right)_{B+V} - \left(C_{n_\psi}\right)_B \tag{11}$$

$$\left(C_{l_\psi}\right)_V = \left(C_{l_\psi}\right)_{B+V} - \left(C_{l_\psi}\right)_B \tag{12}$$

The derivatives with subscript V include the effectiveness of the isolated vertical tail and the fuselage—vertical-tail interference. When subscript V is replaced by $V + H$, equations (10) to (12) are also valid and include the interference effects of the horizontal tail on the vertical-tail effectiveness.

VERTICAL-TAIL FLOW PARAMETERS

The values of the effective angle of attack α'_V of the vertical tail, computed from experimental yawing-moment force data where the vertical-tail incidence was varied from 0° to 4°, were obtained by the following relation:

$$\alpha'_V = \frac{C_{n_V}}{C_{n_{i_V}}} \tag{13}$$

where C_{n_V} is the difference in C_n of a given model configuration with and without the vertical tail. The effective angle of attack α'_V is measured in the plane perpendicular to the vertical-tail axis of rotation. This plane is not the plane in which angle of yaw (ψ) and angle

of sidewash (σ) are measured except when the fuselage is at 0° angle of attack ($\alpha_B = 0$).

The effective dynamic pressure ratio $\left(\frac{q_V}{q}\right)_e$ presented is from experimental yawing-moment force data and was obtained as follows:

$$\left(\frac{q_V}{q}\right)_e = \frac{\left(C_{n_{i_V}}\right)_{\alpha,\psi}}{\left(C_{n_{i_V}}\right)_{\substack{\alpha=0 \\ \psi=0}}} \tag{14}$$

The $\left(C_{n_{i_V}}\right)_{\substack{\alpha=0 \\ \psi=0}}$ value for the wing-fuselage configurations $W + B_1\left(\frac{l_V}{b_W} = 0.396\right)$ and $W + B_2\left(\frac{l_V}{b_W} = 0.500\right)$ is -0.00263 and -0.00288, respectively.

VERTICAL-TAIL EFFECTIVENESS PARAMETER

A vertical-tail effectiveness parameter is defined herein as γ_N and is expressed as follows:

$$\gamma_N = -\frac{\frac{\partial C_{n_V}}{\partial \psi}}{\frac{l_V}{b_W}\frac{S_V}{S_W}\left(C_{L_\alpha}\right)_{V_{is}}} \tag{15}$$

For the present investigation $\left(C_{L_\alpha}\right)_{V_{is}} = 0.035$, which was computed using reference 23 and is the assumed linear lift-curve slope of the isolated vertical tail (based on the projected area of the tail). The values of the tail volume $\frac{l_V}{b_W}\frac{S_V}{S_W}$ determined from the geometry of the models having fuselages B_1 or B_2 are 0.0600 and 0.0758, respectively. Positive values of γ_N indicate that the vertical tail is contributing

stability. The factor γ_N is used to express the effectiveness of the vertical tail on the fuselage configurations without the wing as well as on the wing-fuselage configurations.

Assuming a linear lift-curve slope of the vertical tail, the relation between the vertical-tail effectiveness parameter γ_N and the effective-flow parameters (eqs. (13) and (14)) is as follows:

$$\gamma_N = -\frac{\frac{\partial C_{n_V}}{\partial \psi}}{\frac{l_V}{b_W}\frac{S_V}{S_W}\left(C_{L_\alpha}\right)_{V_{is}}} = \eta\left[\frac{\partial \alpha'_V}{\partial \psi}\left(\frac{q_V}{q}\right)_e + \alpha'_V \frac{\partial\left(\frac{q_V}{q}\right)_e}{\partial \psi}\right] \tag{16}$$

where

$$\eta = -\frac{\left(C_{n_{i_V}}\right)_{\substack{\alpha=0 \\ \psi=0}}}{\frac{l_V}{b_W}\frac{S_V}{S_W}\left(C_{L_\alpha}\right)_{V_{is}}} \tag{17}$$

In reference 24, the vertical-tail effectiveness was expressed as two efficiency factors, that is, (1) for the fuselage—vertical-tail configuration and (2) for the wing—fuselage—vertical-tail configuration. The γ_N defined in equation (15) is the over-all effectiveness parameter of the vertical tail and can be shown to be the equivalent of the product of the two separate efficiency factors of reference 24.

RESULTS AND DISCUSSION

The analysis presented herein has been limited principally to the static directional stability characteristics although the lateral force and effective dihedral data are also presented. Because of the general interrelation of lateral force and yawing moment, any discussion of the general lateral-force characteristics would be repetitious and therefore has been omitted. A figure-number index for plotted data is presented in table II. The static directional stability characteristics and effective dihedral at low yaw angles have been summarized in tables III and IV. The yaw-angle ranges of -5° to 5° and 5° to 28.7° have been designated as the low yaw- and high yaw-angle range, respectively.

Reference 24 has pointed out that one of the major factors controlling the static-lateral-stability derivatives of a complete model is the relative position of the wing and the fuselage. The present investigation is of a midwing fuselage arrangement; therefore, the applicability of the presented experimental data is limited to similar models.

A limited amount of longitudinal aerodynamic characteristics, but no analysis, has been included with these data (see fig. 10).

DIRECTIONAL STABILITY AND LATERAL FORCE

Characteristics of Complete Model

Data for the complete model - wing, fuselage, vertical tail, and horizontal tail - are discussed in this section. The results for configurations without the horizontal tail are used to demonstrate the effects of tail length, scale effect, and fence effect. Although the horizontal tail (located below the fuselage) had a limited effect on the lateral stability characteristics in some instances, the data without the horizontal tail are considered adequate for the aforementioned purpose.

Characteristics of model without flaps at low angles of yaw.- The static lateral stability characteristics of the complete-model configuration at low angles of yaw are presented in figure 11. The C_{n_ψ} variation with angle of attack indicated that the complete-model configuration was directionally stable only for angles of attack up to approximately 23°. At higher angles of attack, the complete model was directionally unstable and had an unstable (positive) value of C_{n_ψ} of 0.0042 at 29° angle of attack. References such as 10, 11, and 12 have shown similar directionally unstable characteristics at high angle of attack (near maximum lift coefficient). Reducing the vertical-tail length (fig. 12) by approximately 20 percent caused a 25-percent reduction in C_{n_ψ} for the low and moderate angle-of-attack range. Above 21° angle of attack the shorter tail length $\left(\frac{l_V}{b_W} = 0.396\right)$ indicated an improvement over the directional stability characteristics shown for the model having the longer tail length.

A comparison of figures 11 and 12 indicated that the horizontal tail $(i_H = -14°)$ had a small directional stabilizing effect at the lower angles of attack and a slight destabilizing effect at angles of attack greater than 16°. Although the data are not presented for the

complete model having horizontal-tail incidence i_H of -6°, the trends and values of C_{n_ψ} through the angle-of-attack range were almost like those of the model $W + B_2 + V$ without the horizontal tail (fig. 12).

Only very small scale effects on the directional stability characteristics were indicated when the Reynolds number was reduced from 4.45×10^6 to 1.2×10^6. Figure 13 is presented as an example to show the small scale effect.

Flap and fence effects.- The effects of flaps and fences on the static lateral stability characteristics of the complete model are shown in figure 11 and the effect of fences on the characteristics of the flapped model configuration without the horizontal tail $\left(i_H = -14^\circ\right)$ is shown in figure 14.

The addition of leading-edge flaps to the complete-model configuration (fig. 11) improved the directional stability characteristics, especially through the angle-of-attack range from approximately 9° to 15°. The large unstable values of C_{n_ψ} were reduced for angles of attack above approximately 27°.

The addition of leading-edge and double slotted flaps to the complete-model configuration (fig. 11) altered the directional-stability-parameter characteristics of the unflapped model configuration by approximately a one-third increase in the directional stability at angles of attack below approximately 7° and some improvement up to 18° angle of attack. Above 18° angle of attack, the addition of these flaps did not prevent the large destabilizing changes shown by the unflapped model.

The addition of f_2 fences ($0.544\ b_W/2$) to the model configurations with leading-edge flaps (figs. 11 and 14) improved the directional stability characteristics for angles of attack above about 10° but did not prevent the directional instability near the stall.

The effect of fence spanwise position (fig. 3) through the entire yaw-angle range is shown in figure 15. Up through 21° angle of attack, inboard f_1 fences ($0.232\ b_W/2$) reduced the directional stability characteristics at low yaw angles; whereas, outboard f_2 and f_3 fences ($0.544\ b_W/2$ and $0.700\ b_W/2$, respectively) improved the directional stability characteristics at low yaw angles (fig. 15(a)) in addition to improving the longitudinal stability characteristics of the sweptback wing (ref. 25). At high angles of attack (27°), however, it should be pointed out that the fences investigated appeared to have no effect (fig. 15(b)) for the entire yaw-angle range.

Characteristics at high angles of yaw.- The data presented in figure 16 indicated that the previously noted directional instability for high angles of attack occurred only at yaw angles below approximately 10° and that the model was directionally stable at the higher yaw angles with or without leading-edge flaps, fences, and double slotted flaps. These same trends are shown (fig. 17) for the unflapped model configurations without the horizontal tail, but with the vertical-tail length $\frac{l_V}{b_W}$ reduced from 0.500 to 0.396.

The indicated surface flow and stall pattern (fig. 18) from wool tufts placed on the surface of the model showed large changes as yaw angle was increased from 0° to 20° at moderate and high angles of attack. These changes in flow are reflected in the data (figs. 16 and 17) and the inboard movement of the stalled flow of the leading wing had a big influence on the air flow experienced by the vertical tail.

In the high angle-of-attack range, it is interesting to note that the directional instability at low yaw angles and the high degree of directional stability at yaw angles above 10° were also encountered with the wing—fuselage—vertical-tail model for which data are presented in reference 9 even though the aspect ratio and sweep angle of the wing are very different from those of the present model.

Characteristics of Wing and Fuselage

The characteristics of the wing alone are presented in figures 19 and 20. Fuselage-alone characteristics are presented in figures 19 and 21. Characteristics of the wing and fuselage combination are presented in figures 19, 22, 23, and 24.

Wing characteristics at low angles of yaw.- The data presented in figure 19 show that the directional stability parameter C_{n_ψ} for the wing alone was small for angles of attack up to about 18°. Above 18° angle of attack ($C_L = 1.0$), the wing alone became directionally unstable ($C_{n_\psi} = 0.0011$ at $\alpha = 27°$).

The addition of leading-edge flaps or leading-edge and double slotted flaps to the wing-alone model configuration improved the characteristics so that the wing was directionally stable through the angle-of-attack range to 24° and 21°, respectively (fig. 19(a)), but had only very slight effects on the directional instability characteristics of the wing at approximately 27° angle of attack.

Characteristics of the fuselage alone.- The static-lateral-stability parameters of the fuselage-alone model configuration B_2 plotted against

angle of attack are shown in figure 19 for low angles of yaw. The directional stability parameter C_{n_ψ} indicated that the fuselage-alone model configuration was directionally unstable with a nearly constant (positive) value of approximately 0.001 through the angle-of-attack range (0° to 28°).

The static lateral stability characteristics at high yaw angles (fig. 21) show that the fuselage-alone model configuration was directionally unstable through the yaw range. The directionally unstable yawing moment at high yaw angles was less at the higher angles of attack such as 20° and 26° than at lower angles of attack.

Characteristics of wing and fuselage combination at low angles of yaw.- The C_{n_ψ} values through the angle-of-attack range of the wing-fuselage model configuration (fig. 19(a)) without flaps were almost identical to the sum of the individual C_{n_ψ} values of the wing-alone model configuration and the fuselage-alone model configuration because the wing-fuselage interference $\left(\Delta_1 C_{n_\psi}\right)$ was small.

The leading-edge flaps or leading-edge and double slotted flaps (fig. 19) contributed approximately the same stabilizing C_{n_ψ} magnitude to the wing-fuselage model configuration as to the wing-alone model configuration. However, the stabilizing contributions of the flaps were not large enough to overcome the unstable fuselage moment.

The destabilizing (positive) wing-fuselage interference, $\Delta_1 C_{n_\psi}$ of the wing-fuselage configuration with flaps (fig. 19(a)) was greater than that of the wing-fuselage configuration without flaps.

The changes of the yawing-moment contributions of the wing-fuselage accounted for approximately 20 to 40 percent of the difference between the C_{n_ψ} of the complete airplane model at 0° and at 26° angle of attack.

Characteristics at high angles of yaw.- At high angles of attack (approx. 21° to 27°), the directional unstable characteristics shown at yaw angles up to approximately 10° (fig. 20) became stable and increased progressively as yaw angles increased for the wing-alone model configuration with or without flaps. The complete-model configuration indicated the same trend (fig. 14).

For the entire yaw-angle range (0° to 28°), the directional stabilizing effect resulting from the addition of leading-edge flaps or leading-edge and double slotted flaps to the wing-alone model configuration became less as angle of attack increased (fig. 20). For example, the addition of the leading-edge and double slotted flaps more than doubled the stable C_n contribution of the leading-edge flaps to the

wing-alone model configuration at approximately 9° angle of attack; whereas, at 27° angle of attack, the leading-edge flaps or the double slotted flaps had only a very small effect on C_n of the unflapped wing-alone model.

Varying the fuselage length (fineness ratios from 6.43 to 12.10) had only a very slight effect on the yawing-moment characteristics (figs. 23 and 24) of the wing fuselage through the yaw-angle range (0° to 28.7°).

Effectiveness of Vertical Tail

The contributions of the vertical tail to the lateral stability derivatives are presented in figures 25 to 27 as the incremental differences of the lateral stability derivatives obtained from the data of the various model configurations with and without the tail. Figure 28 presents a summary of the contributions of the main model components to the directional stability and lateral force of the complete model. Figures 29 and 30 present the vertical-tail-effectiveness parameter γ_N (see eq. 13). Cross-plotted data to demonstrate vertical-tail-length effects are shown in figure 31. Figure 32 shows the effect of the wing on the yawing-moment contribution of the vertical tail through the yaw-angle range.

The rate of change of the effective angle of attack of the vertical tail $\left(\alpha'_V\right)$ with yaw angle (figs. 33 and 34) and the dynamic pressure ratio $\left(\frac{q_V}{q}\right)_e$ are used to demonstrate the effective flow conditions that the vertical tail experienced in the present investigation. Also, the vertical-tail angle of attack α'_V and the effective dynamic-pressure ratio are plotted against yaw angle in figures 35 and 36. A positive increase in the rate of change of α'_V with yaw angle is indicative of a more favorable flow field and an increased possibility of the vertical tail to provide a stabilizing yawing moment.

Air-flow surveys (σ and q_V/q) in the general vicinity of the vertical tail are presented in figures 37 and 38. Note that the surveys were made in a vertical plane (fig. 9) normal to the wind-tunnel center line; therefore, the angle between the superimposed 0.25-chord line of the vertical tail and the plane of survey will increase as angle of attack α increases. The sidewash angle σ and the effective angle of attack of the tail α'_V are not measured in the same plane, except at $\alpha_B = 2°$, since α'_V is the angle of attack of the vertical tail about its own axis of rotation (fig. 4). The local sidewash angles and dynamic pressure ratios are presented only for illustrating the nature of the flow in the vicinity of the tail.

Vertical-tail contribution at low angles of yaw for the tail length of 0.500 wing semispan.- A rather rapid destabilizing reduction of the incremental contribution of the tail $(C_{n_\psi})_V$ or $(C_{n_\psi})_{V+H}$ with increasing angle of attack occurred for angles of attack above approximately 20° - 21° for all wing-fuselage configurations investigated (figs. 25 to 28). The vertical-tail contribution is presented in figure 29 as the effectiveness parameter γ_N. The loss in vertical-tail effectiveness was more rapid above angles of attack of 18° for model configurations with double slotted flaps than for configurations without these flaps.

For all wing-fuselage configurations investigated with or without flaps, 60 to 80 percent of the loss in the directional stability C_{n_ψ} between 0° and 26° angle of attack was due to the change in yawing-moment contribution of the vertical tail. This is shown for the unflapped configurations in figure 28 which is a summary of the contribution of the main model components to the directional stability of the airplane model. The remaining loss of approximately 20 to 40 percent in the directional stability was due to the changes of the yawing-moment contributions of the wing-fuselage configurations without the vertical or horizontal tail.

Only very small scale effects on the directional-stability contribution of the vertical tail were indicated when the Reynolds number was varied from 4.45×10^6 to 1.20×10^6. Other than figure 13, data for the lower Reynolds number have not been presented.

Effectiveness of the vertical tail at high angles of yaw.- The vertical-tail effectiveness parameter γ_N for the high yaw-angle range is presented in figure 30. For all wing-fuselage configurations at angles of attack below approximately 20°, the positive values of γ_N indicated that the vertical tail caused a directionally stabilizing effect through the yaw-angle range with the major changes in the effectiveness generally occurring in the yaw-angle range of approximately 10° to 20°. As angles of attack increased above 20°, γ_N values indicated less stabilizing effectiveness at low yaw angles but large increasing effectiveness for yaw angles of approximately 8° to 20°. As was the case at low angles of yaw, the change in vertical-tail effectiveness was the major factor in altering the slope of the yawing-moment curve for the complete airplane model configurations.

Effect of the horizontal tail.- The directional stability characteristics of the various model configurations with and without the horizontal tail $(i_H = -14°)$ are summarized in table III. At this horizontal-tail incidence of -14°, a comparison of $(C_{n_\psi})_V$ and $(C_{n_\psi})_{V+H}$ in

figures 26, 27, and 28 indicated that the horizontal tail (located below the fuselage) generally had a directional stabilizing effect at the low angles of attack ($<8^\circ$) and a very slight destabilizing effect at angles of attack above 16° for the unflapped configurations. However, when $i_H = -6^\circ$, the horizontal tail had small or no effect on the vertical-tail contribution to the directional-stability parameter. The values of $(C_{n_\psi})_{V+H}$ when $i_H = -6^\circ$ have not been presented because the $(C_{n_\psi})_V$ of the $W + B_2 + V$ model without the horizontal tail were almost identical to the $(C_{n_\psi})_{V+H}$ of the $W + B_2 + V + H$ model with the tail at $i_H = -6^\circ$.

Vertical-tail-length effect.- The vertical-tail length l_V is an important term in the tail volume $\frac{l_V}{b_W}\frac{S_V}{S_W}$ because it determines both the moment arm and the vertical and lateral location of the tail in the flow field behind an airplane. The tail length may be such that a vertical tail is in a favorable or an adverse flow region, from the standpoint of sidewash angle and dynamic pressure ratio. In the present investigation a reduction in tail length by approximately 20 percent caused a 25-percent reduction in the vertical-tail contribution at low angles of attack α but apparently located the vertical tail in a more favorable flow field behind the wing fuselage at the high angles of attack (figs. 25, 29, and 30). The advantage of a short tail length is best demonstrated in figure 31 where the vertical-tail contribution to the directional stability was cross-plotted with data from reference 12. This figure shows that, for a given value of $\frac{l_V}{b_W}\frac{S_V}{S_W}$, the vertical tail remains effective over a greater angle-of-attack range for the short tail lengths than for the long tail lengths.

At angles of attack above approximately 10° to 12°, a more favorable flow field (fig. 33) was shown at low yaw angles for the configuration having the shorter of the two tail lengths. In the low to moderate angle-of-yaw range ($<10^\circ$), figure 35 indicated that the short tail length of $0.396b_W$ positioned the tail in a more favorable flow field than when $\frac{l_V}{b_W}$ was 0.500. At yaw angles above approximately 10° and in a high angle-of-attack attitude (27°), both tail-length configurations had large stabilizing $\frac{\partial \alpha'_V}{\partial \psi}$; however, the $\frac{l_V}{b_W}$ of 0.500 configuration had the larger positive $\frac{\partial \alpha'_V}{\partial \psi}$. This more favorable flow was also reflected in the results for the yawing-moment data shown in figure 17 at angles of yaw above 10°.

Remarks on the wing and the fuselage influence on the vertical tail.- Results from force-test data (figs. 25 and 26) and from air-flow surveys (figs. 37 and 38) indicated that the addition of the wing to the fuselage to form the wing-fuselage configuration had only a small effect on the vertical-tail effectiveness and air flow at low angles of attack. At moderate angles of attack from approximately 10° to 14°, the addition of the wing to the fuselage generally appeared to have some beneficial effects. However, at high angles of attack ($>20^\circ$), force data (figs. 25 and 32) showed that the effectiveness of the vertical tail was considerably reduced at all yaw angles below approximately 10° when the wing was added to the fuselage. This considerable reduction in the tail effectiveness at low yaw angles was apparently due to different flow phenomena at the vertical tail behind the fuselage alone and behind the wing-fuselage combination.

From the limited air-flow-survey data of this investigation, at 21° angle of attack it appeared that the fuselage alone at 5° to 10° yaw angle had a vortex type of flow in the vicinity of the vertical tail (fig. 37). The flow over the fuselage appeared to be the same as that described in reference 27. When the wing was added to the fuselage, the flow in the vicinity of the vertical tail was very different from that of the fuselage alone at 21° angle of attack even though the values of $(C_{n_\psi})_V$ were about the same. At 21° angle of attack, in the vicinity of the vertical tail, the air-flow surveys (fig. 37) indicated that the flow behind the wing-fuselage configurations more nearly resembled the flow behind the wing alone with leading-edge flaps than it did the flow behind the fuselage alone.

The flow at the vertical tail is influenced greatly by the strong vortices behind the wing, particularly at angles of attack greater than approximately 21°. References 16 and 25 showed that this wing had a leading-edge-vortex type of flow and the surveys of reference 18 showed regions of high vorticity behind the wing at an unyawed attitude. With or without the fuselage, this leading-edge vortex developed at the wing inboard (spanwise) sections, moved outboard along the wing, and finally turned into the free-stream direction before reaching the tips. From observations of surface tufts (fig. 18), limited probe studies, and previous observations of sweptback and delta wings (ref. 26), it is indicated that in the yawed attitude the leading-edge vortex of the leading wing moves well inboard and turns in a streamwise direction, whereas the vortex of the trailing wing continues to be shed in the general vicinity of the tip and moves in a streamwise direction after being shed. This vortex type of flow is illustrated schematically in figure 39.

It is apparent (fig. 39) that rapid changes in direction (stabilizing inflow or destabilizing outflow) and magnitude of the sidewash angle can occur, along the spanwise stations of the vertical tail,

depending on the strength of the vortex and the relative position of the vertical tail and the vortex. Reference 6 describes a somewhat similar effect on the sidewash distribution that a vertical tail experienced in a separation vortex.

The flow picture described may be somewhat simplified for a wing-fuselage combination since the flow has been related principally to the wing leading-edge vortex flow. When combining the wing with the fuselage, it should also be remembered that the complex flow at the tail is influenced by such things as the wing vortex sheet (stabilizing sidewash above and destabilizing sidewash below) and the flow field behind high-lift devices such as double slotted flaps.

DIHEDRAL EFFECT

Complete-Model Characteristics

Dihedral effect at low angles of yaw.- The variations of the rolling-moment derivative C_{l_ψ} with angle of attack (figs. 11 and 12) show that reversals of the positive slope of the rolling-moment derivative occurred for the unflapped configuration when large flow separation (fig. 18) of the wing occurred (coincident with longitudinal pitch up). In the vicinity of maximum lift coefficient, the values of C_{l_ψ} are negative. Similar C_{l_ψ} characteristics have been shown for configurations having sweptback wings. The addition of leading-edge flaps, of course, improved the air-flow characteristics on the outboard sections of the wing which prevented the reversal of C_{l_ψ} at moderate angles of attack. Reference 2 has shown similar effects of leading-edge flaps on the C_{l_ψ} characteristics for midwing-fuselage configurations.

The addition of double slotted flaps to the model configuration with leading-edge flaps (figs. 11 and 14) indicated approximately a 0.002 incremental increase in the positive C_{l_ψ} for comparative angles of attack below 12°. This indicated incremental increase was primarily due to a difference in the lift coefficient of the model configurations with leading-edge flaps with and without the double slotted flaps.

The variations of the rolling-moment derivative C_{l_ψ} with angle of attack (fig. 13) show that reducing the Reynolds number decreased the angle of attack at which the reversals of the positive slope of the rolling-moment derivative occurred. Similar effects have been shown in reference 4. As pointed out in reference 4 it is advisable to exercise caution when using lateral-stability parameters obtained at low Reynolds numbers, especially in the moderate to high lift-coefficient range on swept wings with conventional airfoil shapes.

Dihedral effect at high angles of yaw.- For the flapped and unflapped configurations at yaw angles above approximately 10° to 12°, there was generally a decrease in C_{l_ψ} as yaw angle increased (fig. 16). At the highest angle of attack (fig. 16(d)) or near maximum lift coefficient, it should be noted that the configuration with leading-edge flaps and with leading-edge and double slotted flaps had a reversal in C_{l_ψ} in the higher yaw-angle range (>15°).

Wing-Fuselage Characteristics and Interferences

The wing-alone effective dihedral parameter had the usual variations of sweptback wings with increasing angle of attack (fig. 40). As indicated by $\Delta_1 C_{l_\psi}$, the addition of the fuselage caused only very slight changes in the values of C_{l_ψ} of the wing at low angles of attack. However, as angle of attack increased, $\Delta_1 C_{l_\psi}$ increased and the maximum values occurred at approximately the maximum lift coefficient. The maximum values of $\Delta_1 C_{l_\psi}$ for the wing-fuselage configuration with or without flaps occurred at approximately the maximum lift coefficient of the wing-alone configuration having the corresponding flap configuration (fig. 10(a)).

Summary of Contributions to Effective Dihedral

A summary of the contributions of the main model components to the effective dihedral parameter of the complete model is shown in figure 41. This figure indicates that the wing provides the only significant contribution of C_{l_ψ} of the complete airplane model.

The vertical-tail contribution $\left(C_{l_\psi}\right)_{V+H}$ was of similar magnitude as the wing-fuselage interference $\Delta_1 C_{l_\psi}$ for angles of attack of 10° to 18° as the wing outboard sections stall (fig. 18).

SUMMARY OF RESULTS

The low-speed static lateral stability characteristics of an airplane model having a 47.7° sweptback wing of aspect ratio 6 and the contribution of various model components to the lateral stability characteristics at a Reynolds number of 4.45×10^6 may be summarized as follows:

1. The complete airplane model was directionally stable through the yaw-angle range (0° to 28.7°) for angles of attack up to approximately 23°. The model became very unstable at higher angles of attack for angles of yaw below approximately 10° even though a high degree of directional stability existed at higher yaw angles. Adding leading-edge flaps and double slotted flaps generally increased the directional stability at low to moderate angles of attack but did not prevent the directional instability at higher angles of attack shown by the unflapped airplane model.

2. At low angles of yaw ($\pm 5^\circ$) for all wing-fuselage model configurations investigated (with or without leading-edge and double slotted flaps), 60 to 80 percent of the loss in the directional stability between 0° and 26° angle of attack was due to the change in yawing-moment contribution of the vertical tail. The remaining 20 to 40 percent loss was due to the unstable change of the yawing-moment contributions of the wing-fuselage configurations without the vertical or horizontal tail. As angle of yaw was increased above approximately 10°, the major stabilizing contribution to the high degree of directional stability that existed in the high angle-of-attack range was due to the vertical tail.

3. A reduction in the vertical-tail length (0.500 wing semispan) by approximately 20 percent caused a 25-percent reduction (at 0° angle of attack) of the directional-stability contribution of the vertical tail at low angles of yaw ($\pm 5^\circ$). At high angles of attack, the reduction in tail length located the vertical tail in a more favorable flow field whereby the vertical-tail effectiveness parameter had less variation with yaw angle and indicated a more stabilizing contribution of the vertical tail.

4. The directional-stability parameter of the airplane model was only slightly affected by the horizontal tail or by the unflapped wing—fuselage mutual interference.

5. Changing the Reynolds number from 4.45×10^6 to 1.2×10^6 had no appreciable effect on the directional stability of any of the configurations investigated but did decrease the angle of attack at which a rapid decrease occurred in the value of the effective dihedral parameter.

Langley Aeronautical Laboratory,
National Advisory Committee for Aeronautics,
Langley Field, Va., June 25, 1953.

REFERENCES

1. Campbell, John P., and McKinney, Marion O.: Summary of Methods for Calculating Dynamic Lateral Stability and Response and for Estimating Lateral Stability Derivatives. NACA Rep. 1098, 1952. (Supersedes NACA TN 2409.)

2. Salmi, Reino J., Conner, D. William, and Graham, Robert R.: Effects of a Fuselage on the Aerodynamic Characteristics of a 42° Sweptback Wing at Reynolds Numbers to 8,000,000. NACA RM L7E13, 1947.

3. Salmi, Reino J., and Fitzpatrick, James E.: Yaw Characteristics and Sidewash Angles of a 42° Sweptback Circular-Arc Wing With a Fuselage and With Leading-Edge and Split Flaps at a Reynolds Number of 5,300,000. NACA RM L7I30, 1947.

4. Salmi, Reino J.: Yaw Characteristics of a 52° Sweptback Wing of NACA 64_1-112 Section With a Fuselage and With Leading-Edge and Split Flaps at Reynolds Number From 1.93×10^6 to 6.00×10^6. NACA RM L8H12, 1948.

5. Guryansky, Eugene R., and Lipson, Stanley: Effect of High-Lift Devices on the Longitudinal and Lateral Characteristics of a 45° Sweptback Wing With Symmetrical Circular-Arc Sections. NACA RM L8D06, 1948.

6. Whittle, Edward F., Jr., and Lovell, J. Calvin: Full-Scale Investigation of an Equilateral Triangular Wing Having 10-Percent-Thick Biconvex Airfoil Sections. NACA RM L8G05, 1948.

7. McCormack, Gerald M., and Walling, Walter C.: Aerodynamic Study of a Wing-Fuselage Combination Employing a Wing Swept Back 63°.- Investigation of a Large-Scale Model at Low Speed. NACA RM A8D02, 1949.

8. Purser, Paul E., and Spearman, M. Leroy: Wind-Tunnel Tests at Low Speed of Swept and Yawed Wings Having Various Plan Forms. NACA TN 2445, 1951. (Supersedes NACA RM L7D23.)

9. McCormack, Gerald M.: Aerodynamic Study of a Wing-Fuselage Combination Employing a Wing Swept Back 63°.- Aerodynamic Characteristics in Sideslip of a Large-Scale Model Having a 63° Swept-Back Vertical Tail. NACA RM A9F14, 1949.

10. Anderson, Adrien E.: An Investigation at Low Speed of a Large-Scale Triangular Wing of Aspect Ratio Two.- III. Characteristics of Wing With Body and Vertical Tail. NACA RM A9H04, 1949.

11. Brewer, Jack D., and Lichtenstein, Jacob H.: Effect of Horizontal Tail on Low-Speed Static Lateral Stability Characteristics of a Model Having 45° Sweptback Wing and V Tail Surfaces. NACA TN 2010, 1950.

12. Queijo, M. J., and Wolhart, Walter D.: Experimental Investigation of the Effect of Vertical-Tail Size and Length and of Fuselage Shape and Length on the Static Lateral Stability Characteristics of a Model With 45° Sweptback Wing and Tail Surfaces. NACA Rep. 1049, 1951. (Supersedes NACA TN 2168.)

13. Goodman, Alex: Effects of Wing Position and Horizontal-Tail Position on the Static Stability Characteristics of Models With Unswept and 45° Sweptback Surfaces With Some Reference to Mutual Interference. NACA TN 2504, 1951.

14. Goodman, Alex, and Wolhart, Walter D.: Experimental Investigation of the Low-Speed Static and Yawing Stability Characteristics of a 45° Sweptback High-Wing Configuration With Various Twin Vertical Wing Fins. NACA TN 2534, 1951.

15. Bird, John D., Lichtenstein, Jacob H., and Jacquet, Byron M.: Investigation of the Influence of Fuselage and Tail Surfaces on Low-Speed Static Stability and Rolling Characteristics of a Swept-Wing Model. NACA TN 2741, 1952. (Supersedes NACA RM L7H15.)

16. Salmi, Reino J., and Carros, Robert J.: Longitudinal Characteristics of Two 47.7° Sweptback Wings With Aspect Ratios of 5.1 and 6.0 at Reynolds Numbers up to 10×10^6. NACA RM L50A04, 1950.

17. Salmi, Reino J.: Effects of Leading-Edge Devices and Trailing-Edge Flaps on Longitudinal Characteristics of Two 47.7° Sweptback Wings of Aspect Ratios 5.1 and 6.0 at a Reynolds Number of 6.0×10^6. NACA RM L50F20, 1950.

18. Salmi, Reino J.: Horizontal-Tail Effectiveness and Downwash Surveys for Two 47.7° Sweptback Wing-Fuselage Combinations with Aspect Ratios of 5.1 and 6.0 at a Reynolds Number of 6.0×10^6. NACA RM L50K06, 1951.

19. Sivells, James C., and Spooner, Stanley H.: Investigation in the Langley 19-Foot Pressure Tunnel of Two Wings of NACA 65-210 and 64-210 Airfoil Sections With Various Type Flaps. NACA Rep. 942, 1949. (Supersedes NACA TN 1579.)

20. Foster, Gerald V., and Griner, Roland F.: A Study of Several Factors Affecting the Stability Contributed by a Horizontal Tail at Various Vertical Positions on a Sweptback-Wing Airplane Model. NACA RM L9H19, 1949.

21. Sivells, James C., and Salmi, Rachel M.: Jet-Boundary Corrections for Complete and Semispan Swept Wings in Closed Circular Wind Tunnels. NACA TN 2454, 1951.

22. House, Rufus O., and Wallace, Arthur R.: Wind-Tunnel Investigation of Effect of Interference on Lateral-Stability Characteristics of Four NACA 23012 Wings, an Elliptical and a Circular Fuselage, and Vertical Fins. NACA Rep. 705, 1941.

23. DeYoung, John: Theoretical Additional Span Loading Characteristics of Wings With Arbitrary Sweep, Aspect Ratio, and Taper Ratio. NACA TN 1491, 1947.

24. Schlichting, H.: Aerodynamics of the Mutual Influence of Aircraft Parts (Interference). Library Translation No. 275, British R.A.E., Oct. 1948.

25. Furlong, G. Chester, and McHugh, James G.: A Summary and Analysis of the Low-Speed Longitudinal Characteristics of Swept Wings at High Reynolds Number. NACA RM L52D16, 1952.

26. Bird, John D., and Riley, Donald R.: Some Experiments on Visualization of Flow Fields Behind Low-Aspect-Ratio Wings by Means of a Tuft Grid. NACA TN 2674, 1952.

27. Allen, H. Julian, and Perkins, Edward W.: Characteristics of Flow Over Inclined Bodies of Revolution. NACA RM A50L07, 1951.

TABLE I.- AIR-FLOW SURVEY-PLANE LOCATION

(See fig. 9).

Configuration	α, deg	ψ, deg	$\frac{l_S}{\bar{c}_W}$	$\frac{l_S}{b_W/2}$
*B_2	2	0, 5, 10	2.776	1.008
	2	20	2.611	.948
	8	0, 5, 10	2.776	1.008
	8	20	2.611	.948
	20	0, 5, 10	2.677	.972
	20	20	2.512	.912
W + B_2	2.3	0, 5, 10	2.776	1.008
	2.3	20	2.611	.948
	8.7	0, 5, 10	2.776	1.008
	8.7	20	2.611	.948
	21.1	0, 5, 10	2.677	.972
	21.1	20	2.512	.912
W + B_2 + F	2.2	0, 5, 10	2.776	1.008
	2.2	20	2.611	.948
	8.7	0, 5, 10	2.776	1.008
	8.7	20	2.611	.948
	21.1	0, 5, 10	2.677	.972
	21.1	20	2.512	.912
W + B_2 + F + D	2.9	0, 5, 10	2.776	1.008
	2.9	20	2.611	.948
	9.2	0, 5, 10	2.776	1.008
	9.2	20	2.611	.948
	21.4	0, 5, 10	2.677	.972
	21.4	20	2.512	.912
W + F	21.1	0, 5, 10	2.677	.972
	21.1	20	2.512	.912

*$\alpha_B = \alpha - 2^\circ$.

TABLE II.- FIGURE-NUMBER INDEX FOR PLOTTED DATA

Configuration			Lateral Characteristics						Longitudinal characteristics	Air-flow characteristics
			Force and moments		Derivatives					
Basic	Flaps	Fences	Basic	Tail contribution	[a]Stability parameters	Wing-fuselage interference	Tail contributions	Effectiveness parameter γ_N		
$W + B_2 + V + H$	Off On On	Off Off On	16 16 16		11, 28, 41 11 11	----------	27, 28, 41 27 27		10(c) 10(c)	
$W + B_2 + V$	Off On On	Off Off On	17, 32 15 15	32	12, 13, 28, 41 14 14	----------	25, 26, 28, 31, 32, 41 26 26	29, 30 29, 30 29		[b]33, 34, 35, 36 34, 36
$W + B_1 + V$	Off	Off	17		12	----------	25, 31	29, 30		[b]33, 35
$W + B_1$	Off	Off	24	---	23	----------	----------			
$W + B_2$	Off On On	Off Off On	22, 24, 32 22	---	19, 23, 28, 40, 41 19, 40 19, 40	19, 28, 40, 41 19, 40	----------		10(b), 22 10(b), 22	37, 38 37, 38
$W + B_3$	Off	Off	24	---		----------	----------			
$W + B_4$	Off	Off	24	---		----------	----------			
W	Off On	Off Off	20 20	---	19, 28, 40, 41 19, 40	----------	----------		10(a) 10(a)	37, 38
B_2	---	---	21, 32	---	19, 21, 28, 40, 41	----------	----------		10(b), 21	37, 38
$B_2 + V$	---	---	32	32		----------	25	29		

[a]See tables III and IV for summaries and additional configurations.

[b]Effective flow conditions.

TABLE III.- SUMMARY OF THE STATIC DIRECTIONAL STABILITY CHARACTERISTICS OF THE COMPONENT PARTS AND THE COMPLETE AIRPLANE MODEL HAVING A MIDWING SWEPTBACK 47.7°. R = 4.45 × 10^6

Basic configuration	Type and span of flaps	Vertical tail off Horizontal tail off	Vertical tail on Horizontal tail off	Vertical tail on Horizontal tail on
Fuselage B_2		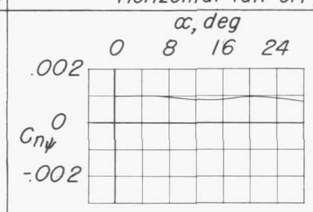	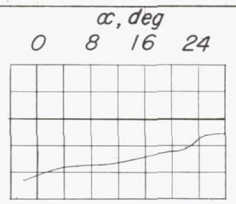	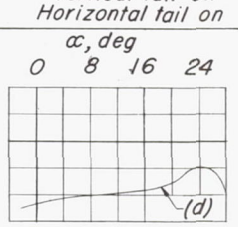
Wing and fuselage B_2	Off	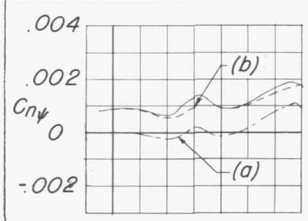	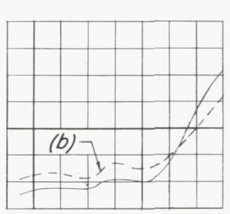	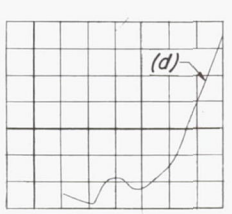
	0.481 $b_w/2$ leading edge	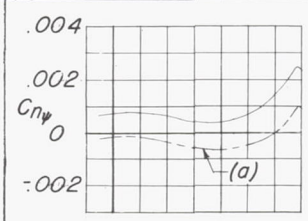	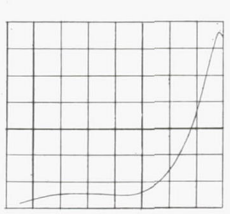	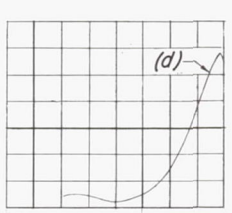
	(c) 0.481 $b_w/2$ leading edge	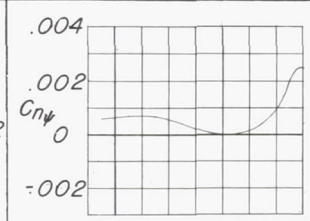	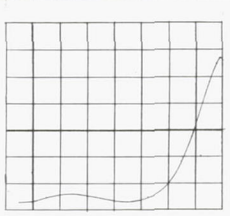	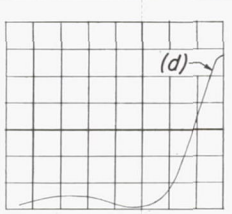
	0.481 $b_w/2$ leading edge 0.462 $b_w/2$ double slotted	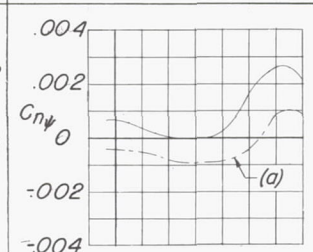	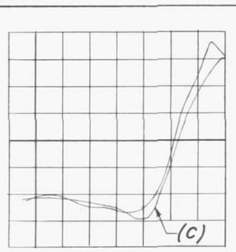	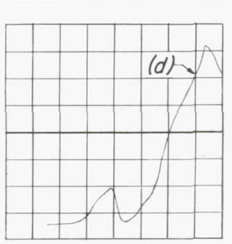

(a) Wing alone
(b) Fuselage B_1 + wing
(c) Fences located at 0.544 $b_w/2$
(d) Horizontal tail incidence of -14°

TABLE IV.- SUMMARY OF THE EFFECTIVE DIHEDRAL CHARACTERISTICS OF THE COMPONENT PARTS AND THE COMPLETE AIRPLANE MODEL HAVING A MIDWING SWEPTBACK 47.7°. $R = 4.45 \times 10^6$

Basic configuration	Type and span of flaps	Vertical tail off Horizontal tail off	Vertical tail on Horizontal tail off	Vertical tail on Horizontal tail on
Fuselage B_2.		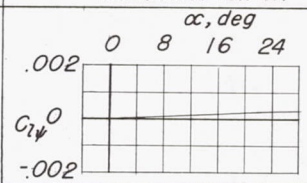	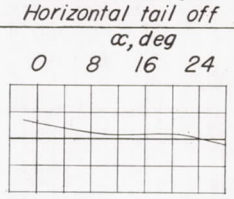	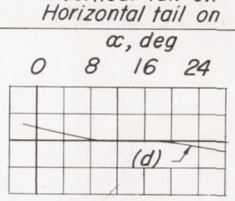
Wing and fuselage B_2	Off	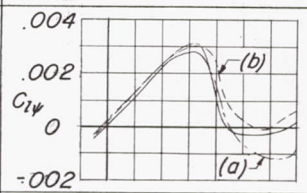	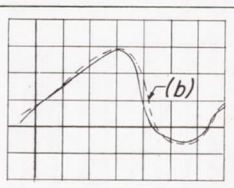	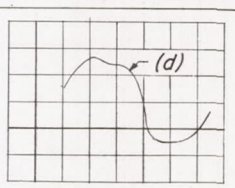
	0.481 $b_w/2$ leading edge	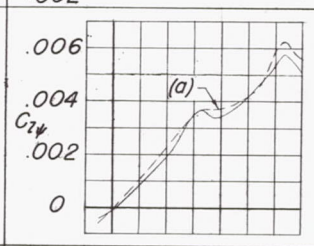	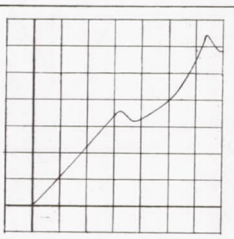	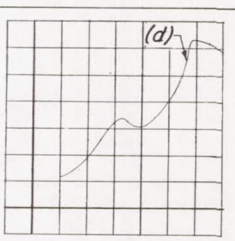
	(c) 0.481 $b_w/2$ leading edge	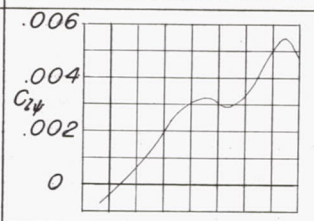	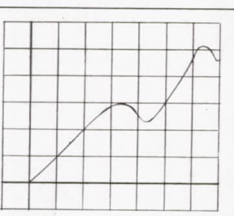	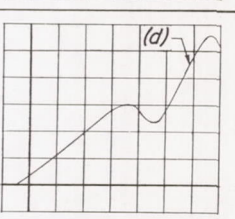
	0.481 $b_w/2$ leading edge 0.462 $b_w/2$ double slotted	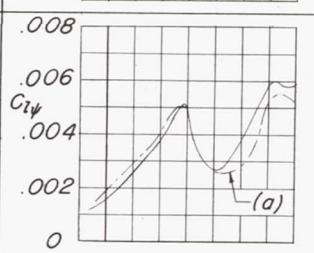	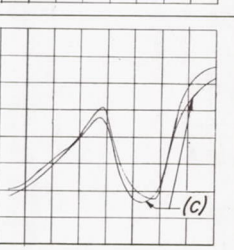	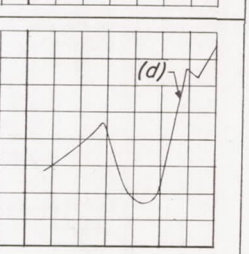

(a) Wing alone
(b) Fuselage B_1 + wing
(c) Fences located at 0.544 $b_w/2$
(d) Horizontal tail incidence of -14°

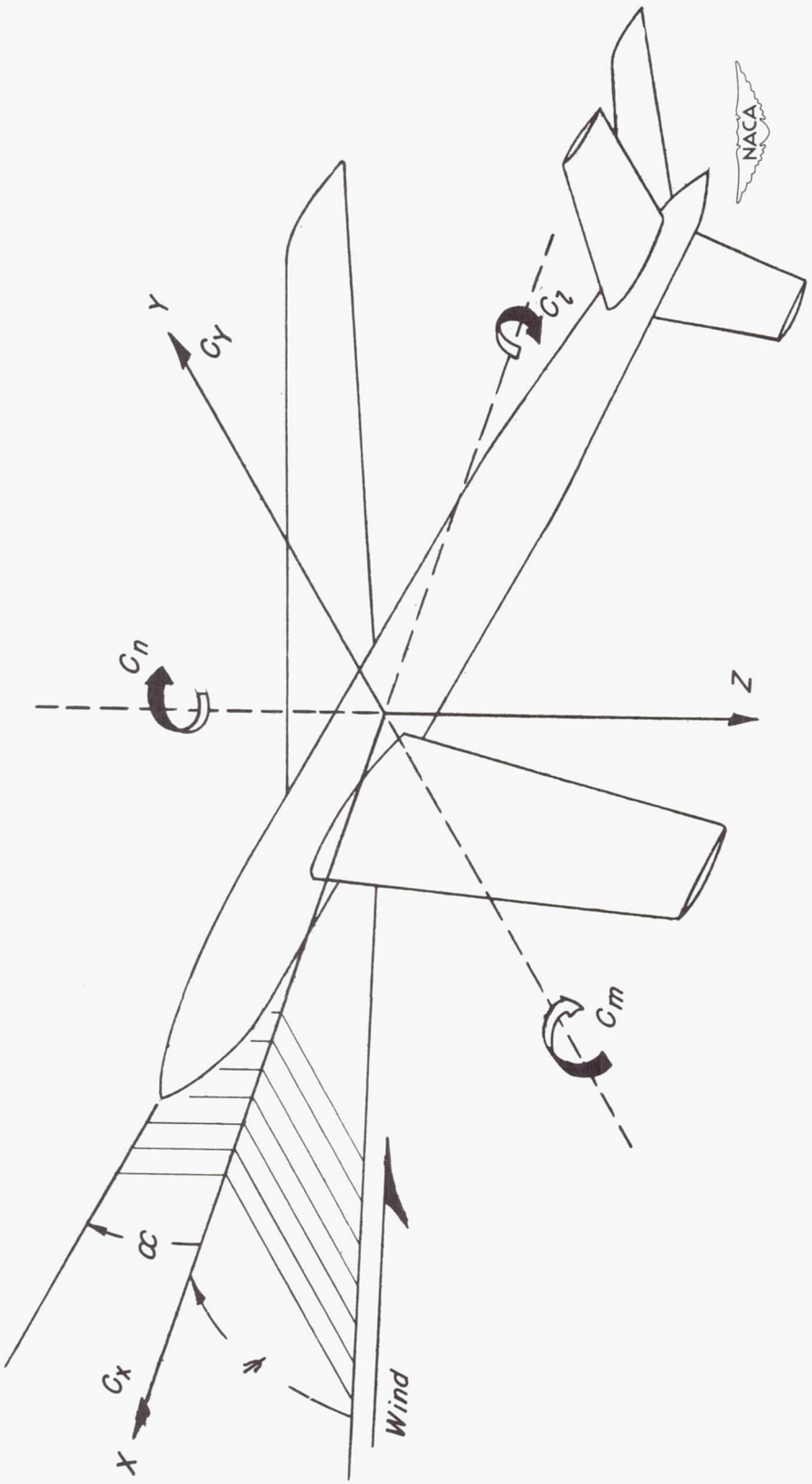

Figure 1.- System of axes. Arrows indicate positive directions.

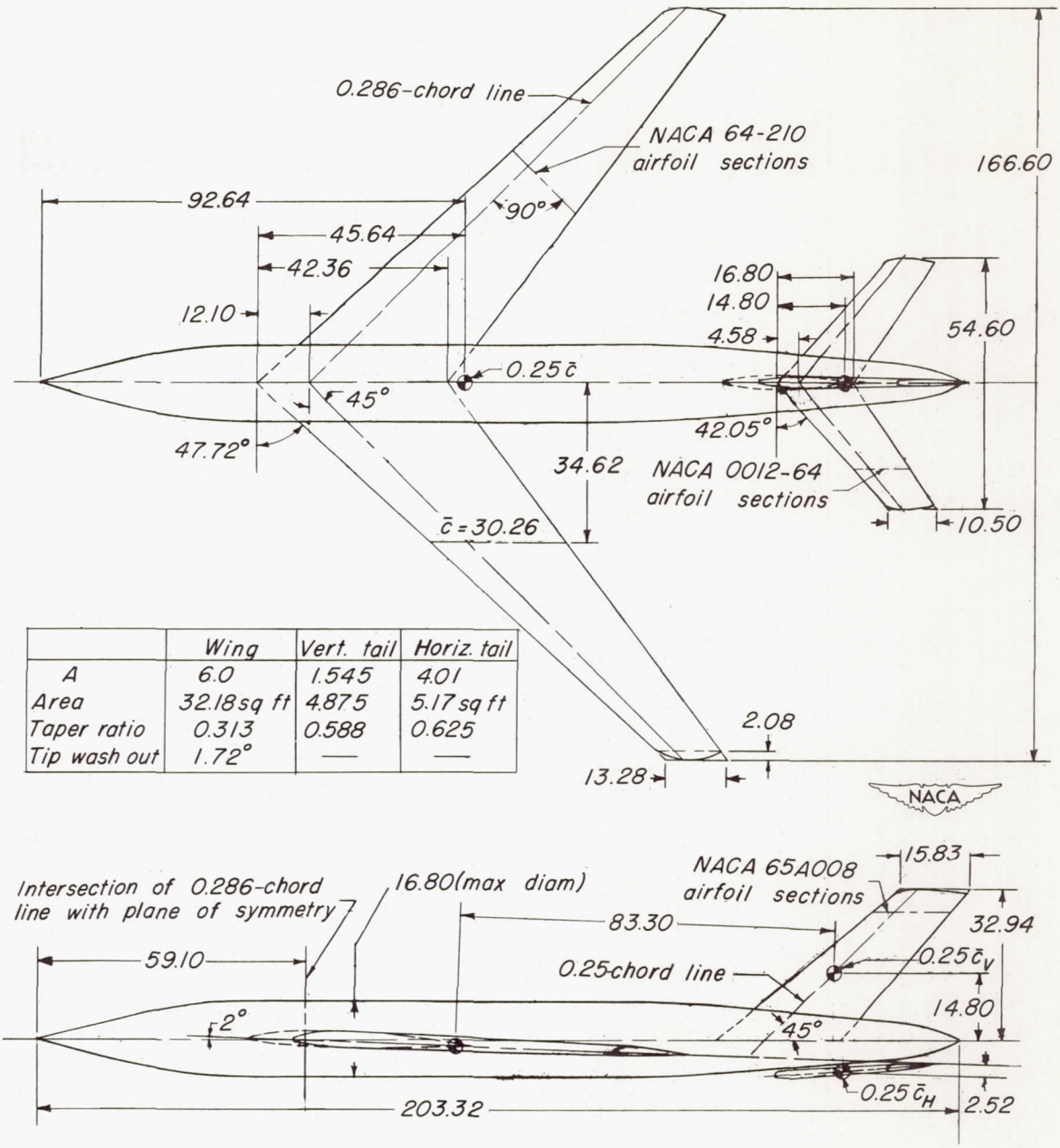

	Wing	Vert. tail	Horiz. tail
A	6.0	1.545	4.01
Area	32.18 sq ft	4.875	5.17 sq ft
Taper ratio	0.313	0.588	0.625
Tip wash out	1.72°	—	—

Figure 2.- Geometry of the 47.7° sweptback-wing airplane model. All dimensions are in inches unless otherwise noted.

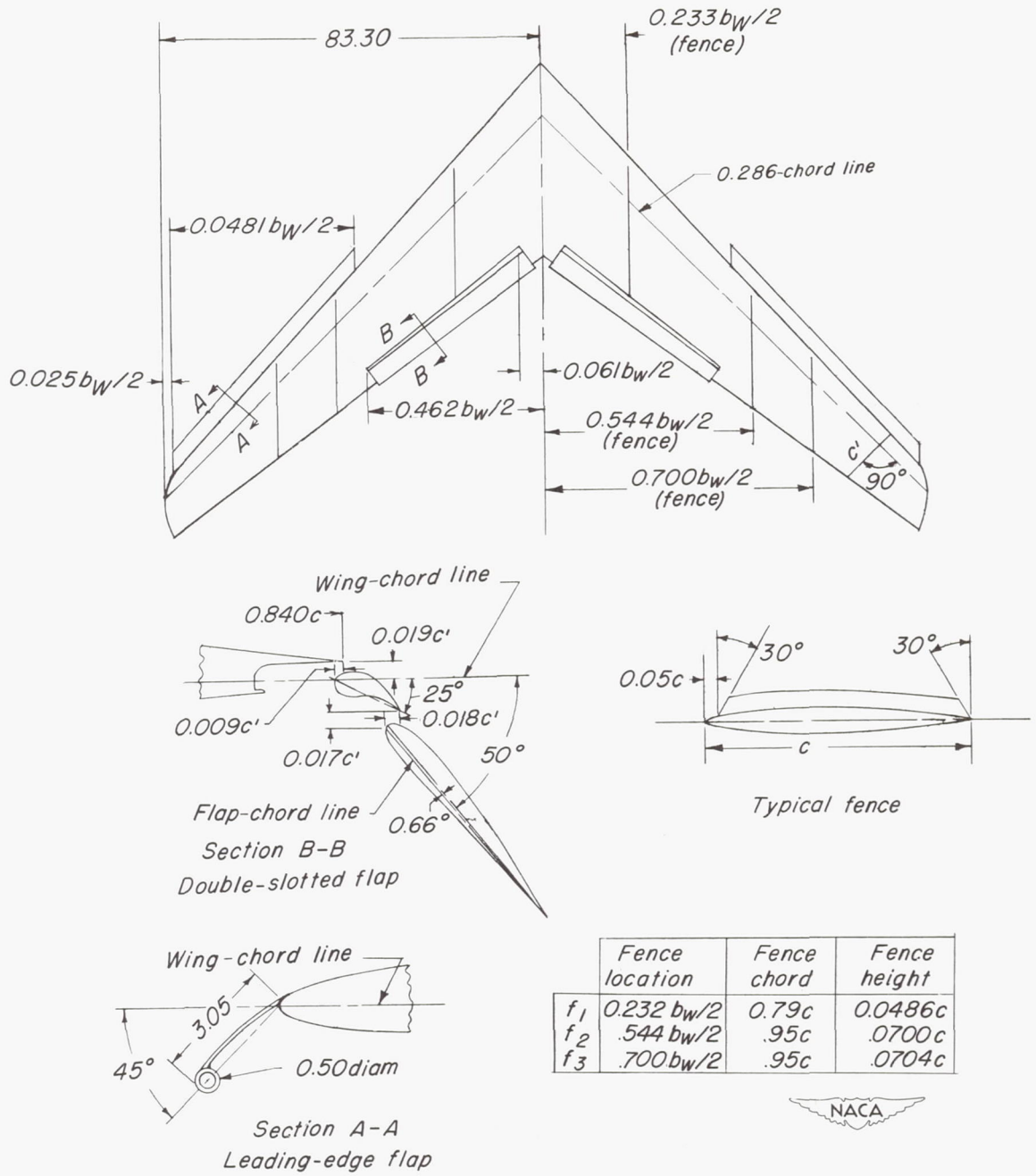

	Fence location	Fence chord	Fence height
f_1	0.232 bw/2	0.79c	0.0486c
f_2	.544 bw/2	.95c	.0700c
f_3	.700 bw/2	.95c	.0704c

NACA

Figure 3.- Geometric details of the high-lift and stall-control devices. All dimensions are in inches unless otherwise noted.

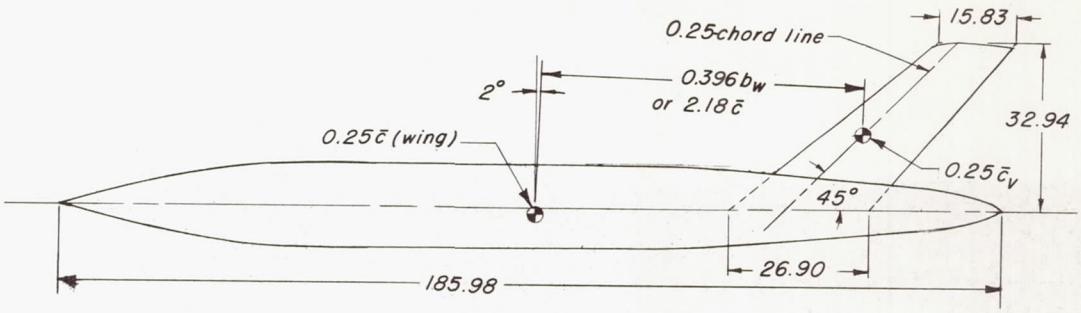

(a) Fuselage B_1 with vertical tail.

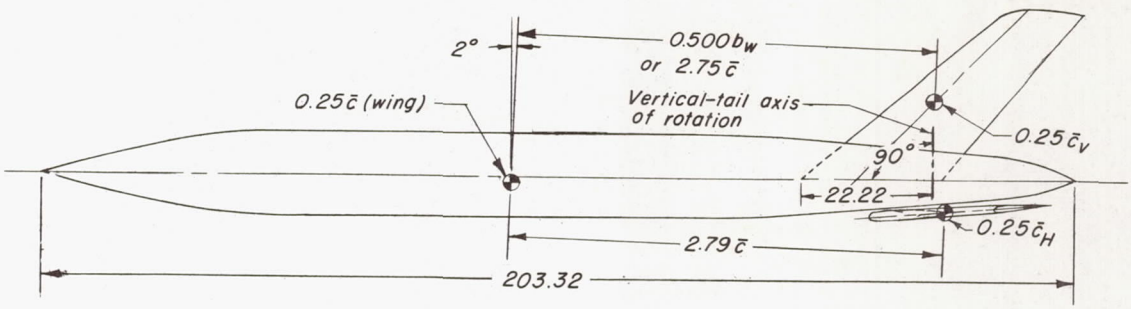

(b) Fuselage B_2 with vertical tail and horizontal tail.

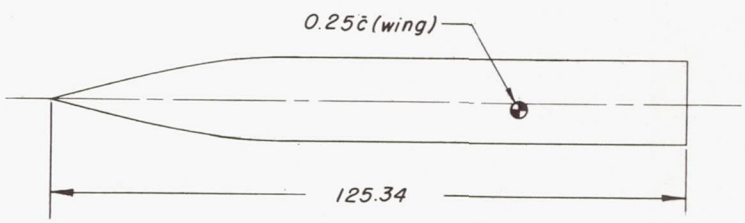

(c) Fuselage B_3.

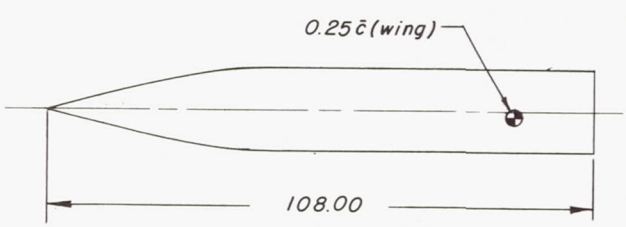

(d) Fuselage B_4.

Figure 4.- Geometric details of the vertical tail and the various fuselage configurations. All dimensions are in inches unless otherwise noted.

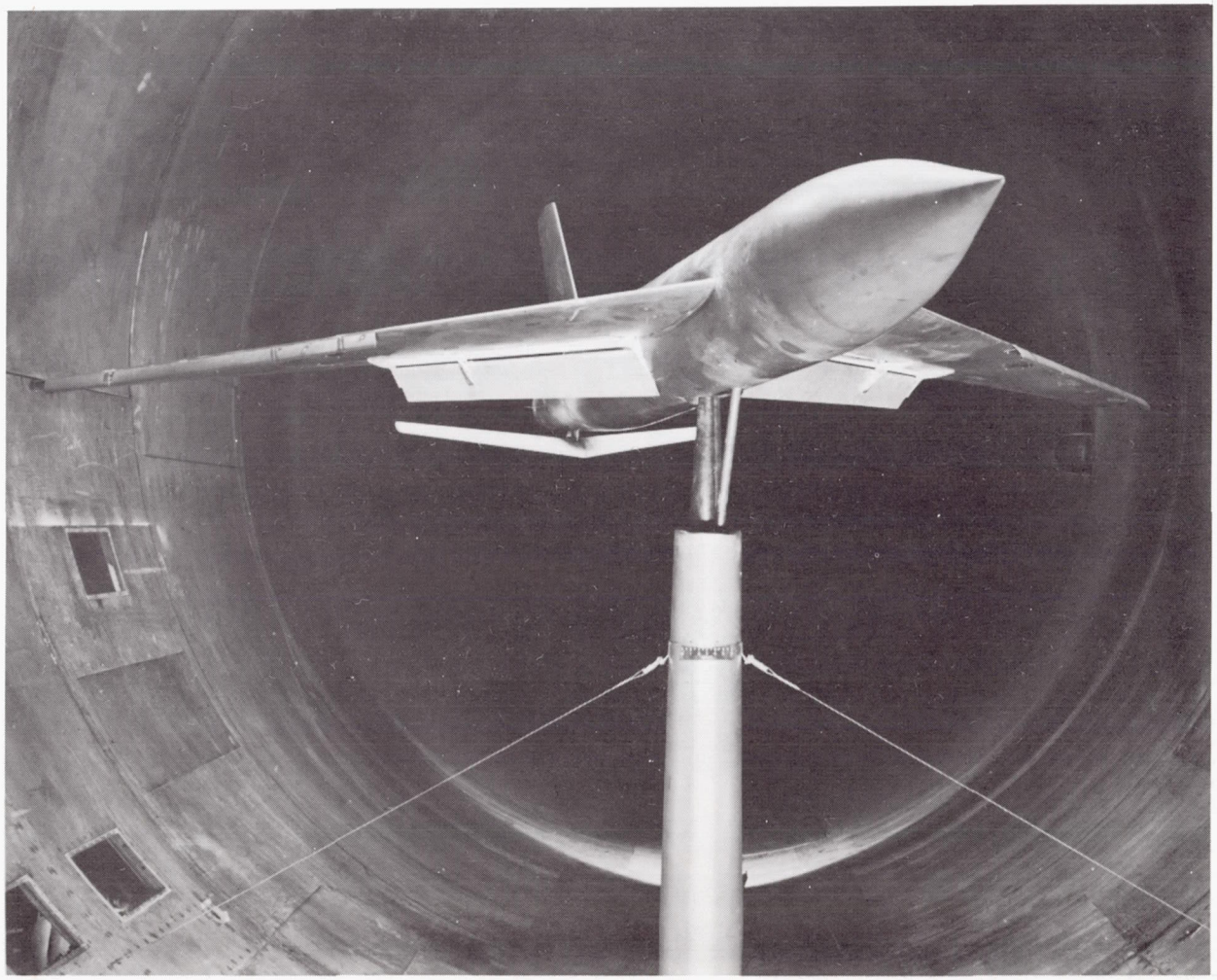

L-74445

Figure 5.- The 47.7° sweptback-wing airplane model of aspect ratio 6.0, with flaps deflected, mounted on the yaw support strut in Langley 19-foot pressure tunnel.

L-73445

Figure 6.- The fuselage of fineness ratio 12.01 with the 45° sweptback vertical tail of aspect ratio 1.545 mounted on the yaw support strut in the Langley 19-foot pressure tunnel.

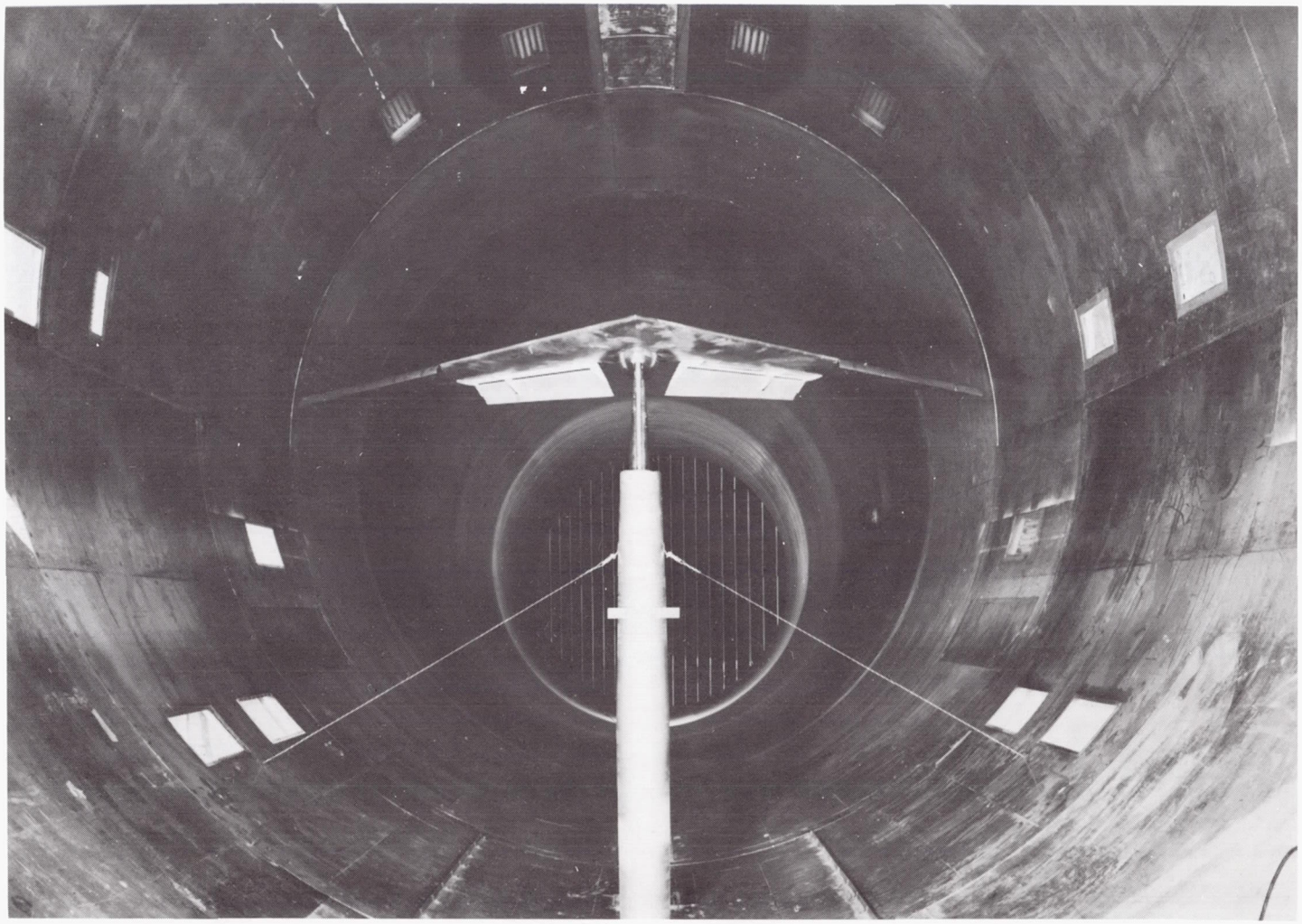

L-74727

Figure 7.- The 47.7° sweptback wing of aspect ratio 6.0, with flaps deflected, mounted on the yaw support strut of the Langley 19-foot pressure tunnel.

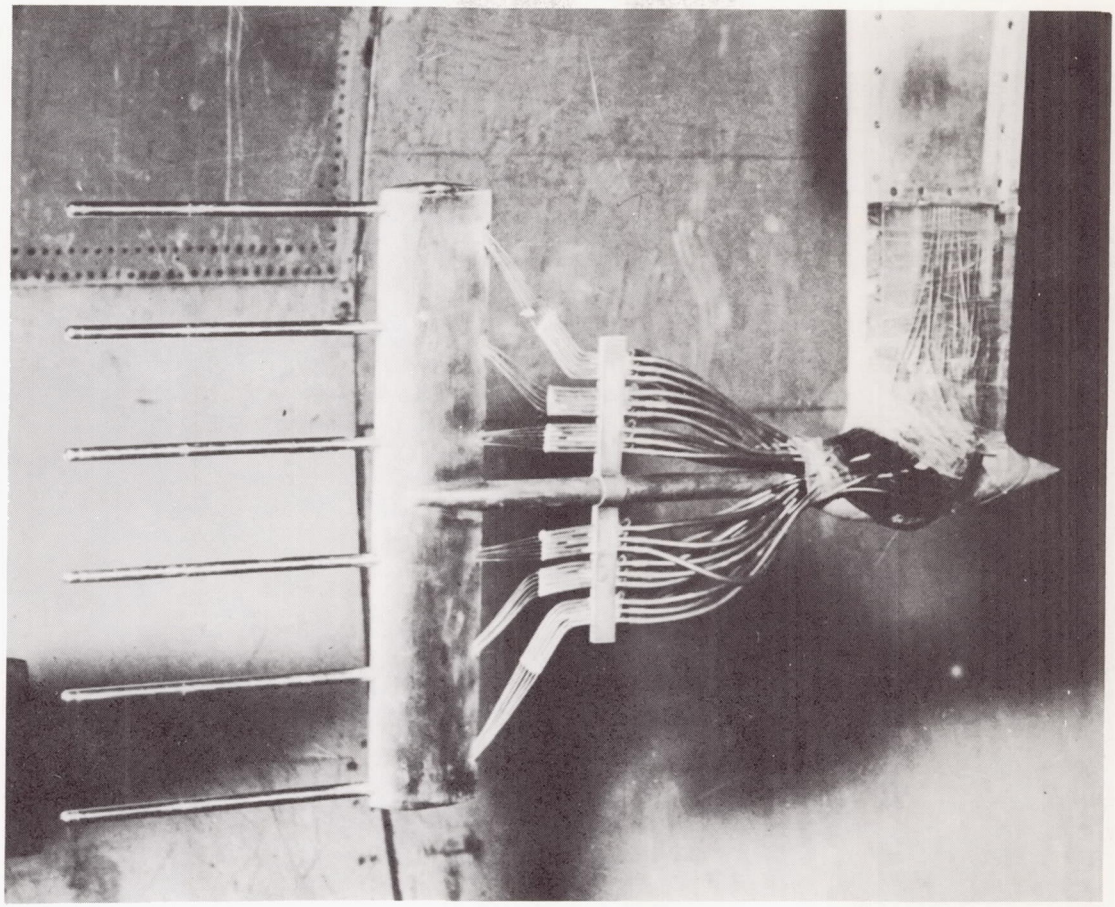

L-47123.1

(a) Photograph of rake head.

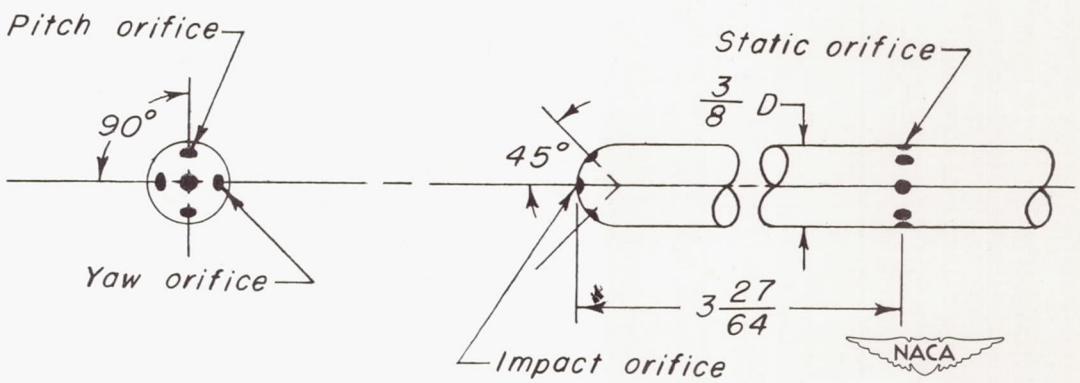

(b) Sketch of tube head.

Figure 8.- Air-flow survey rake used in Langley 19-foot pressure tunnel. All dimensions are in inches.

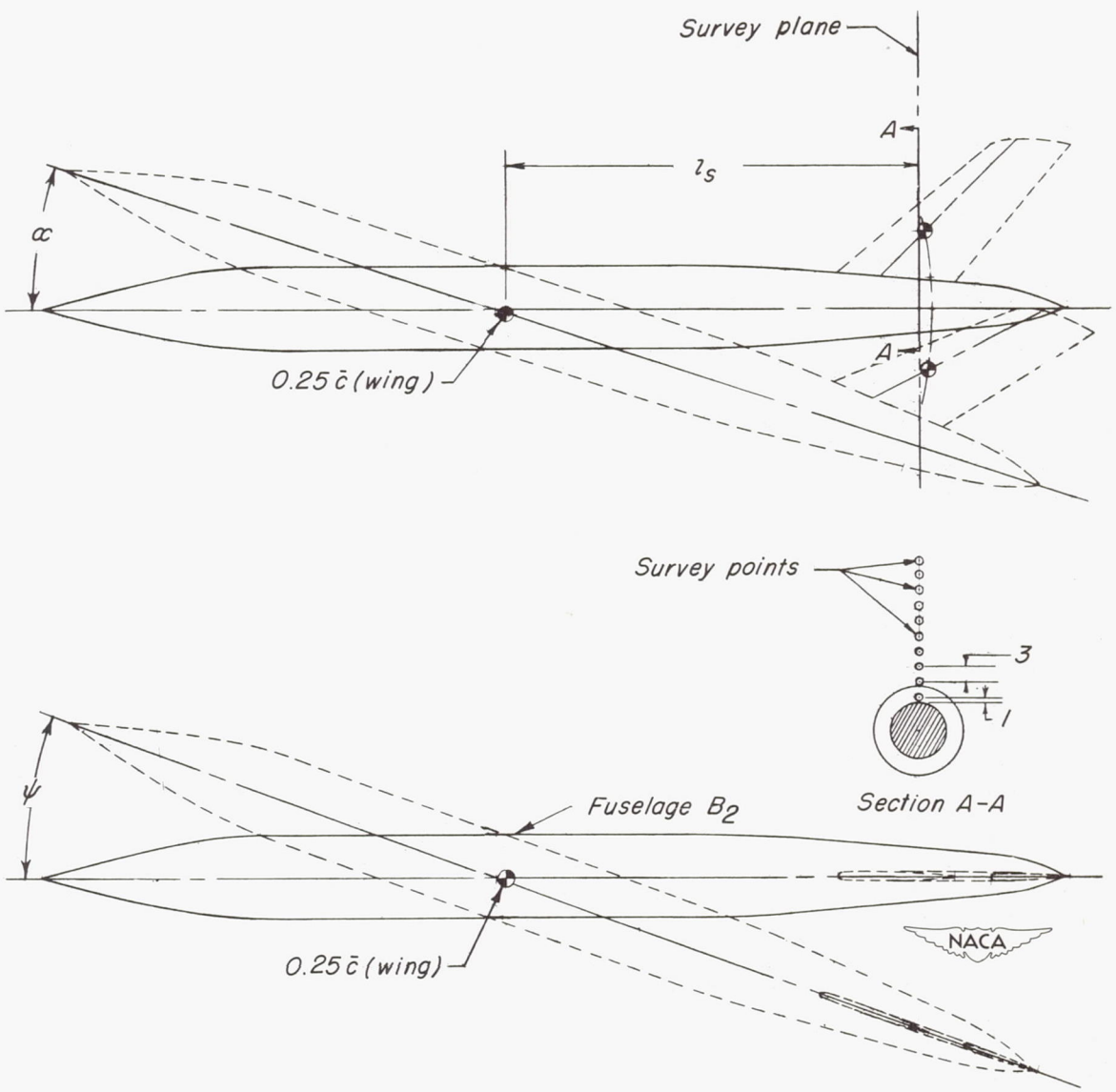

Figure 9.- Location of the air-flow survey plane for various angles of attack and yaw angles. See table I. All dimensions are in inches unless otherwise noted.

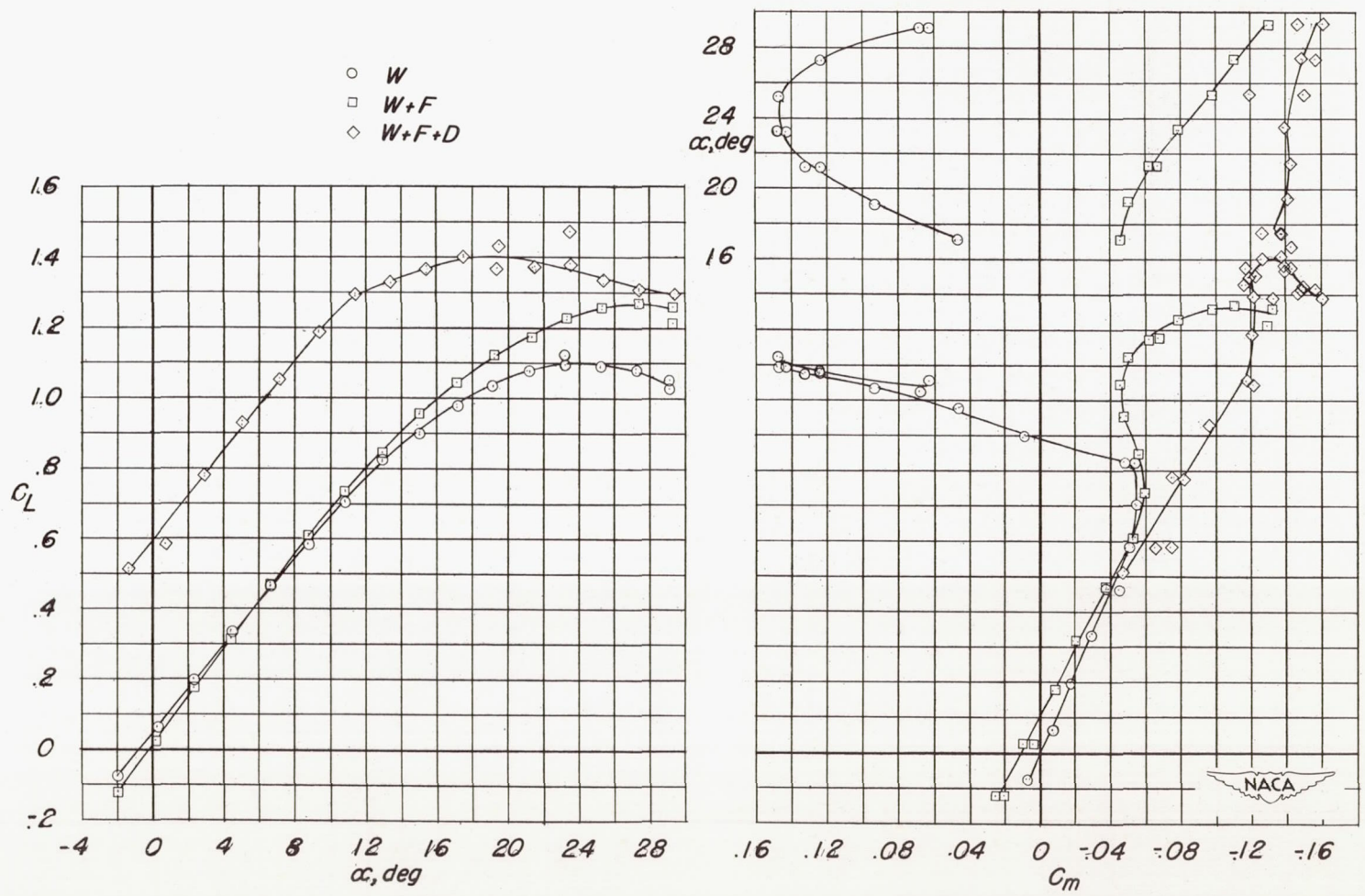

(a) Effect of flaps on the wing alone.

Figure 10.- Aerodynamic characteristics of wing, fuselage, wing-fuselage, and the complete model. R = 4.45×10^6.

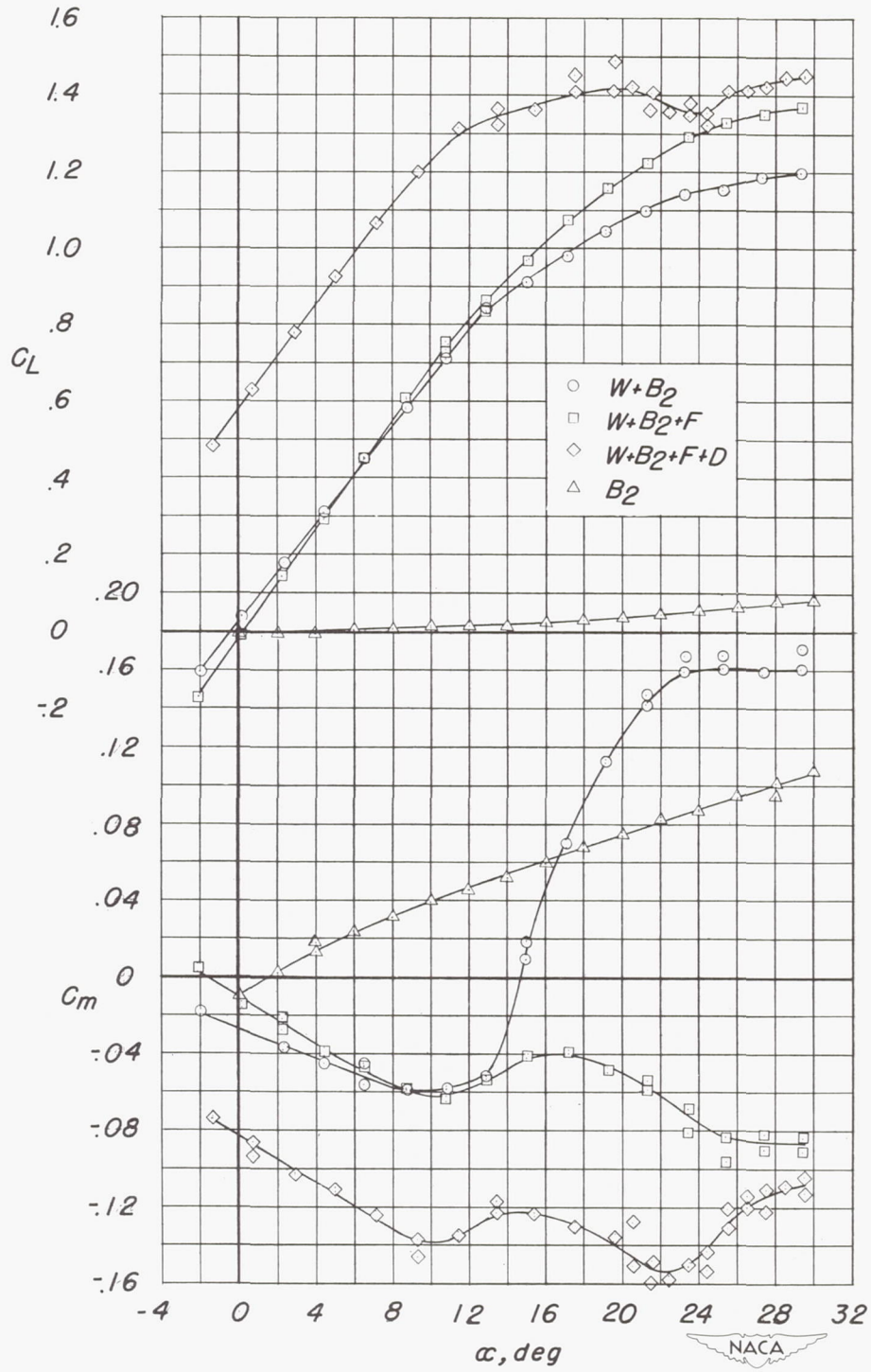

(b) Characteristics of the fuselage and effect of flaps on wing-fuselage configuration.

Figure 10.- Continued.

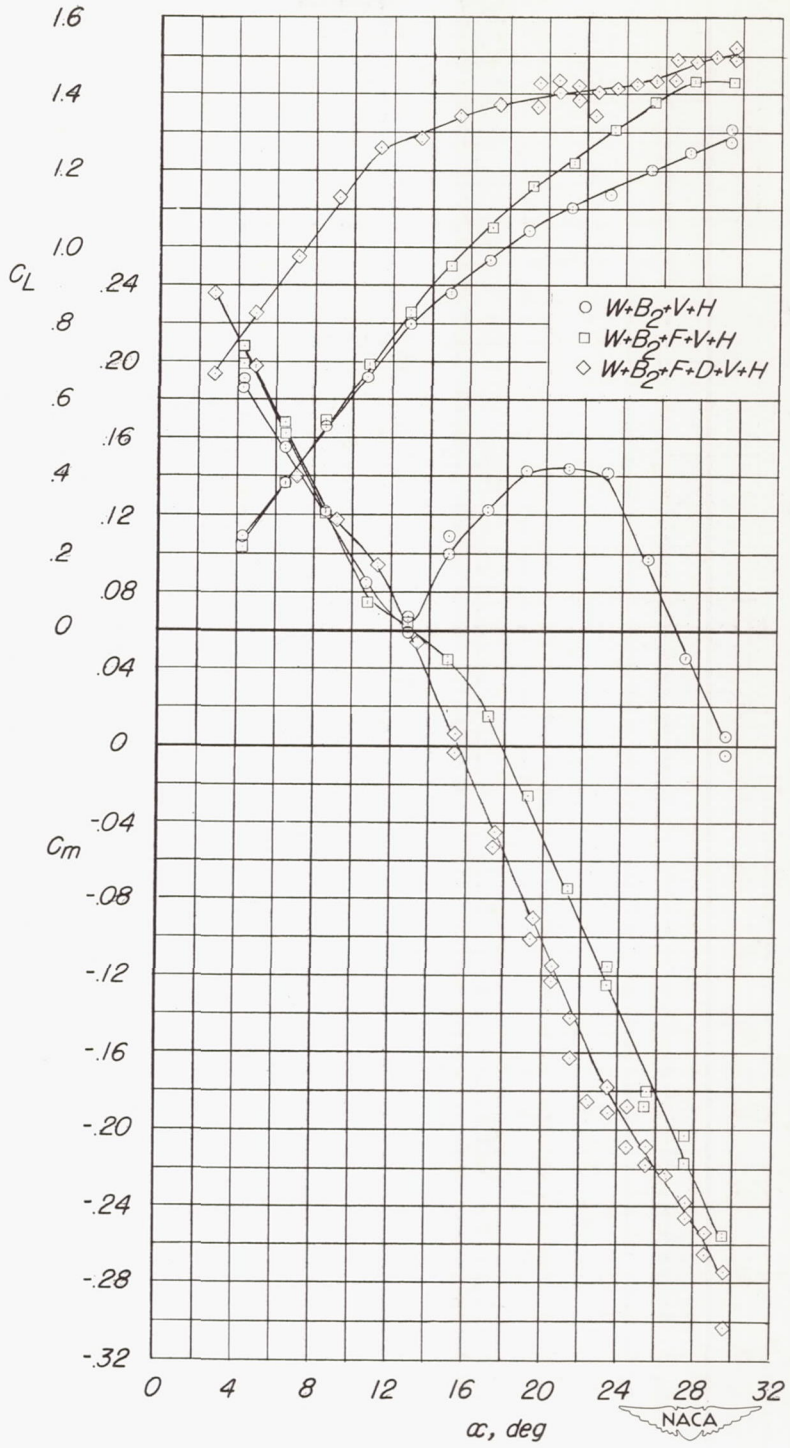

(c) Effect of flaps on the complete model. $l_V/b_W = 0.500$.

Figure 10.- Concluded.

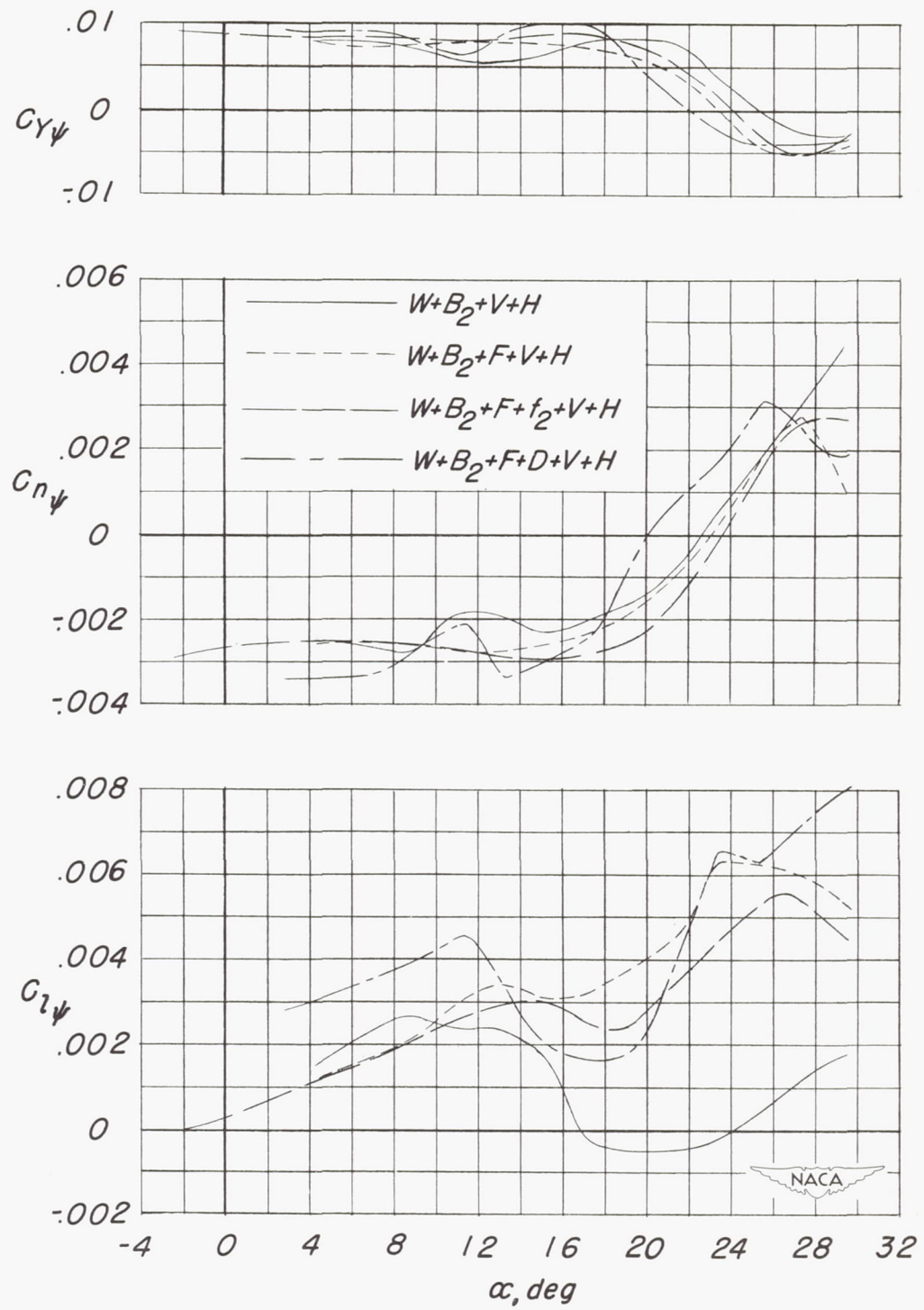

Figure 11.- Variations of C_{Y_ψ}, C_{n_ψ}, and C_{l_ψ} with angle of attack for the complete airplane model configuration with and without flaps and fences. Vertical-tail length is $0.500b_w$; $i_H = -14^\circ$; and $R = 4.45 \times 10^6$.

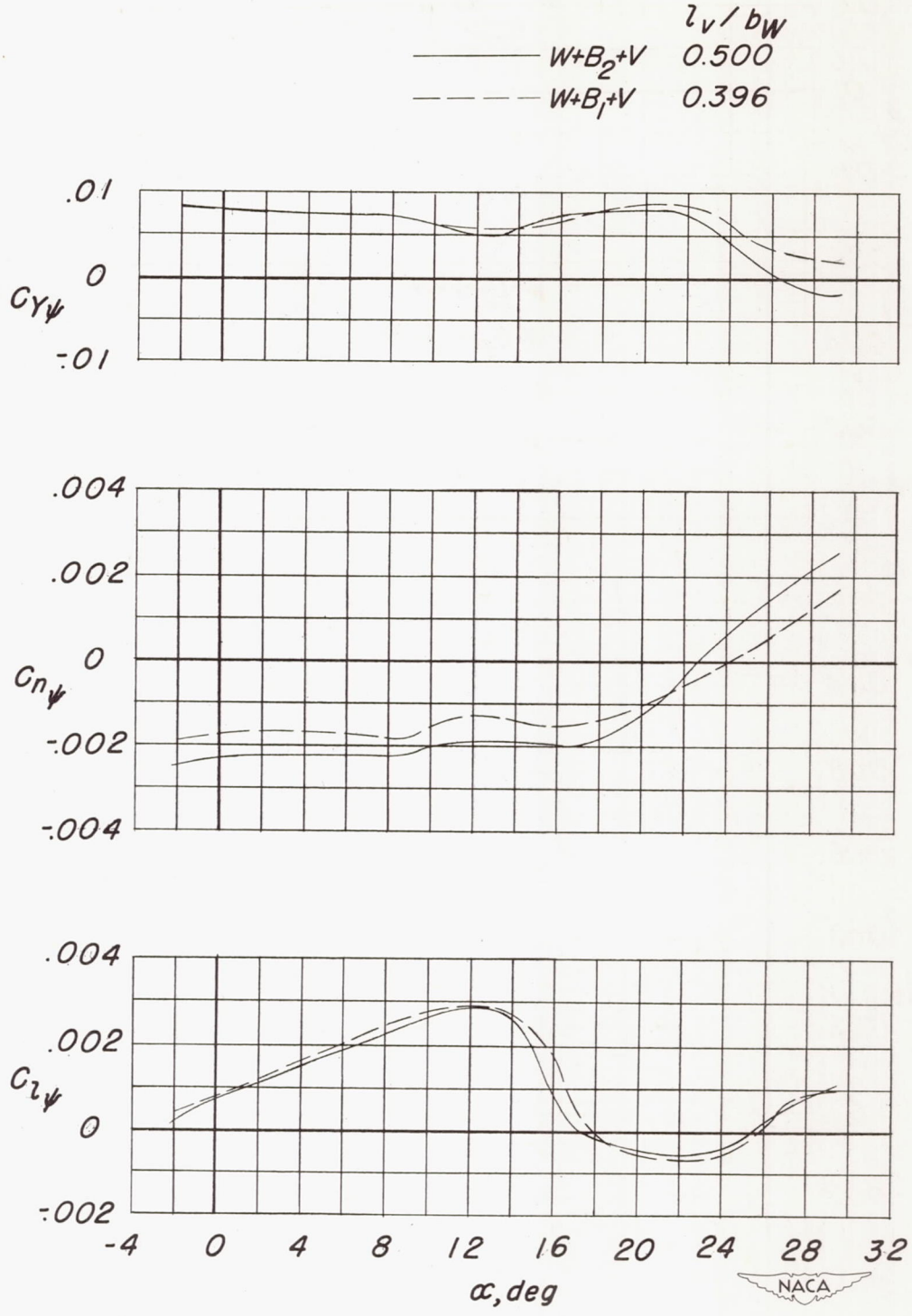

Figure 12.- Effect of vertical-tail length on the variations of C_{Y_ψ}, C_{n_ψ}, and C_{l_ψ} with angle of attack for airplane model configuration without the horizontal tail. $R = 4.45 \times 10^6$.

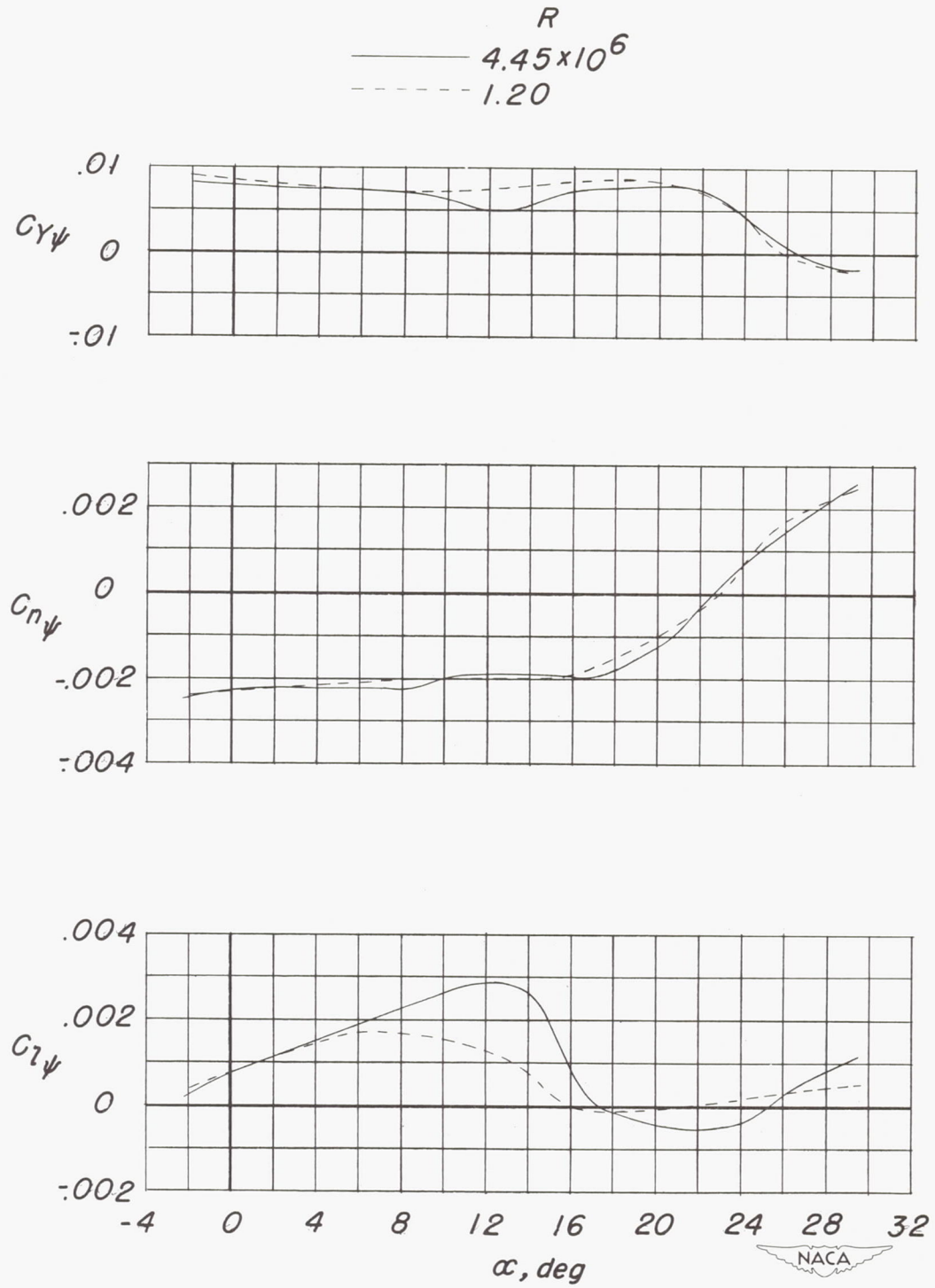

Figure 13.- Scale effects on the variations of C_{Y_ψ}, C_{n_ψ}, and C_{l_ψ} with angle of attack of the airplane model configuration without the horizontal tail. Vertical-tail length is $0.500b_w$ and $R = 4.45 \times 10^6$.

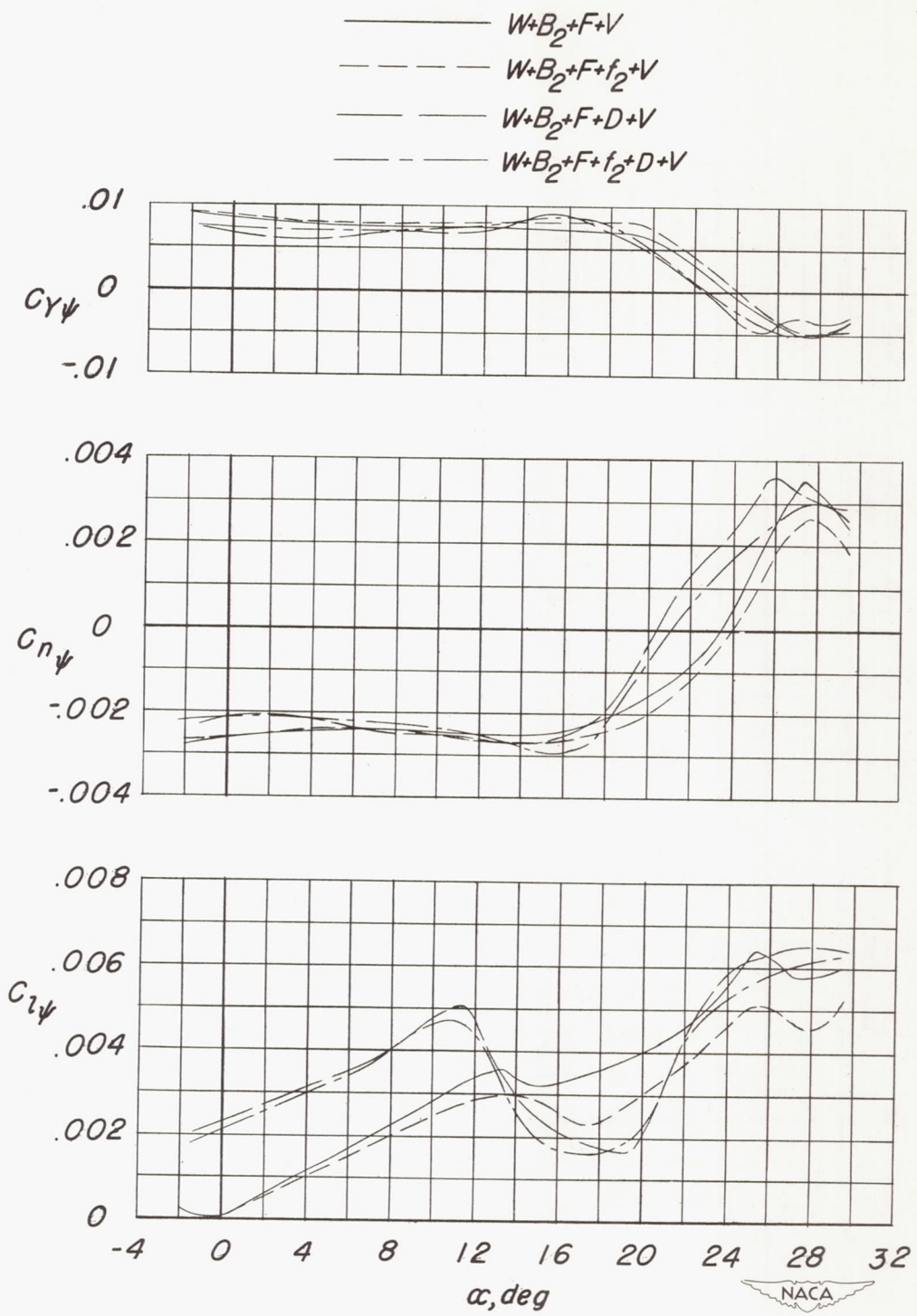

Figure 14.- Effect of fences on the variations of C_{Y_ψ}, C_{n_ψ}, and C_{l_ψ} with angle of attack of the airplane model configuration with leading-edge flaps but without the horizontal tail. Vertical-tail length is $0.500b_w$ and $R = 4.45 \times 10^6$.

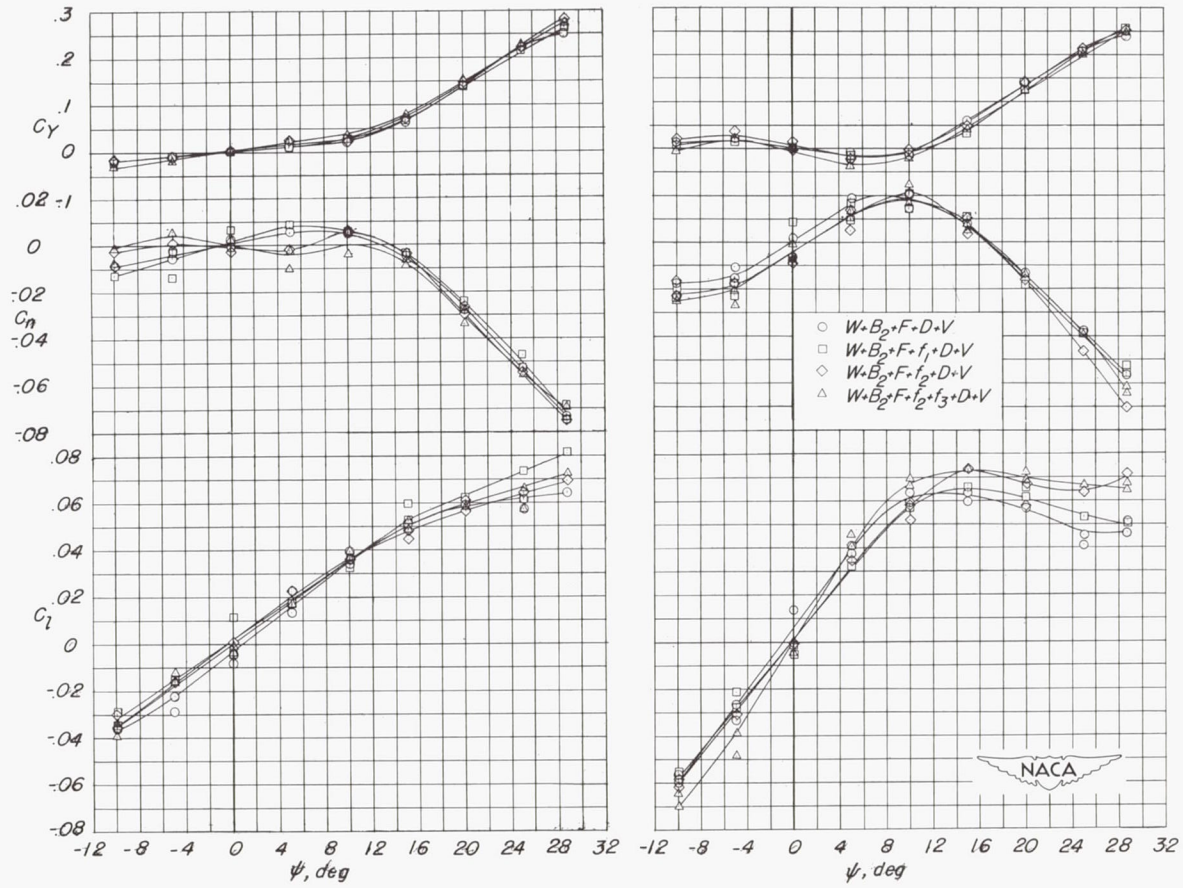

(a) $\alpha \approx 21.5^\circ$.

(b) $\alpha \approx 27.5^\circ$.

Figure 15.- Fence spanwise position effect on the yaw characteristics for the airplane model configuration with leading edge and double slotted flaps but without the horizontal tail. Vertical-tail length is $0.500b_W$ and $R = 4.45 \times 10^6$.

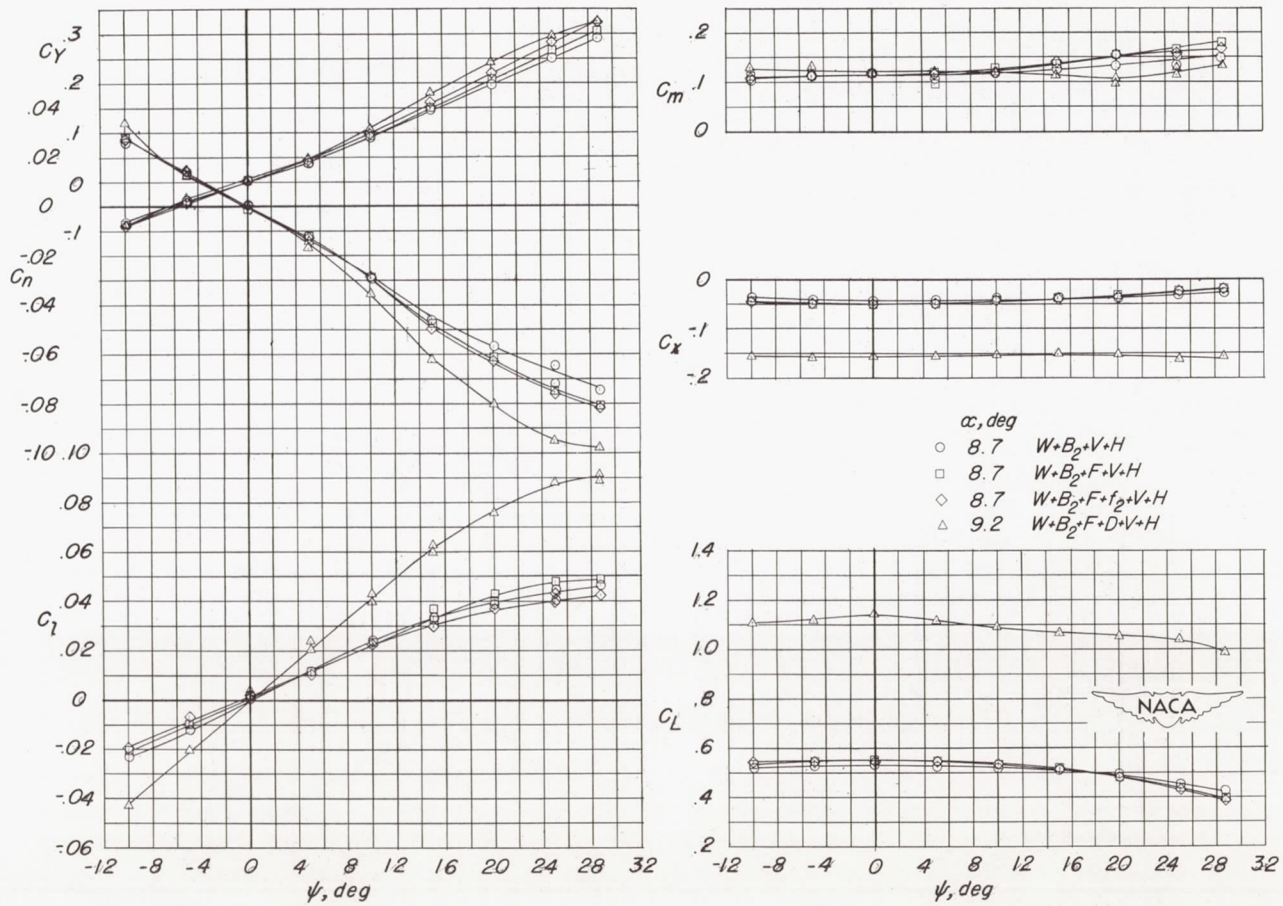

(a) $\alpha \approx 9^\circ$.

Figure 16.- Aerodynamic characteristics in yaw for the complete airplane model configuration with and without flaps and fences. Vertical-tail length is $0.500b_w$; $i_H = -14^\circ$; and $R = 4.45 \times 10^6$.

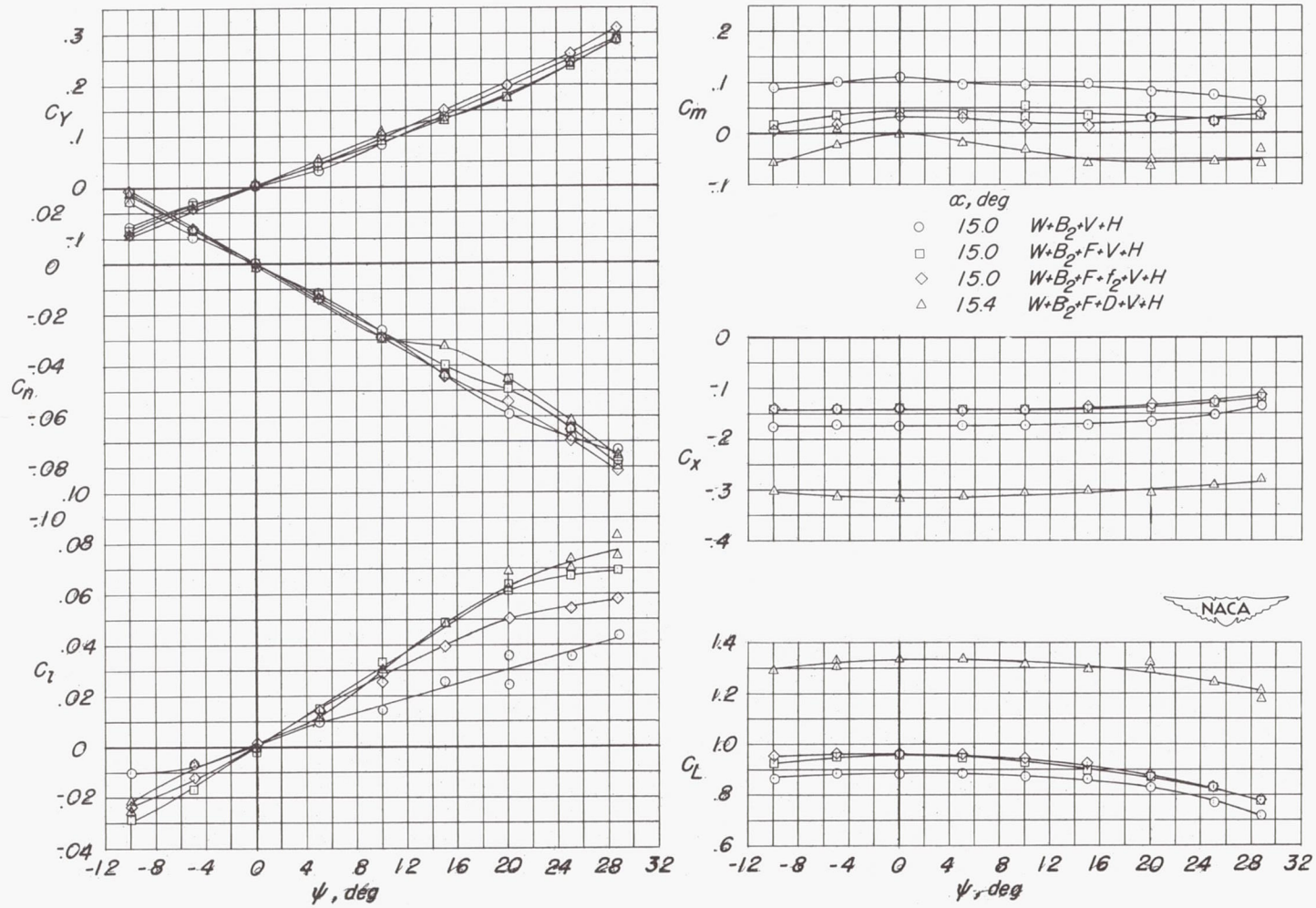

(b) $\alpha \approx 15^\circ$.

Figure 16.- Continued.

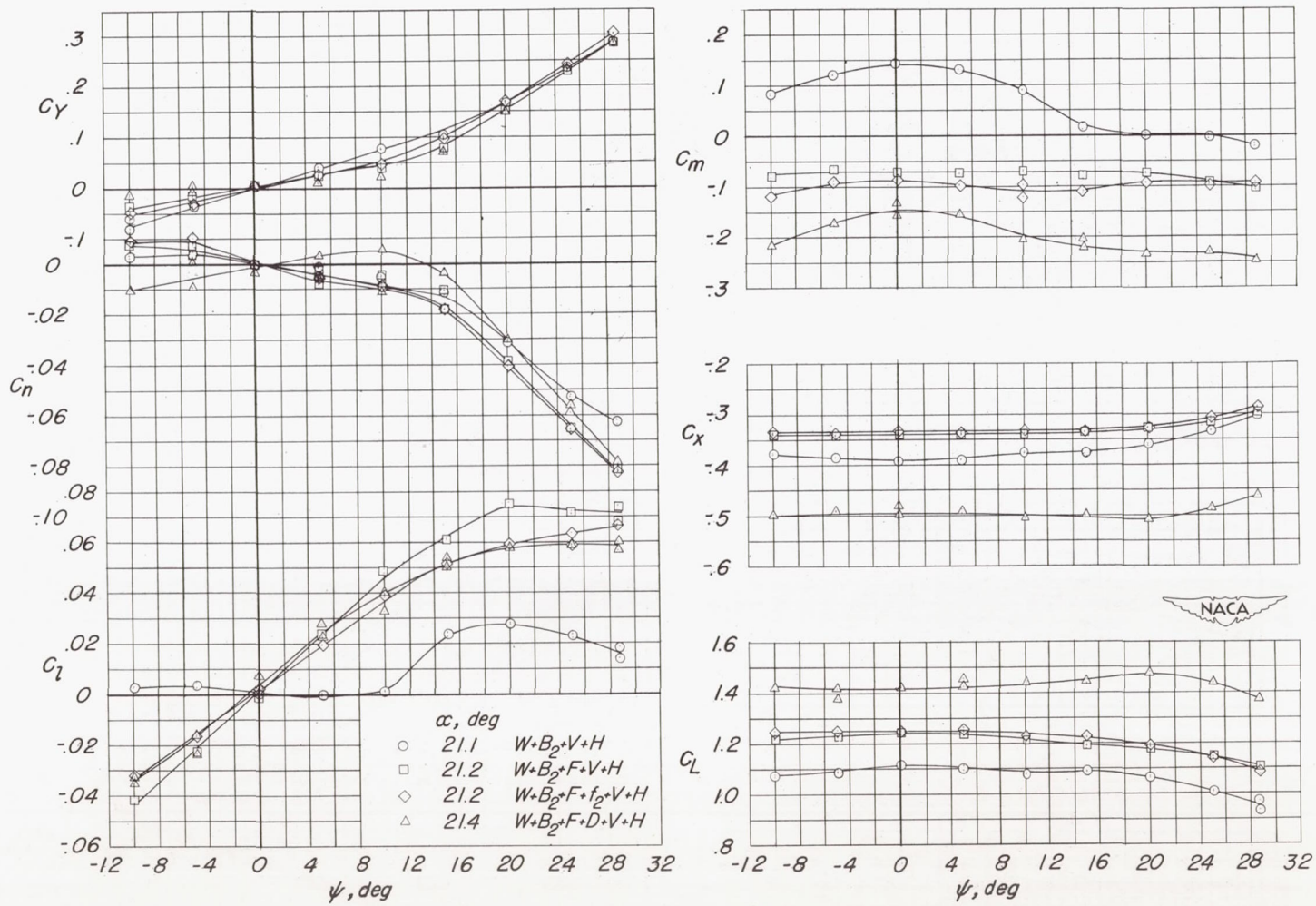

(c) $\alpha \approx 21^\circ$.

Figure 16.- Continued.

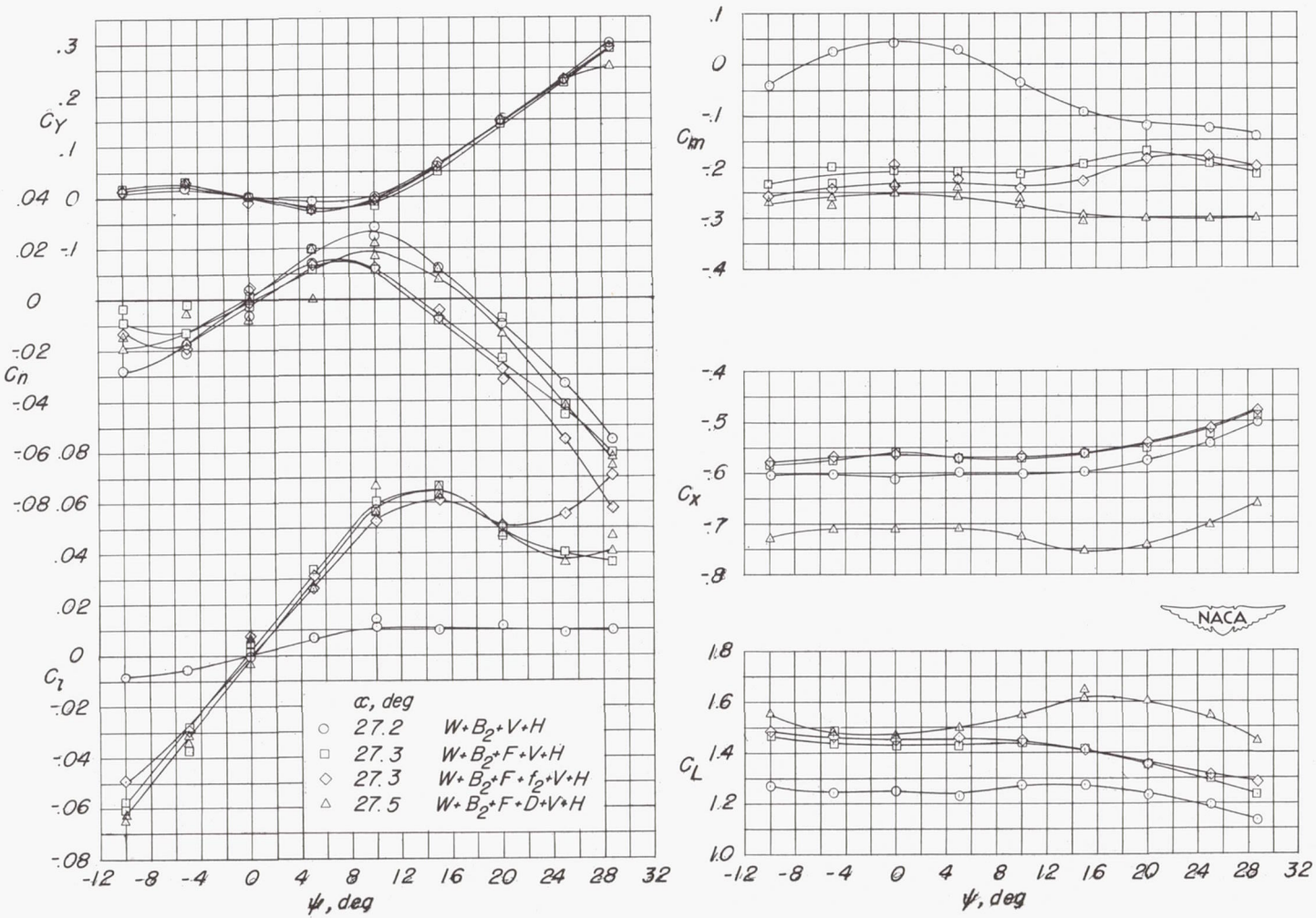

(d) $\alpha \approx 27^\circ$.

Figure 16.- Concluded.

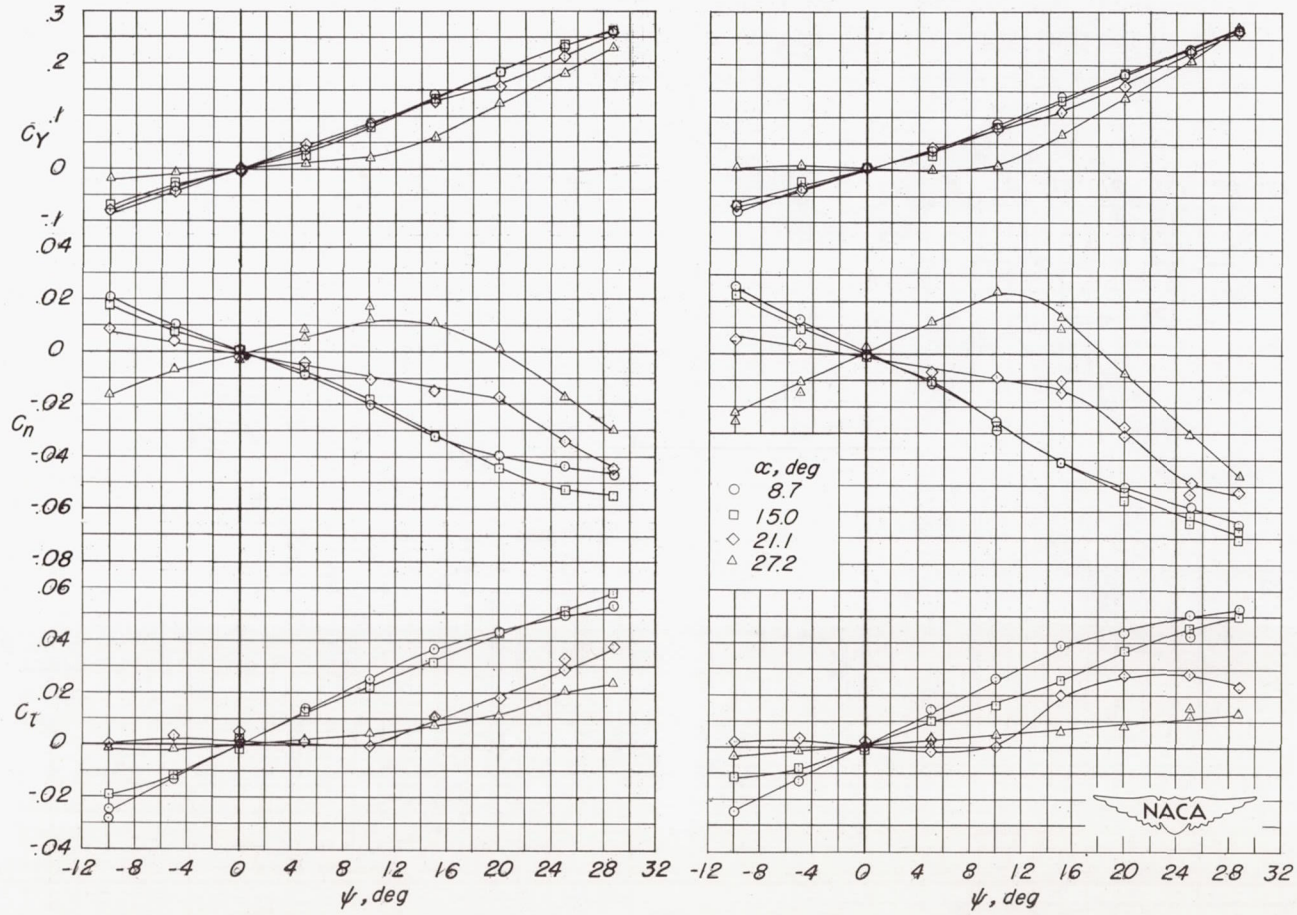

(a) $l_V/b_W = 0.396$.

(b) $l_V/b_W = 0.500$.

Figure 17.- Effect of tail length on the yaw characteristics for the airplane model configuration without the horizontal tail. $R = 4.45 \times 10^6$.

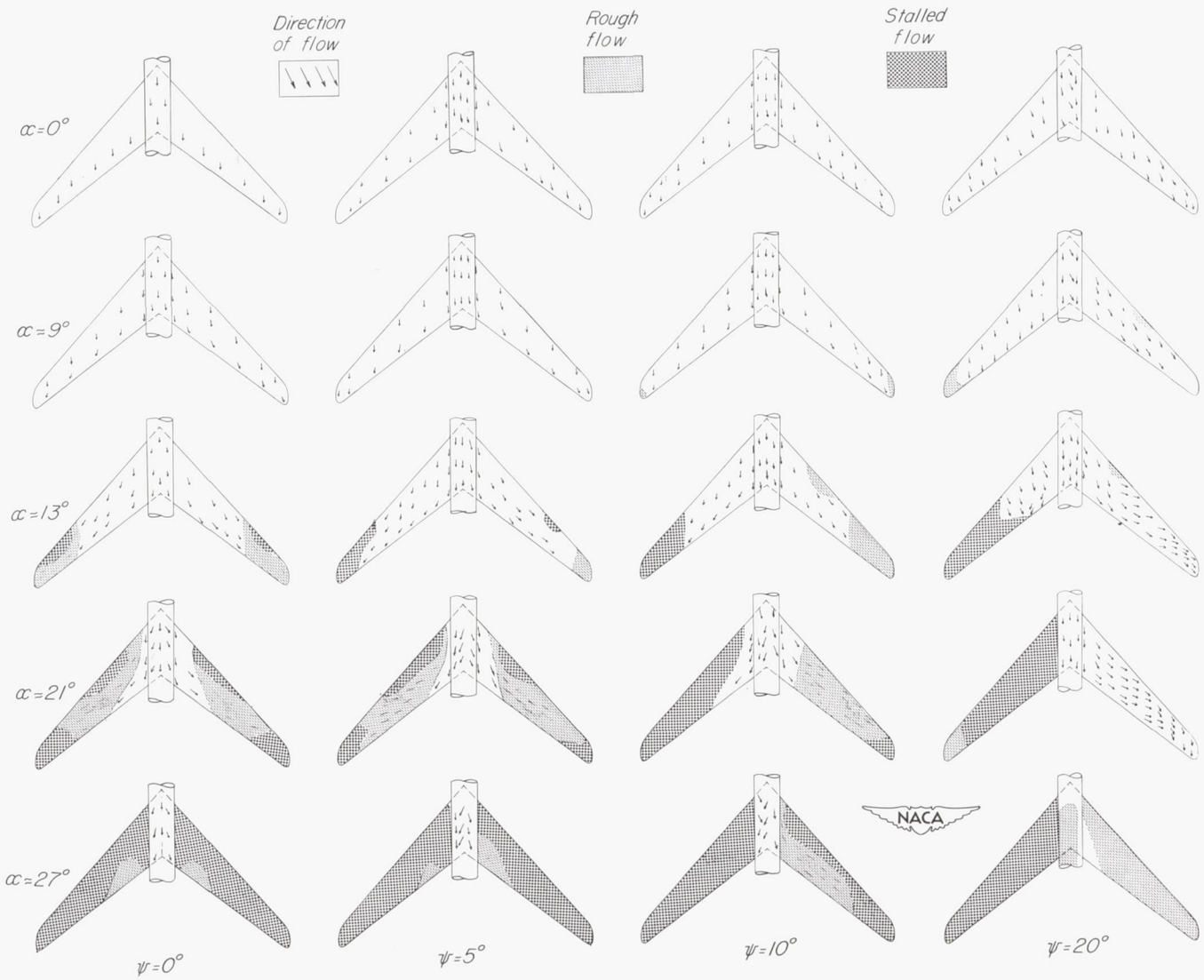

Figure 18.- Observed stalling characteristics of the wing indicated by wool tufts located on the upper surfaces of the unflapped airplane model. $R = 4.45 \times 10^6$.

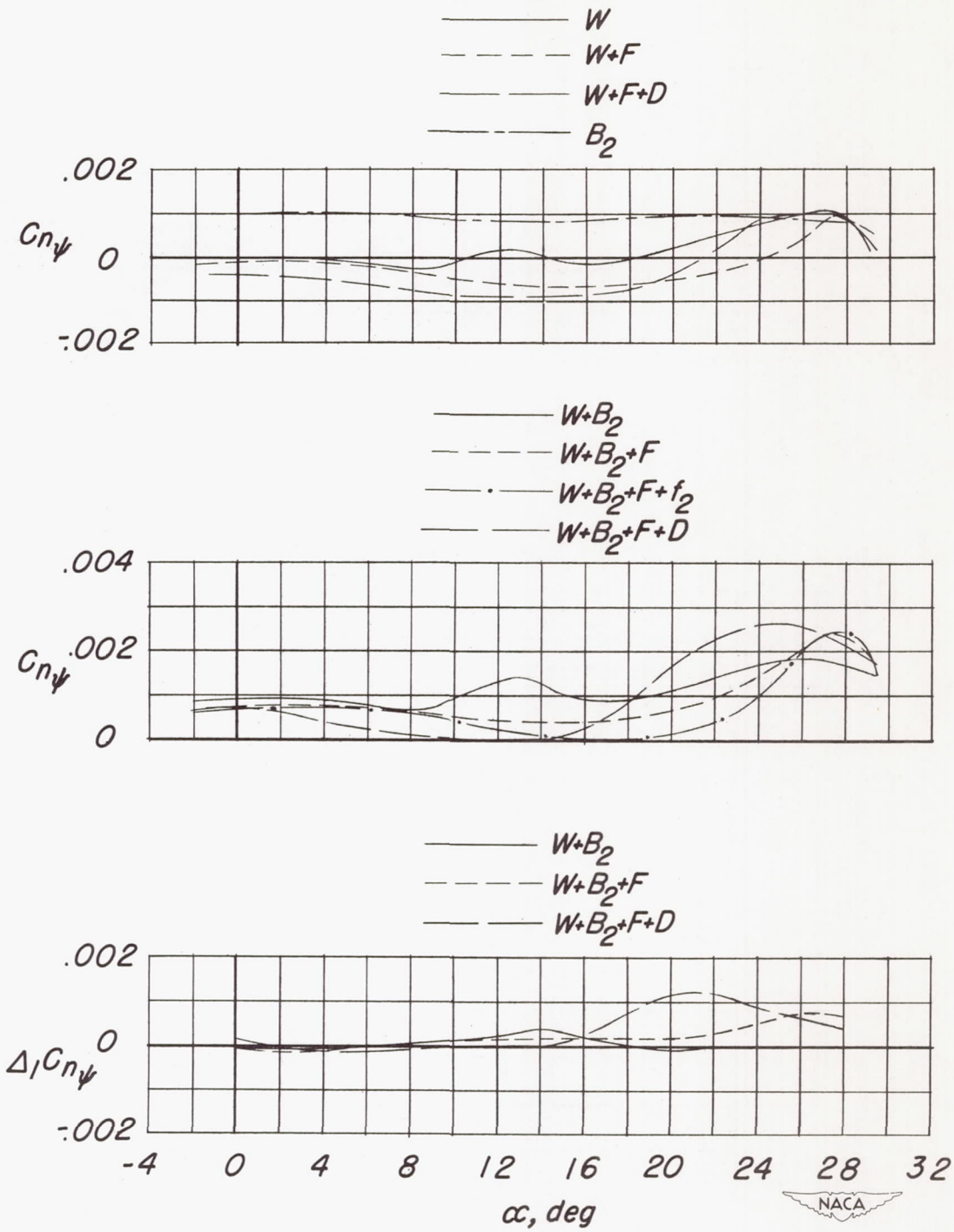

(a) C_{n_ψ} and $\Delta_1 C_{n_\psi}$ against α.

Figure 19.- Variations with angle of attack of the directional-stability and lateral-force parameters for the wing, fuselage, and wing-fuselage combination and the increments caused by the wing-fuselage interference. $R = 4.45 \times 10^6$.

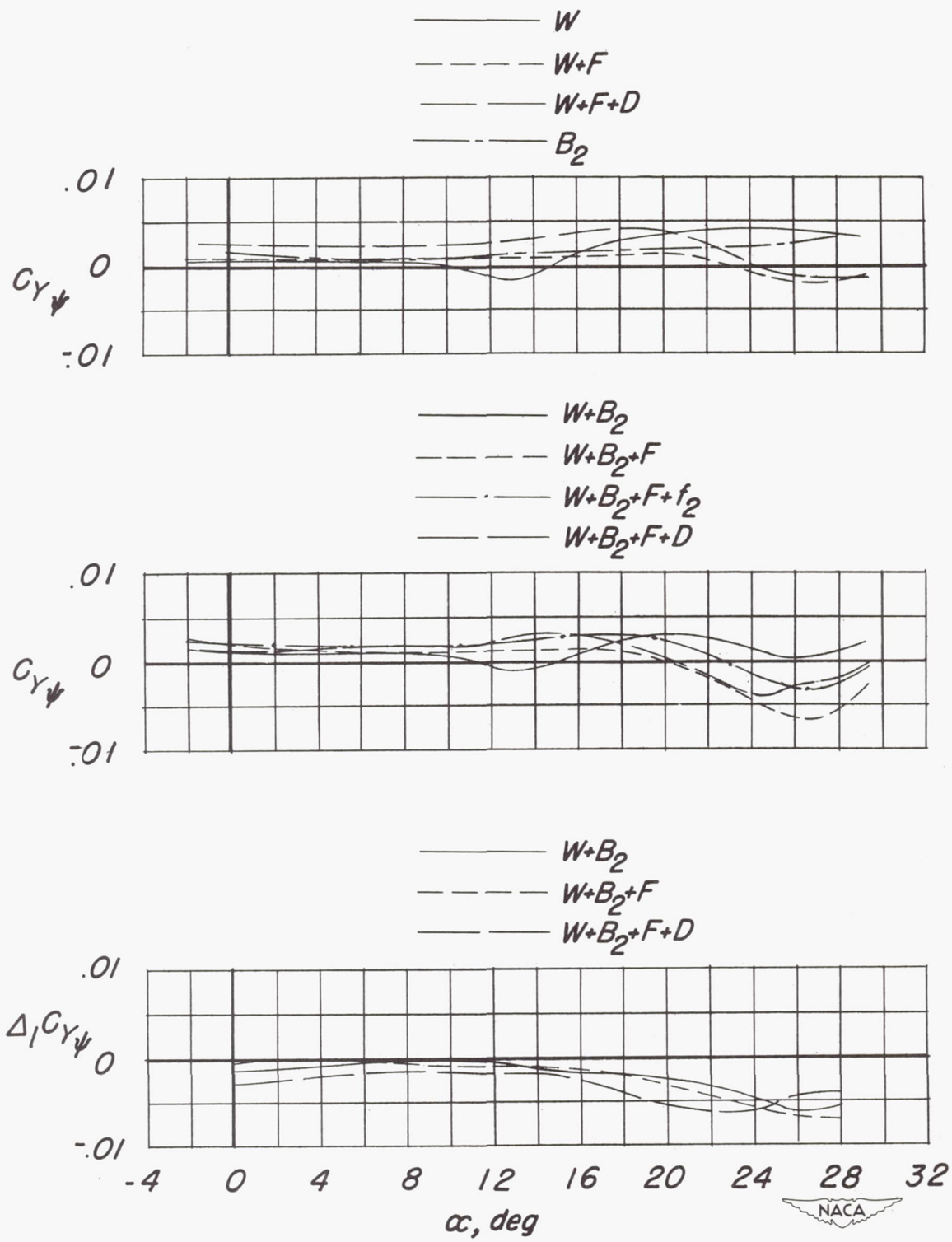

(b) C_{Y_ψ} and $\Delta_1 C_{Y_\psi}$ against α.

Figure 19.- Concluded.

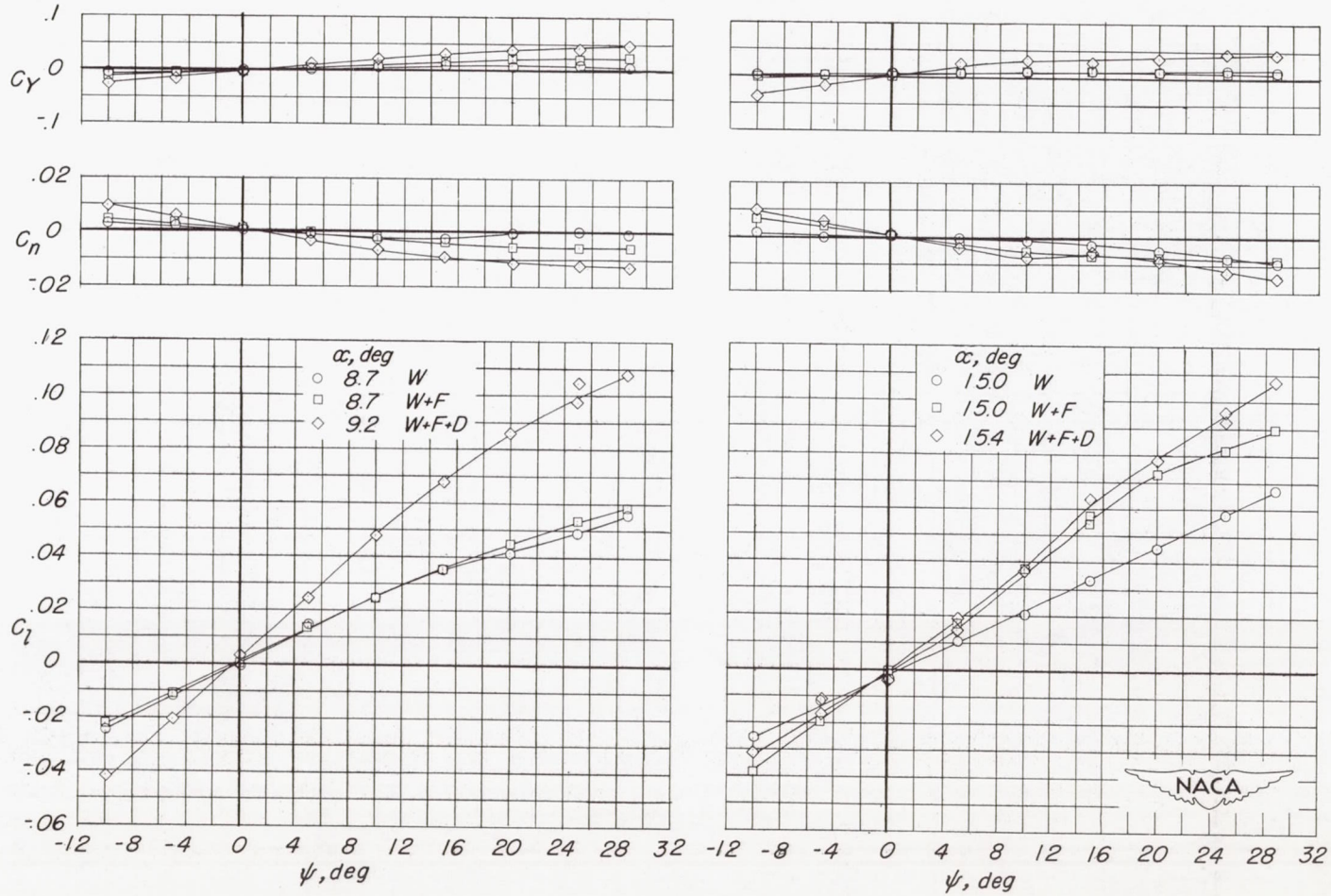

(a) $\alpha \approx 9^\circ$.

(b) $\alpha \approx 15^\circ$.

Figure 20.- Effect of flaps on the yaw characteristics for the wing.
$R = 4.45 \times 10^6$.

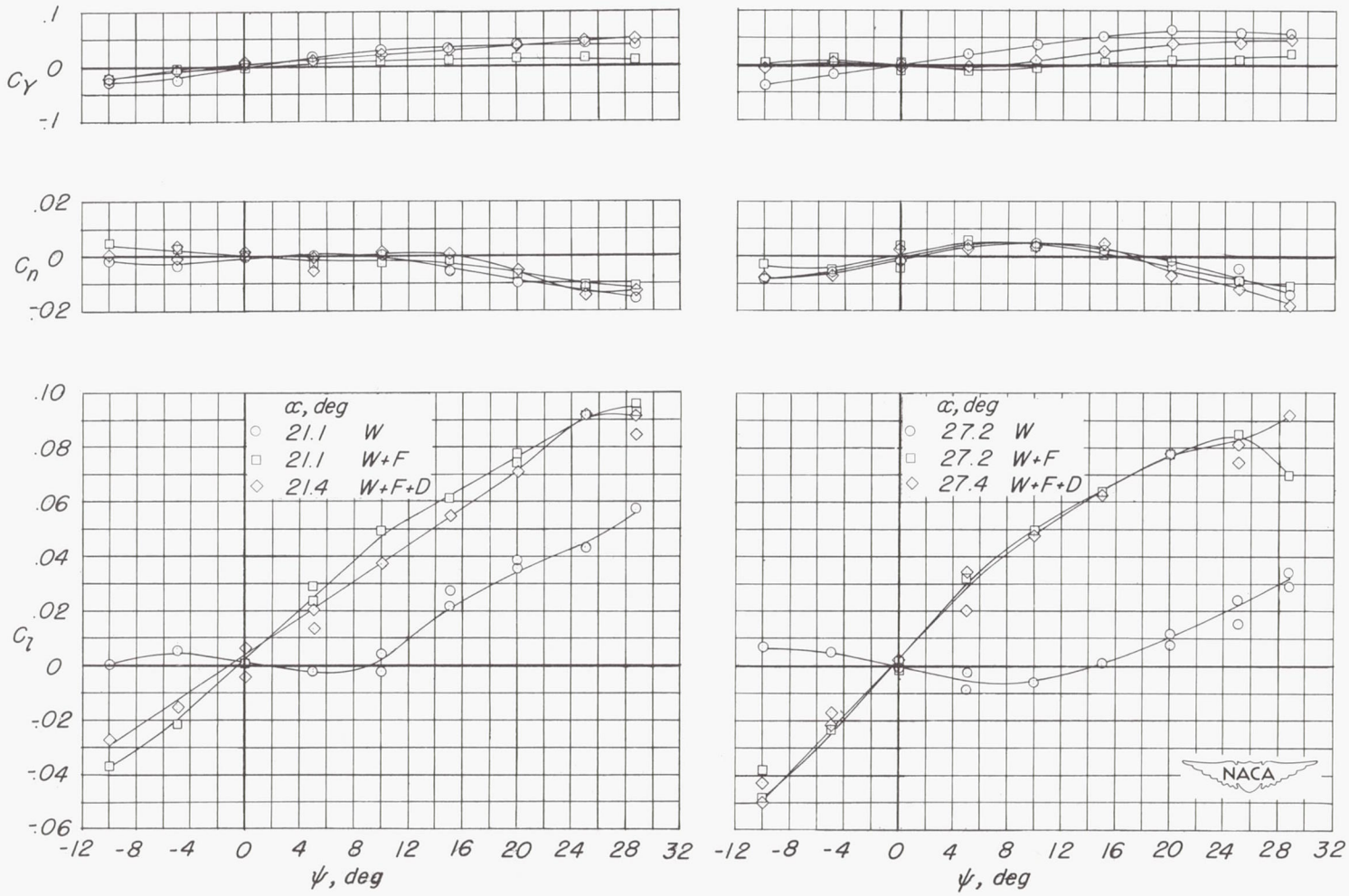

(c) $\alpha \approx 21^\circ$.

(d) $\alpha \approx 27^\circ$.

Figure 20.- Concluded.

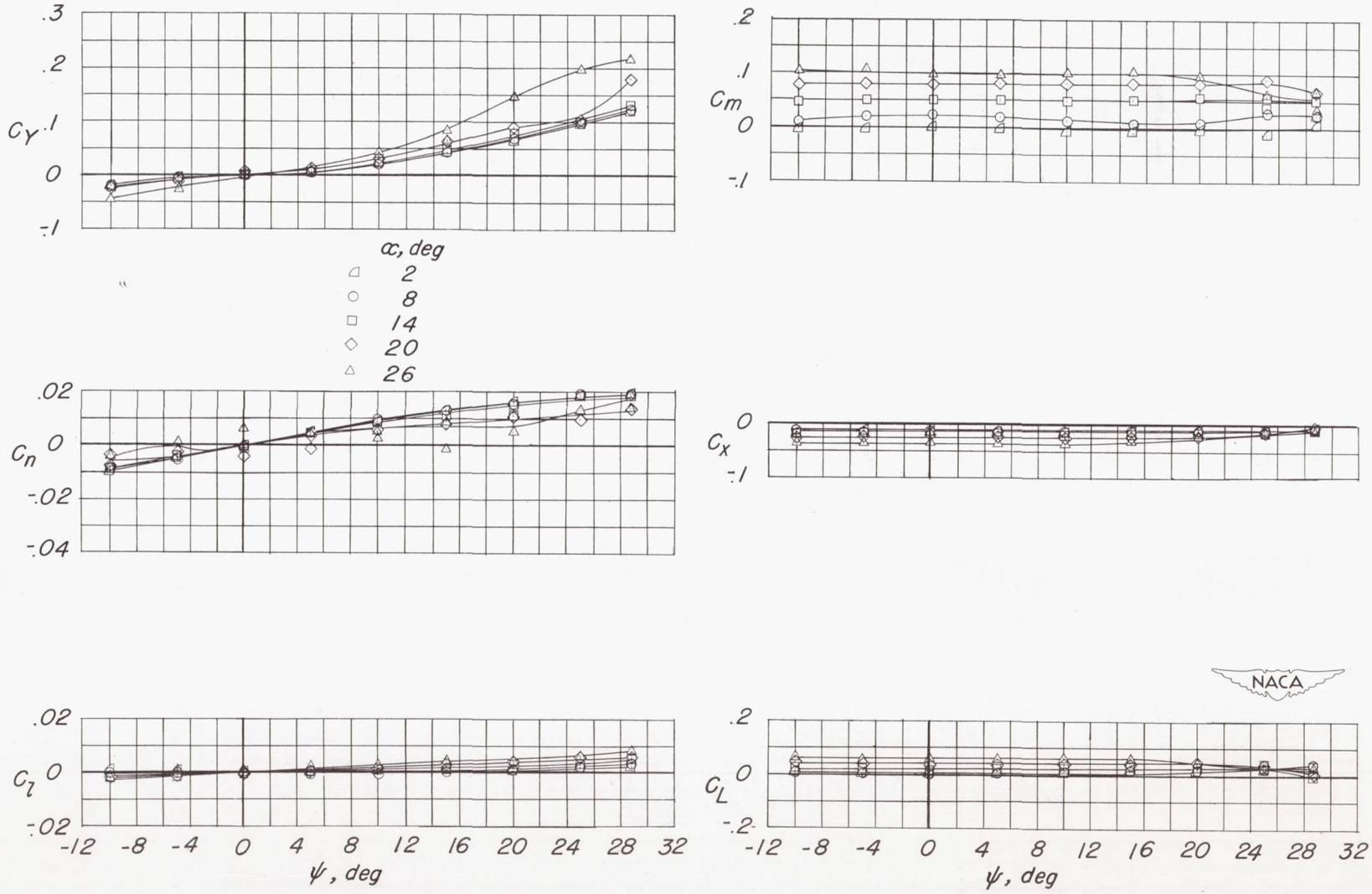

Figure 21.- Aerodynamic characteristics in yaw for the fuselage B_2.
$R = 4.45 \times 10^6$ (based on wing mean aerodynamic chord).

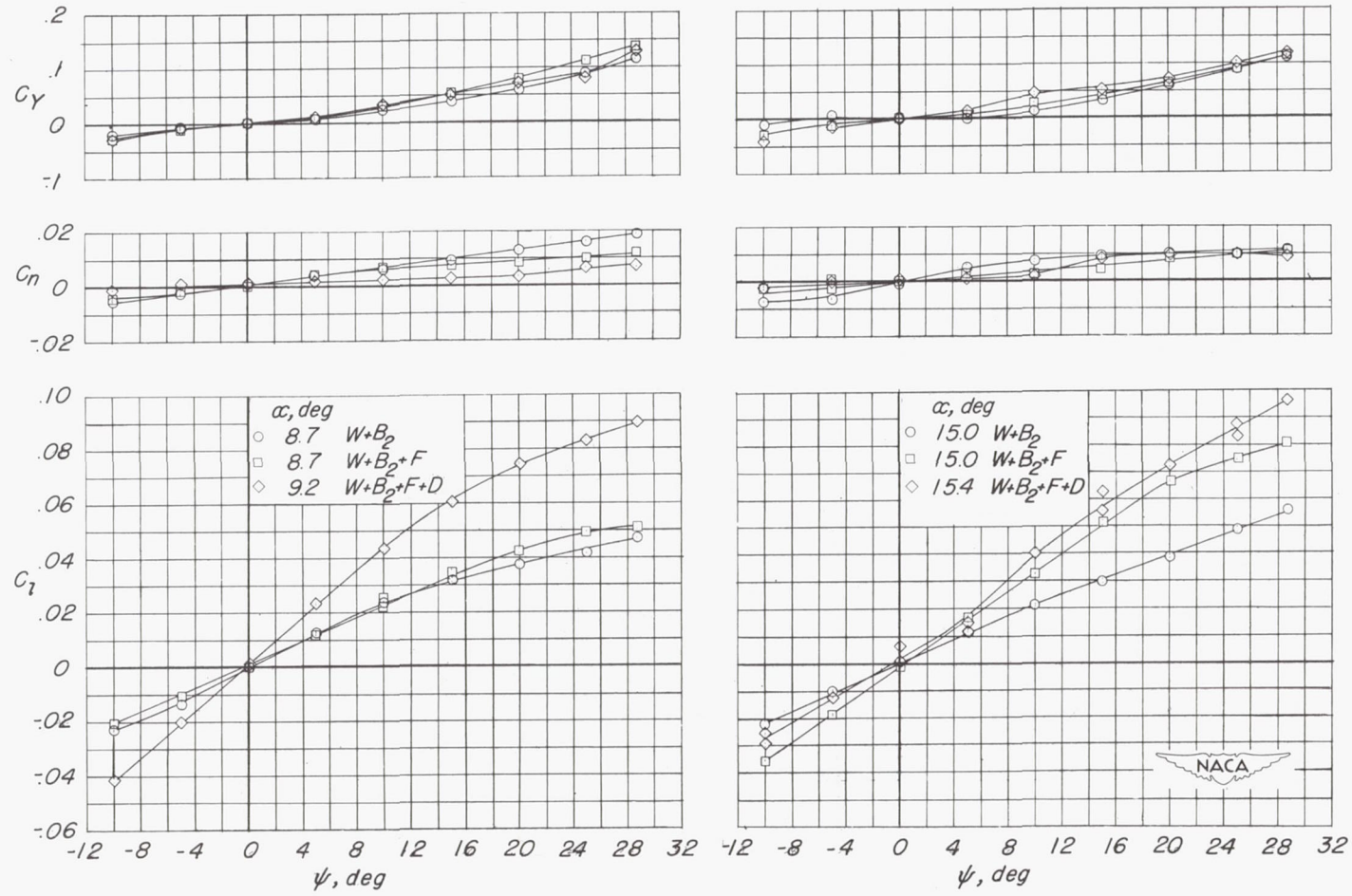

(a) $\alpha \approx 9^\circ$.

(b) $\alpha \approx 15^\circ$.

Figure 22.- Effect of flaps on the yaw characteristics for the wing-fuselage configuration. $R = 4.45 \times 10^6$.

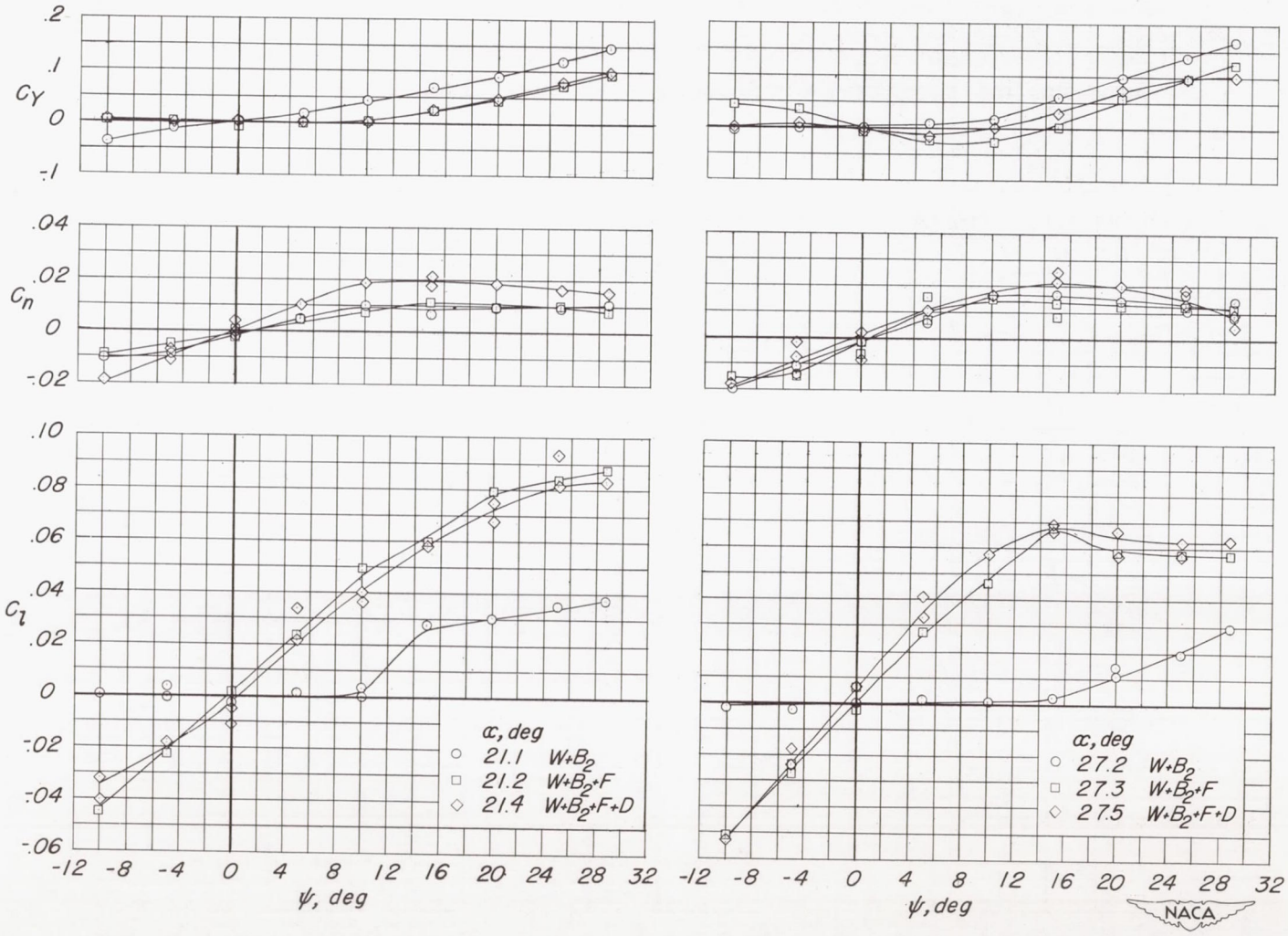

(c) $\alpha \approx 21^\circ$.

(d) $\alpha \approx 27^\circ$.

Figure 22.- Concluded.

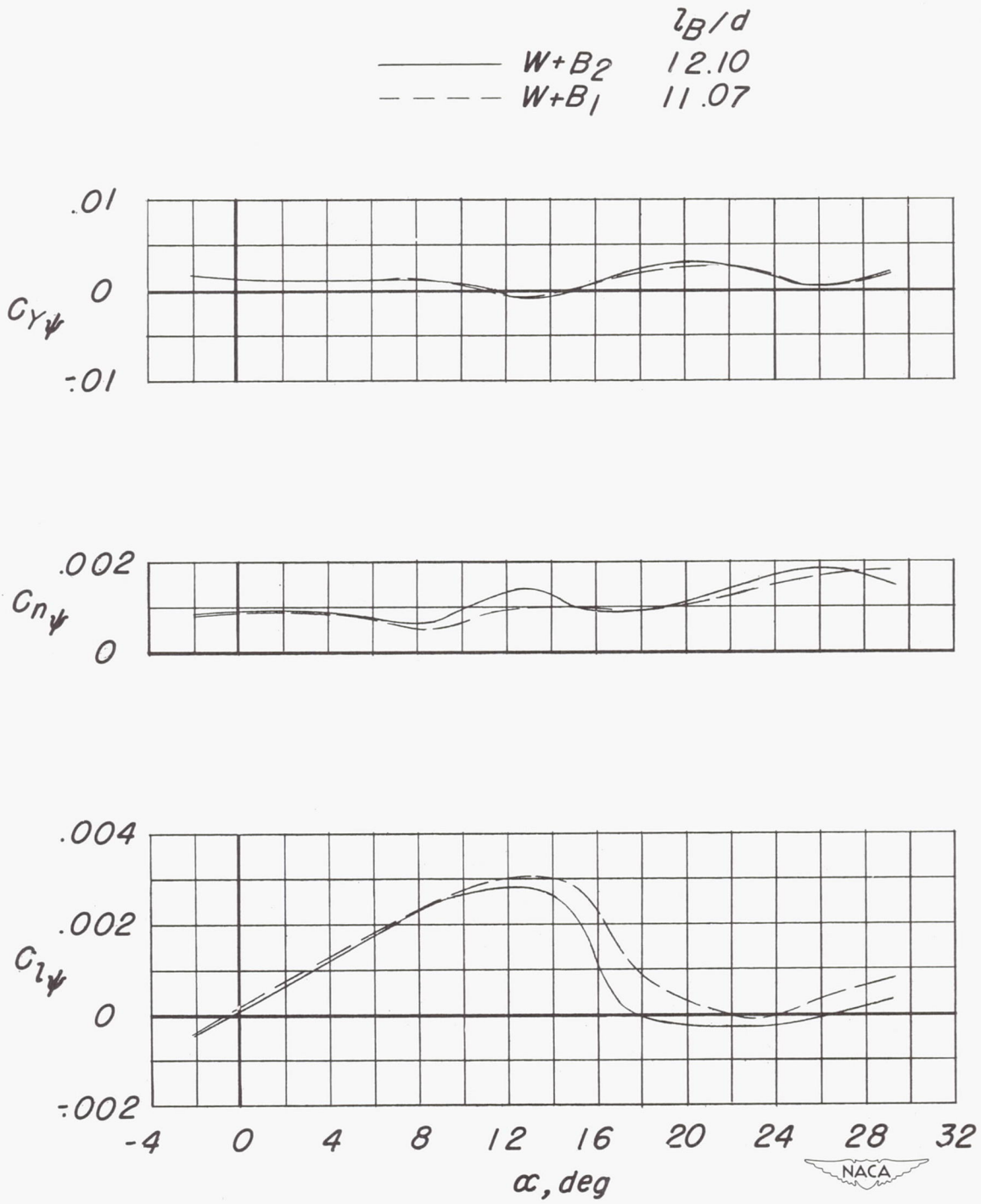

Figure 23.- Effect of fuselage length on the variations of C_{Y_ψ}, C_{n_ψ}, and C_{l_ψ} with angle of attack of the wing-fuselage configuration. $R = 4.45 \times 10^6$.

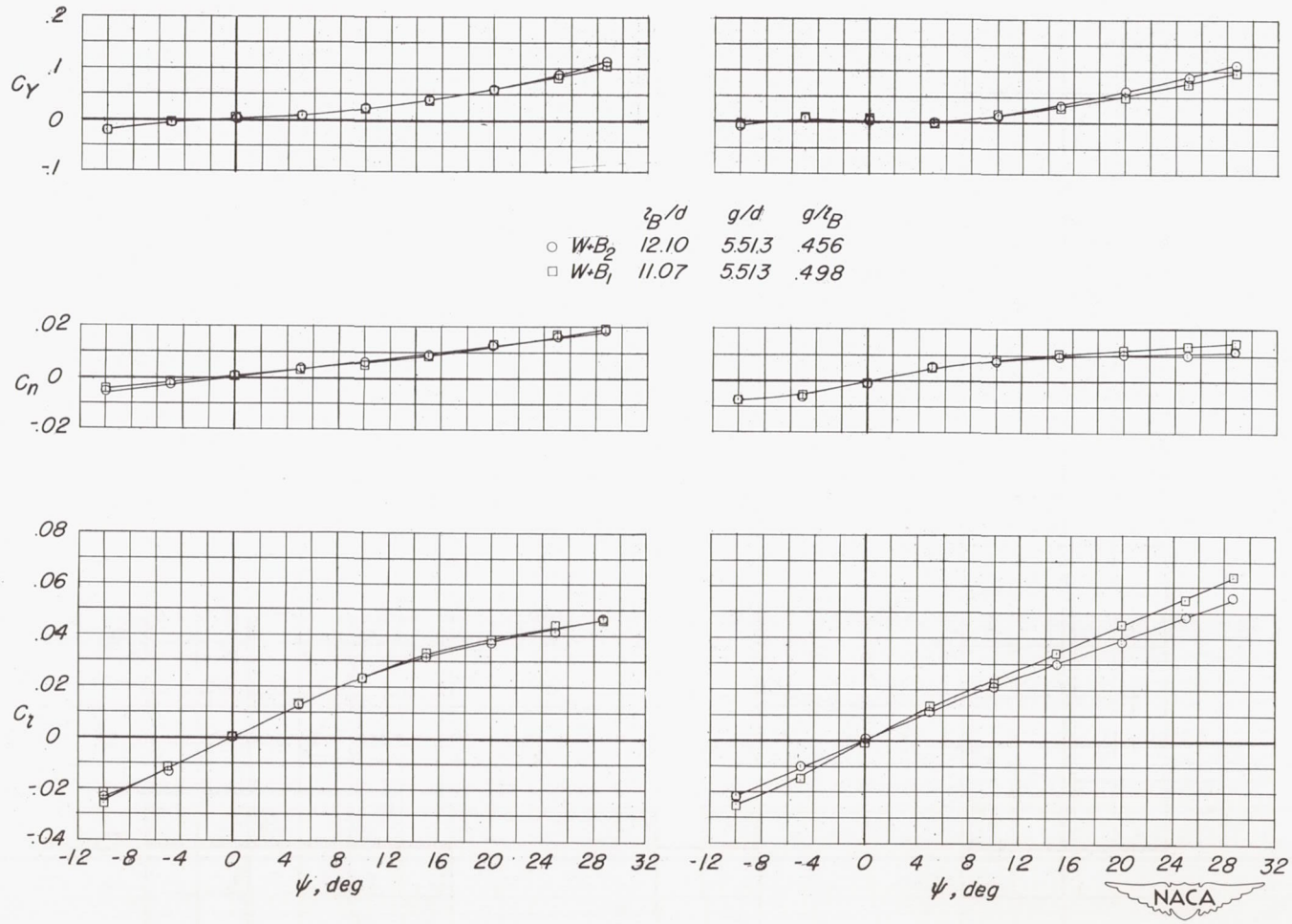

(a) $\alpha \approx 8.7^\circ$.

(b) $\alpha \approx 15.0^\circ$.

Figure 24.- Effect of fuselage length on the yaw characteristics for the wing-fuselage configuration. $R = 4.45 \times 10^6$.

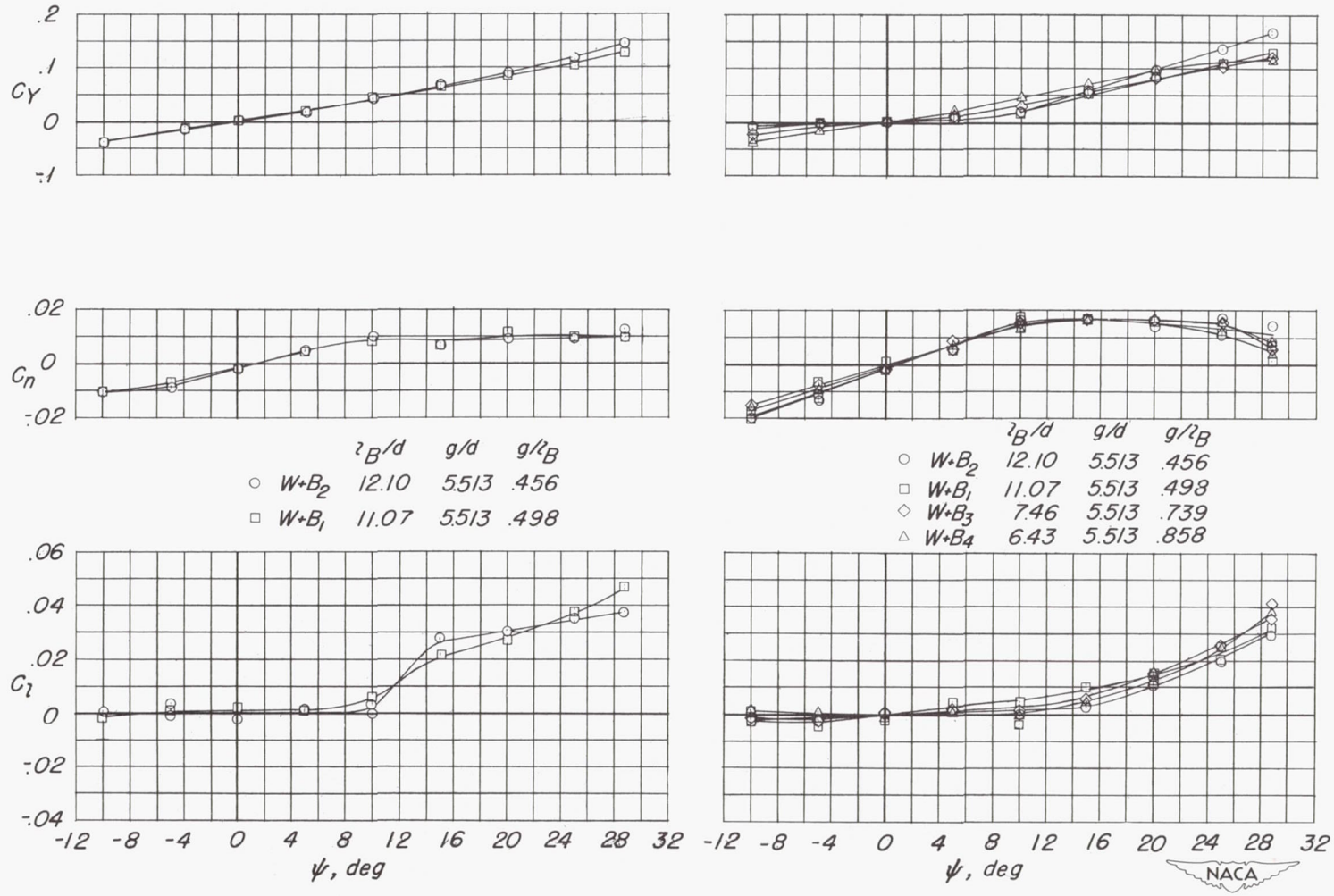

(c) $\alpha \approx 21.1^\circ$.

(d) $\alpha \approx 27.2^\circ$.

Figure 24.- Concluded.

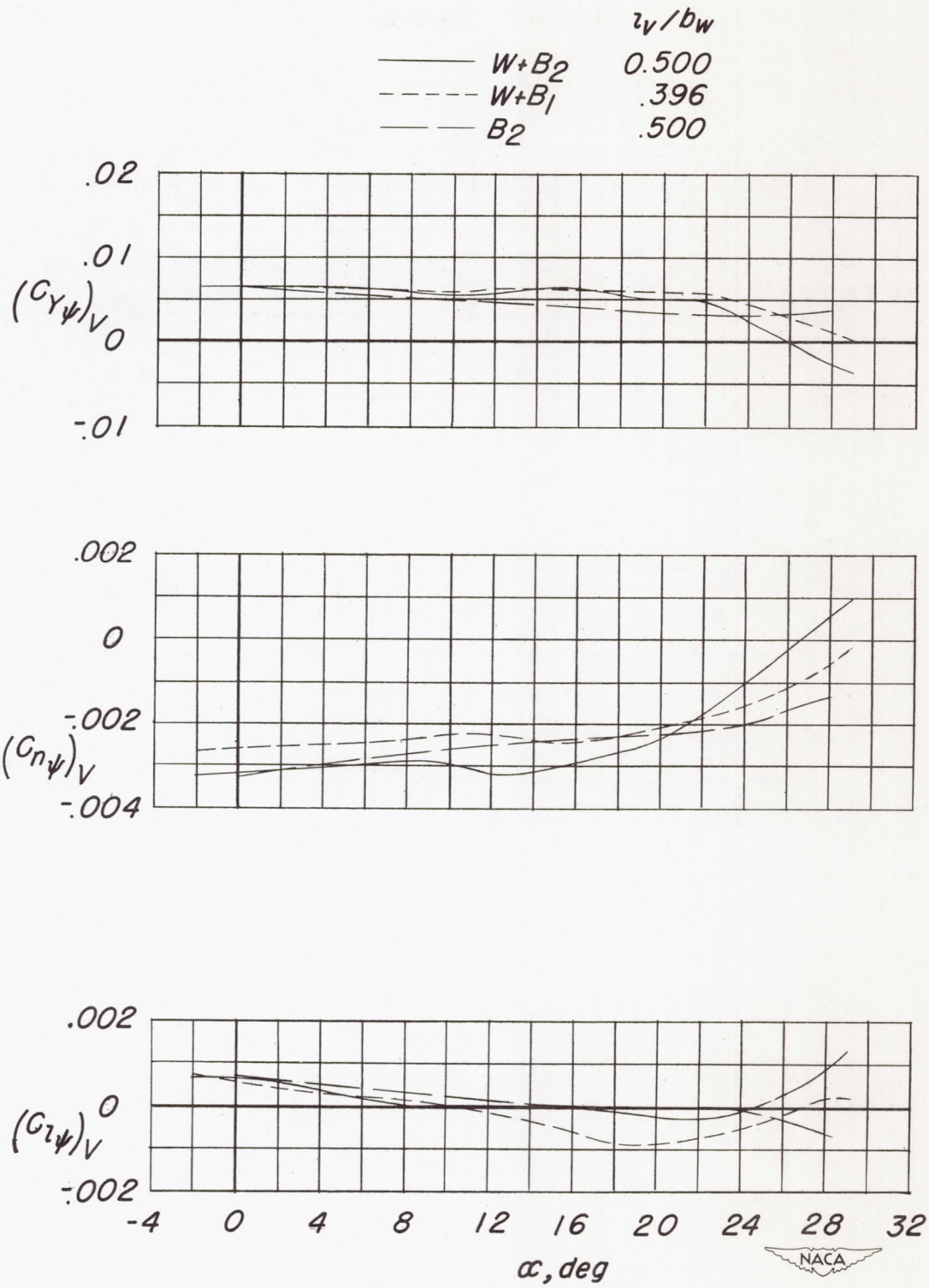

Figure 25.- The incremental contribution of the vertical tail to the static-lateral-stability derivatives of the fuselage and to the wing-fuselage configuration. $R = 4.45 \times 10^6$.

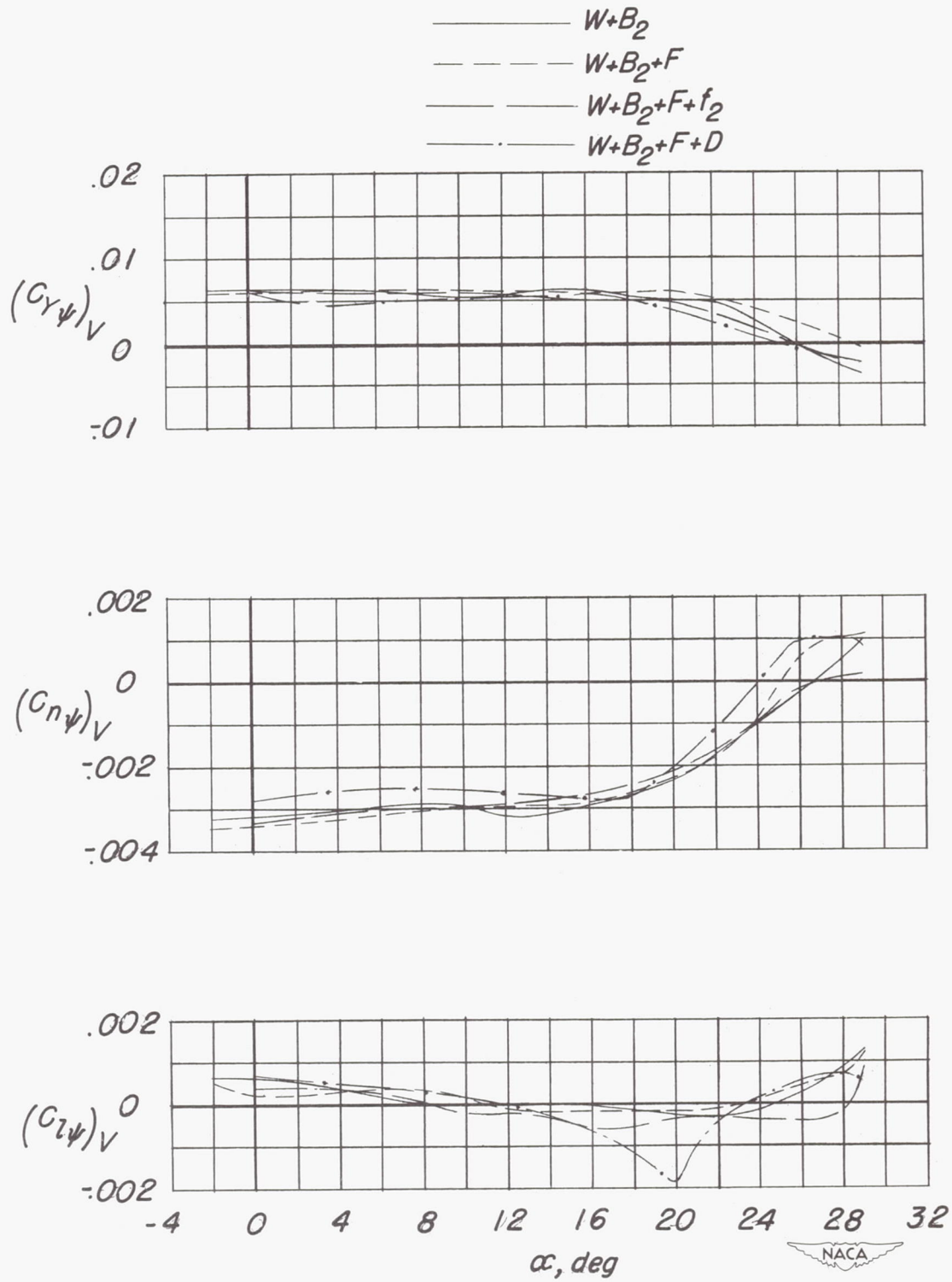

Figure 26.- The incremental contribution of the vertical tail to the static-lateral-stability derivatives of the wing-fuselage configuration with and without flaps and fence. $R = 4.45 \times 10^6$ and $l_V/b_W = 0.500$.

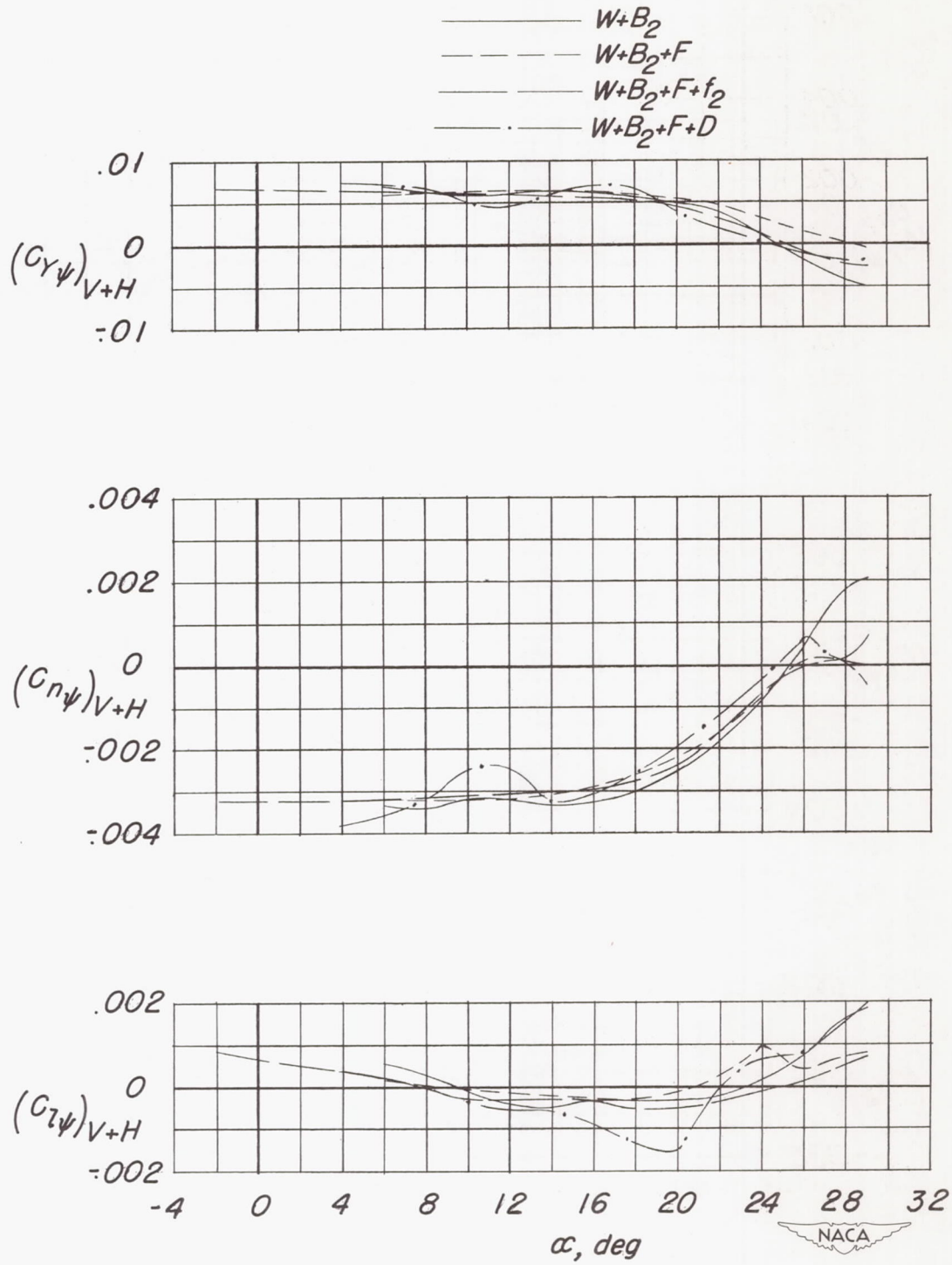

Figure 27.- The incremental contribution of the vertical and horizontal tail to the static-lateral-stability derivatives of the wing-fuselage configuration with and without flaps and fences. Vertical-tail length is $0.500b_W$, $i_H = -14^\circ$; and $R = 4.45 \times 10^6$.

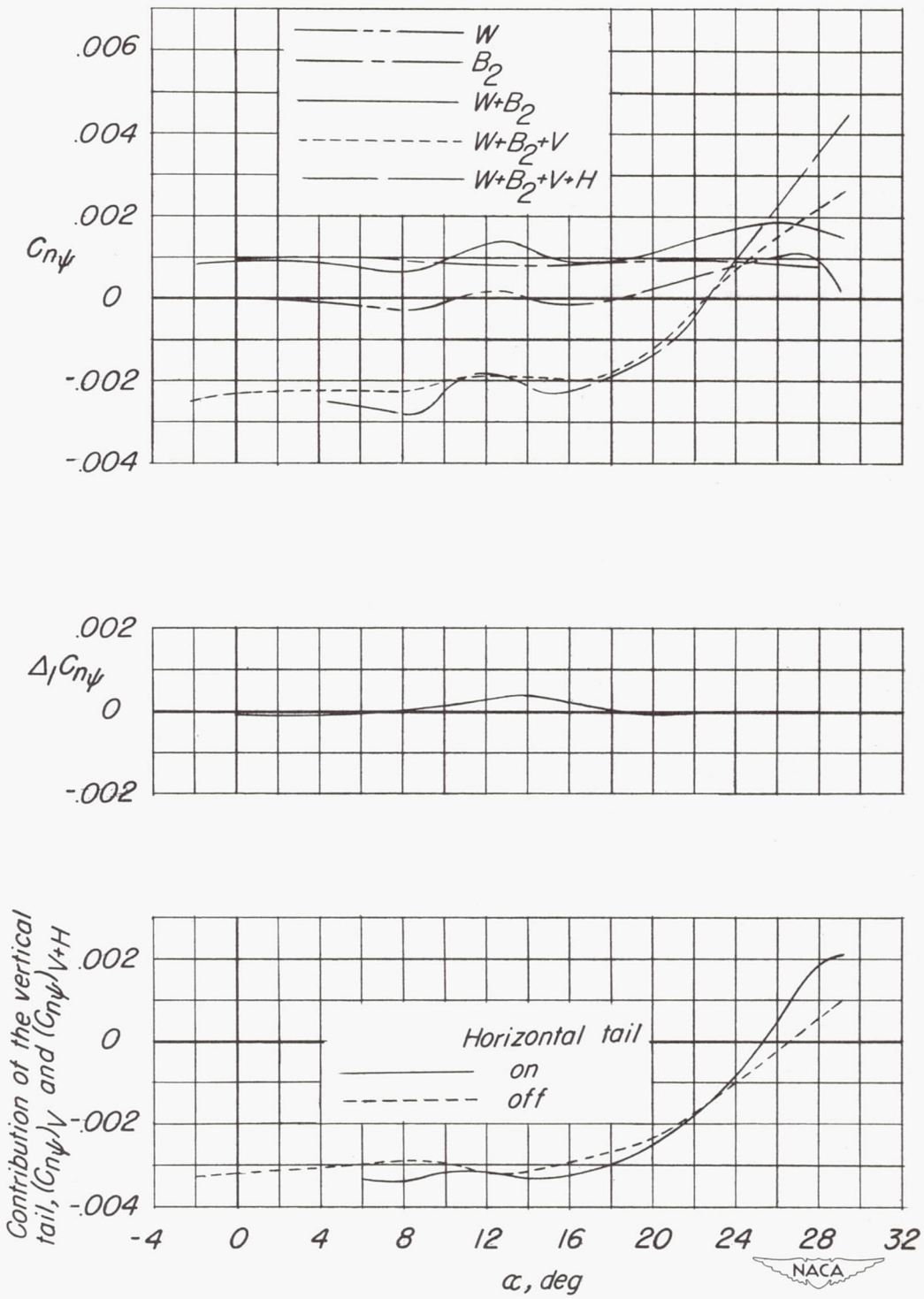

(a) Directional stability.

Figure 28.- Summary of the contributions of the main model components to the directional stability and lateral force of the airplane model. Vertical-tail length is $0.500b_W$ and $R = 4.45 \times 10^6$.

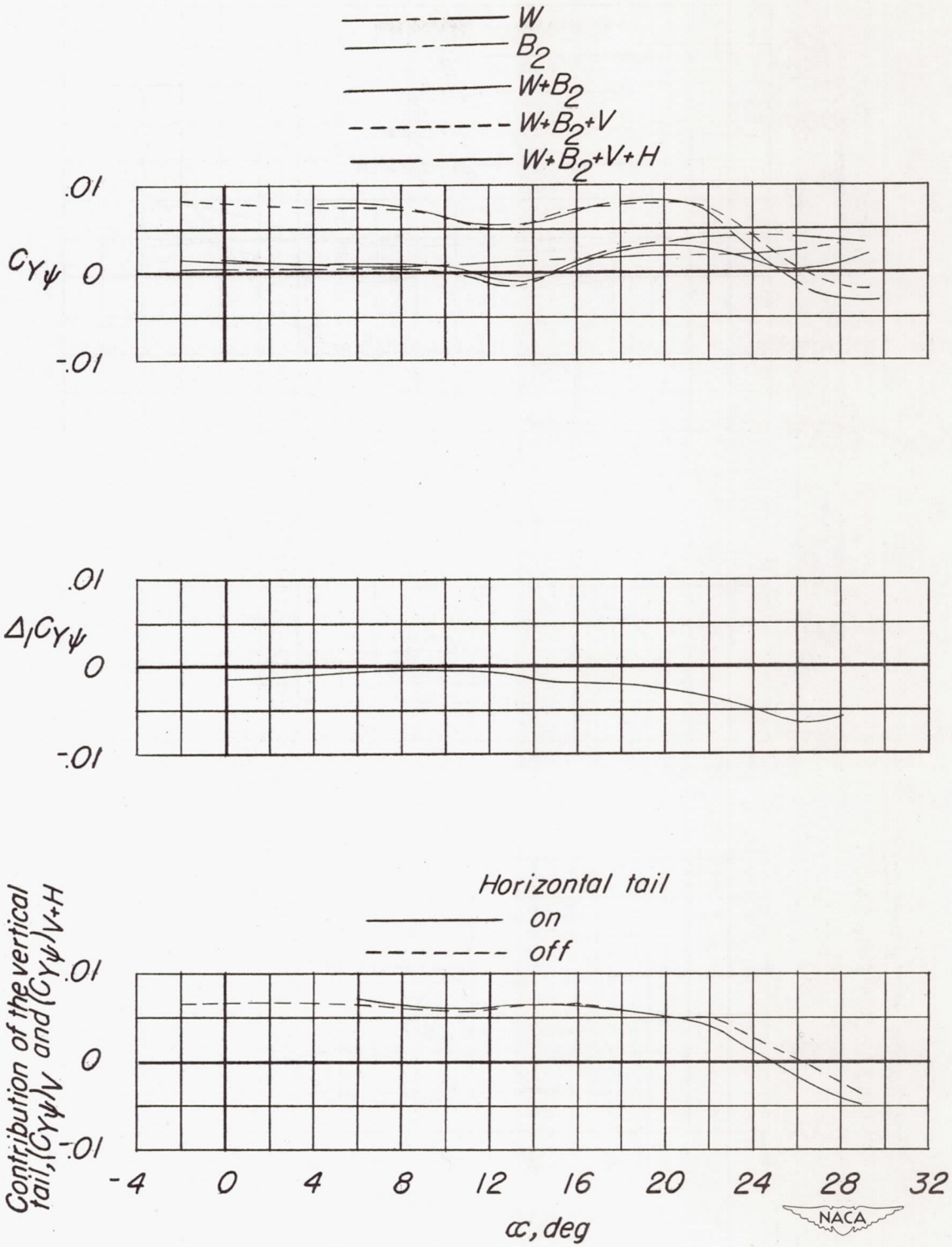

(b) Lateral force.

Figure 28.- Concluded.

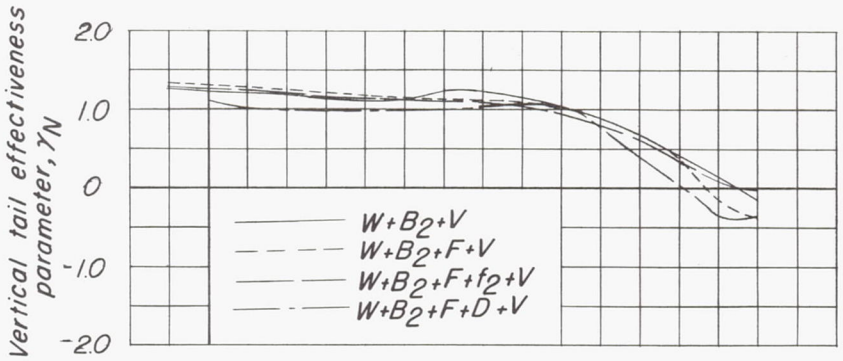

(a) Flap and fence effect of the vertical-tail effectiveness parameter for the vertical tail with the wing-fuselage combination $l_V/b_W = 0.500$.

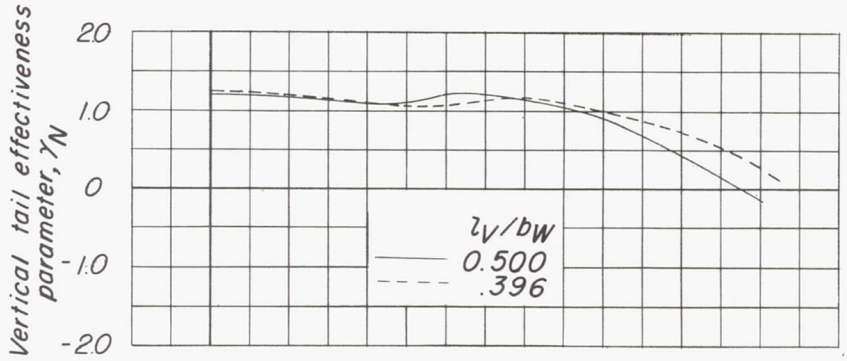

(b) Tail-length effect of the vertical-tail effectiveness parameter for vertical tail with the wing-fuselage configuration without flaps or fences.

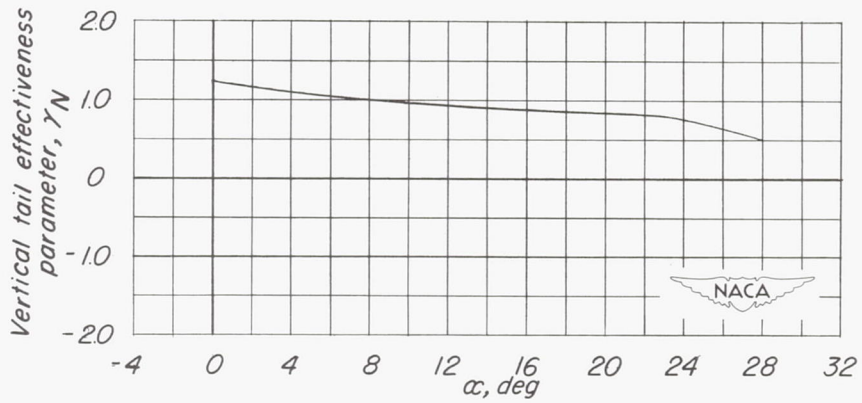

(c) Vertical-tail effectiveness parameter for the vertical tail with the fuselage. $l_V/b_W = 0.500$.

Figure 29.- Variation of the vertical-tail effectiveness parameter with angle of attack. Data presented are based on experimental yawing moments at $R = 4.45 \times 10^6$.

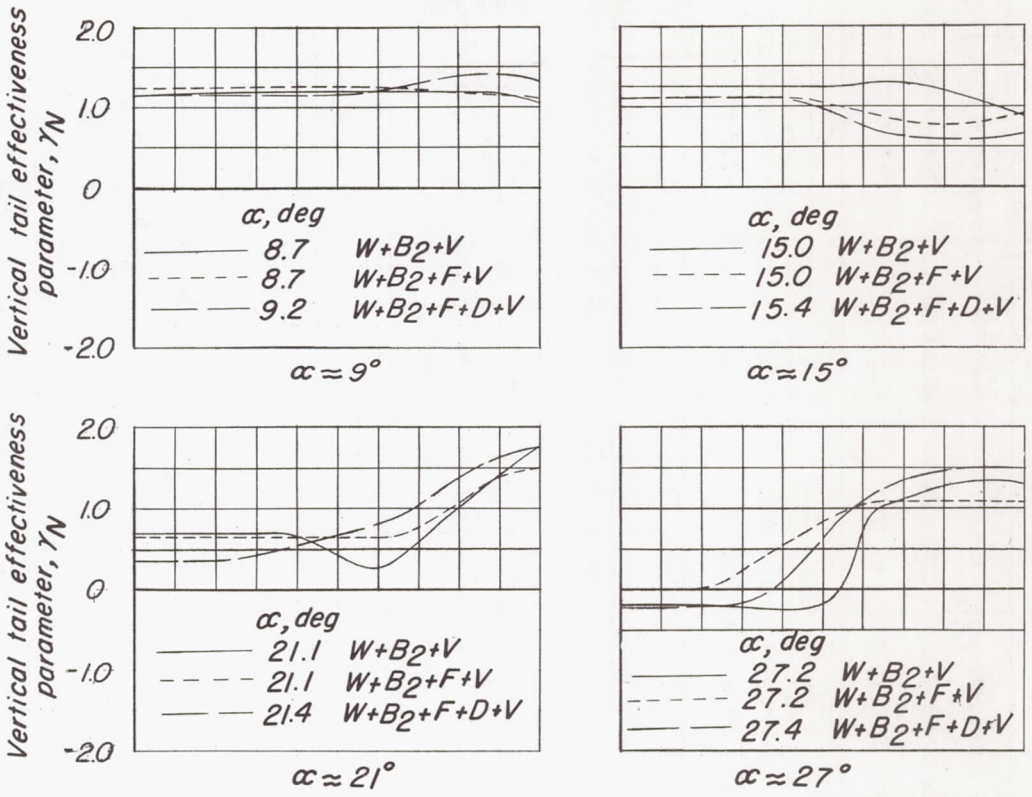

(a) Flap effects on γ_N of the wing-fuselage combination. $l_V/b_W = 0.500$.

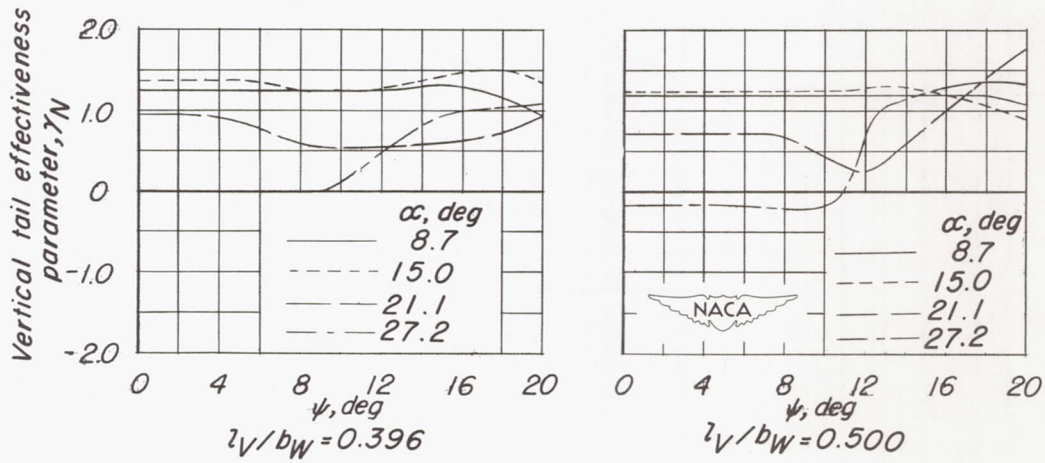

(b) Vertical-tail-length effect on γ_N of the wing-fuselage configurations without flaps.

Figure 30.- Variation of vertical-tail effectiveness parameter with yaw angle. Data presented are based on experimental yawing moments at $R = 4.45 \times 10^6$.

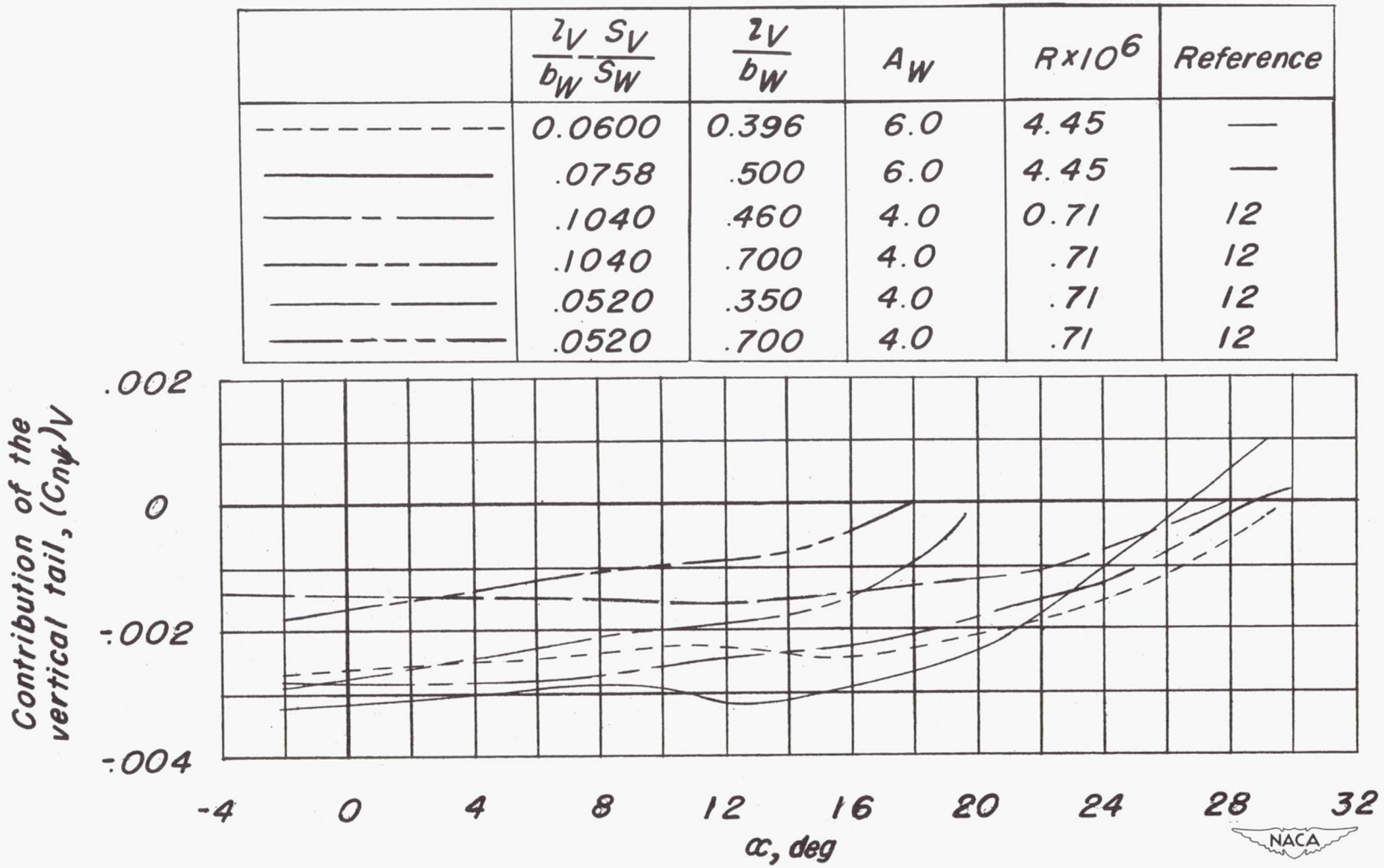

Figure 31.- Effect of tail length on the directional-stability-parameter contribution of vertical tails to midwing fuselage configurations where the wing quarter chord was swept back 45°.

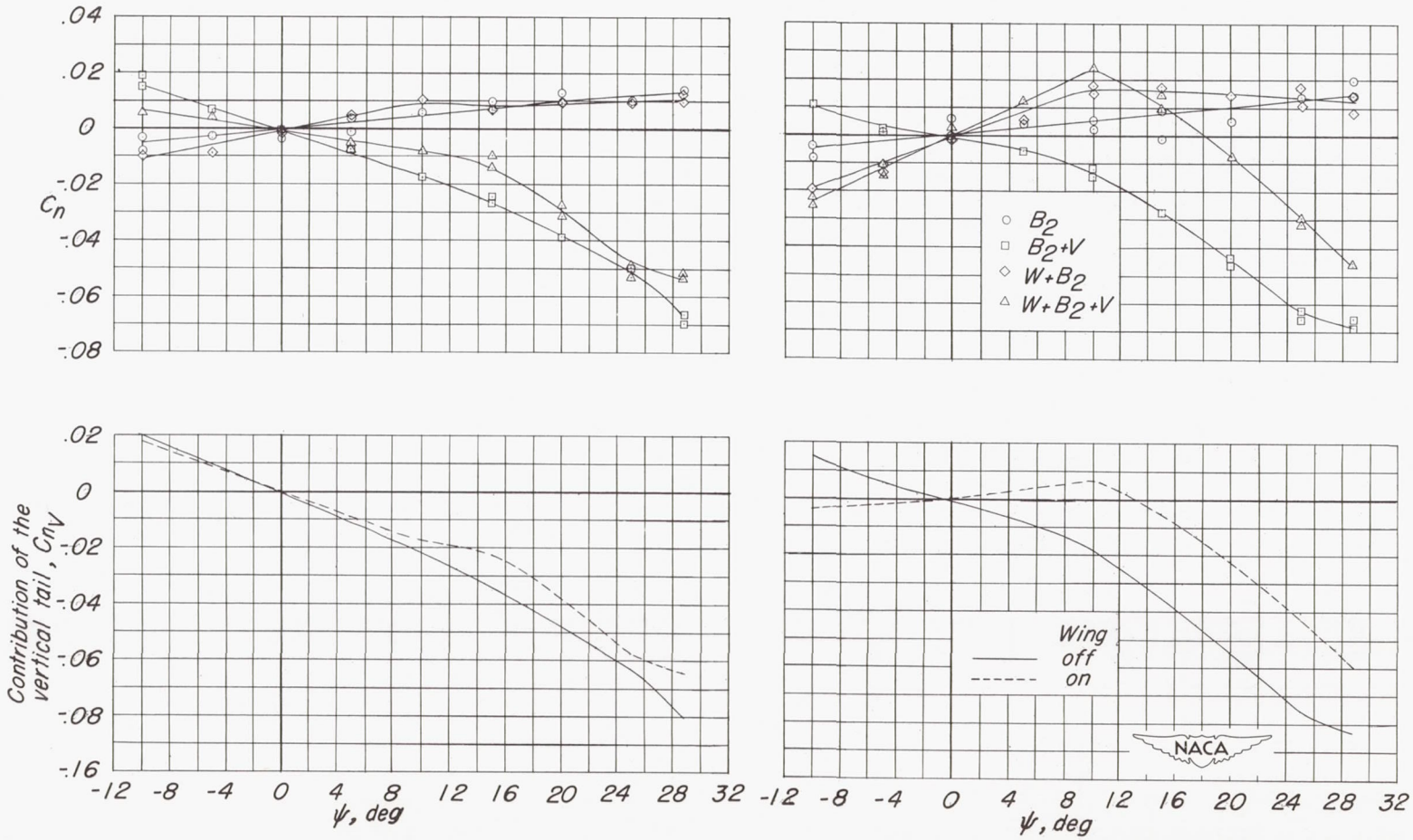

(a) $\alpha \approx 21^\circ$.

(b) $\alpha \approx 27^\circ$.

Figure 32.- Comparison of the vertical-tail contribution of the fuselage—vertical-tail model configuration with and without the 47.7° sweptback wing of aspect ratio 6 at high angles of attack. Vertical-tail length is $0.500b_W$ and $R = 4.45 \times 10^6$.

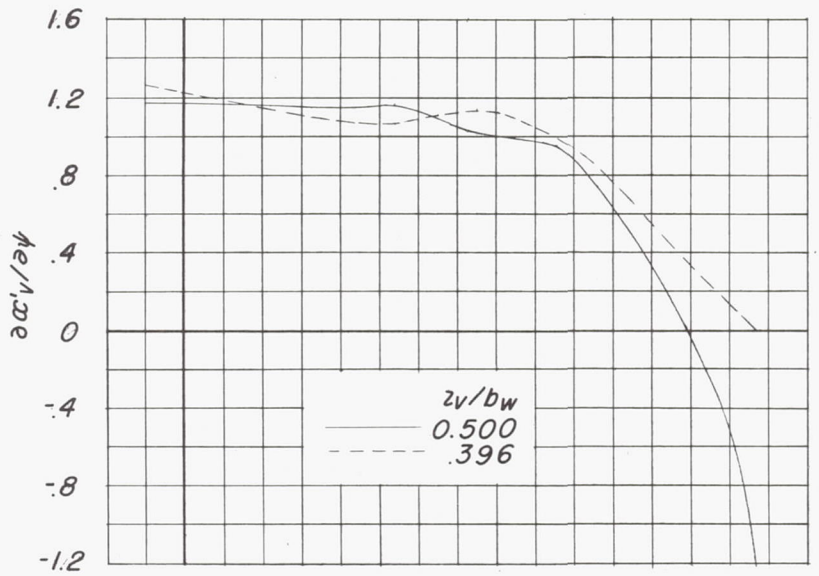

(a) Vertical-tail-length effect on $\partial\alpha'_V/\partial\psi$ against α.

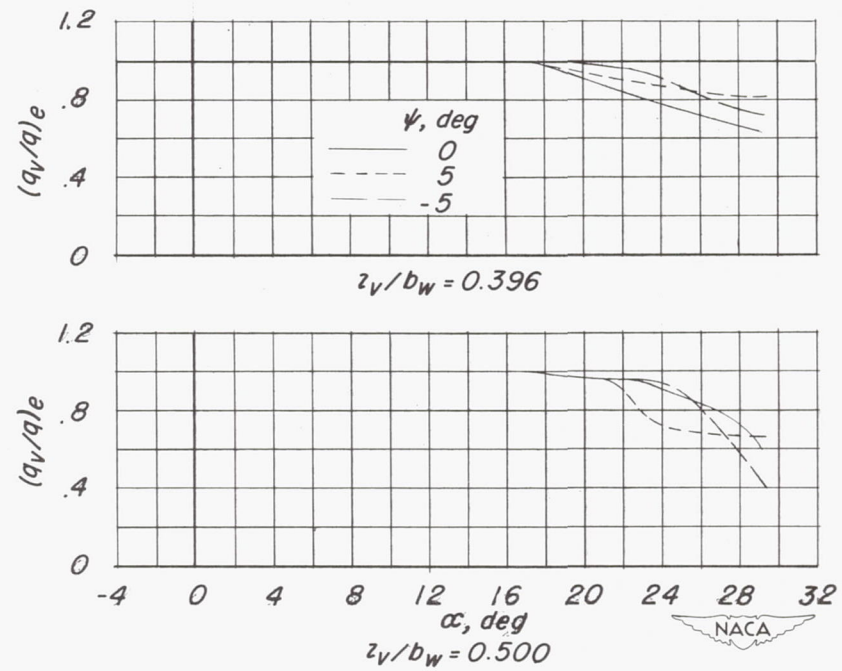

(b) Variation of $(q_V/q)_e$ against α for vertical-tail lengths z_V/b_W of 0.396 and 0.500, respectively.

Figure 33.- Vertical-tail-length effect on $\partial\alpha'_V/\partial\psi$ and $(q_V/q)_e$ with angle of attack of the unflapped wing-fuselage configuration in the low yaw-angle range (-5° to 5°). Data presented are based on experimental yawing moments at $R = 4.45 \times 10^6$.

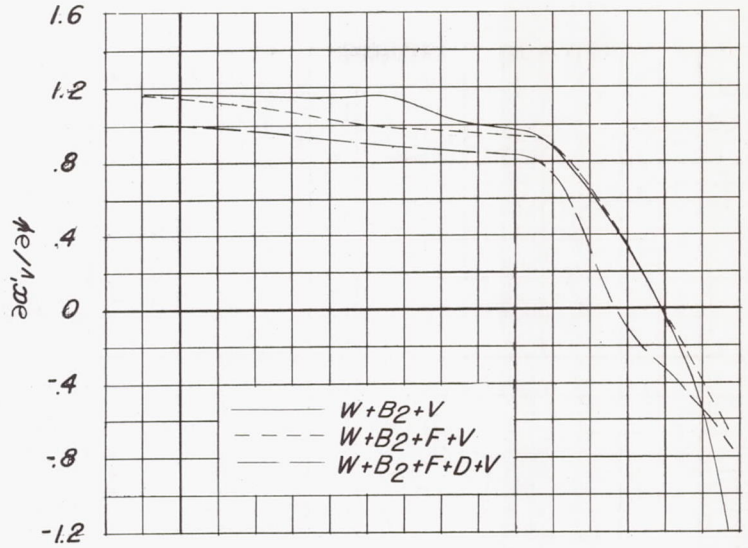

(a) Flap effects on $\partial\alpha'_V/\partial\psi$ against α.

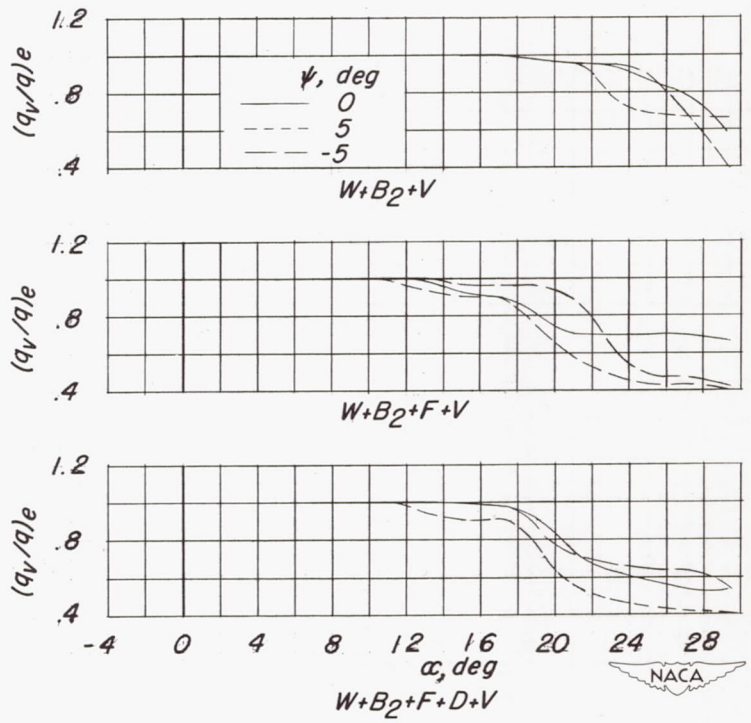

(b) Flap effects on $(q_V/q)_e$ against α.

Figure 34.- Flap effects on $\partial\alpha'_V/\partial\psi$ and $(q_V/q)_e$ with angle of attack of the wing-fuselage configuration, when l_V/b_W was 0.500, in the low yaw-angle range (-5° to 5°). Data presented are based on experimental yawing moments at $R = 4.45 \times 10^6$.

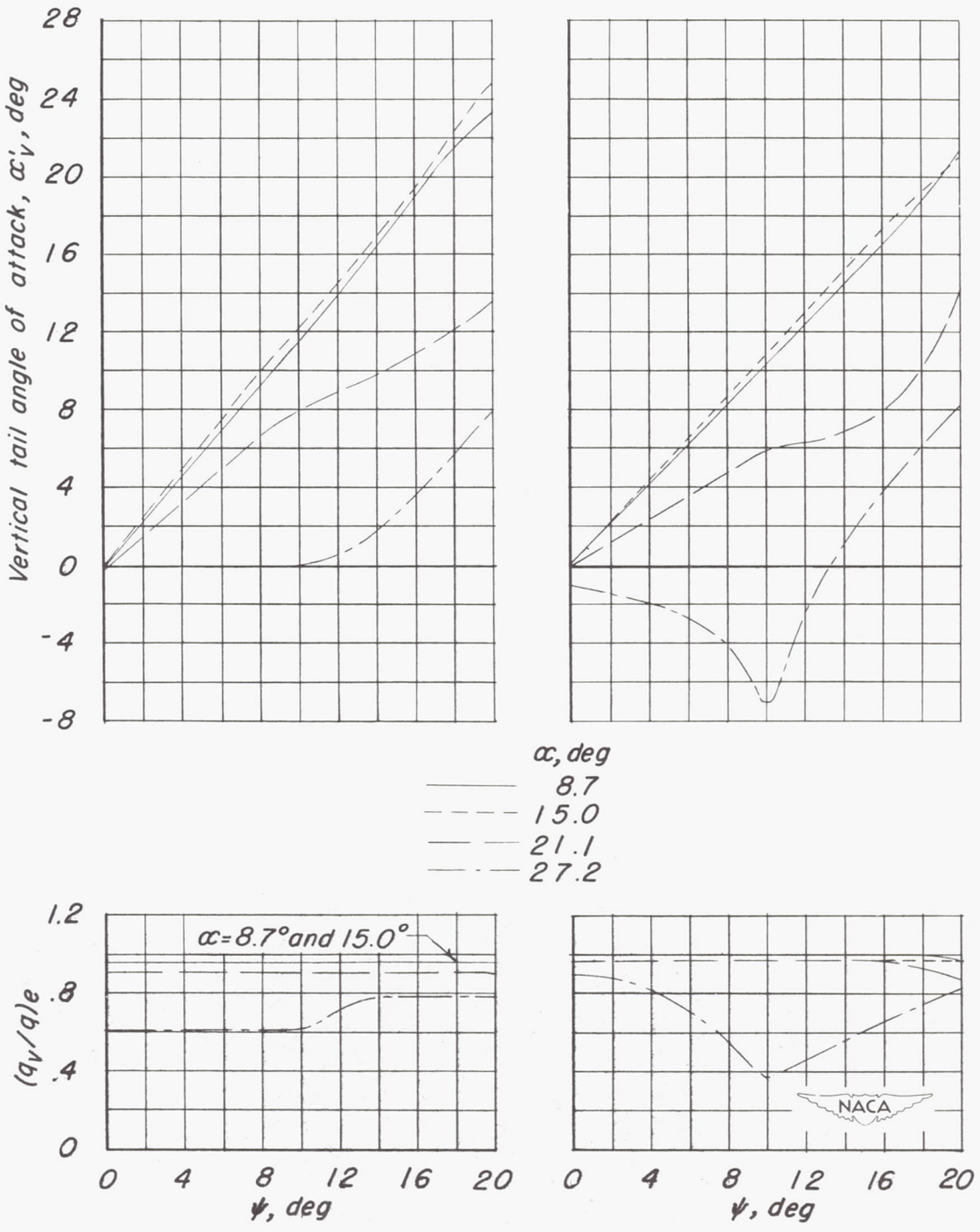

(a) $l_V/b_W = 0.396$. (b) $l_V/b_W = 0.500$.

Figure 35.- Effect of tail length on the angle of attack α'_V and the dynamic pressure ratio of the vertical tail with the unflapped wing-fuselage configurations in a yawed attitude. Data presented are based on experimental yawing moments at $R = 4.45 \times 10^6$.

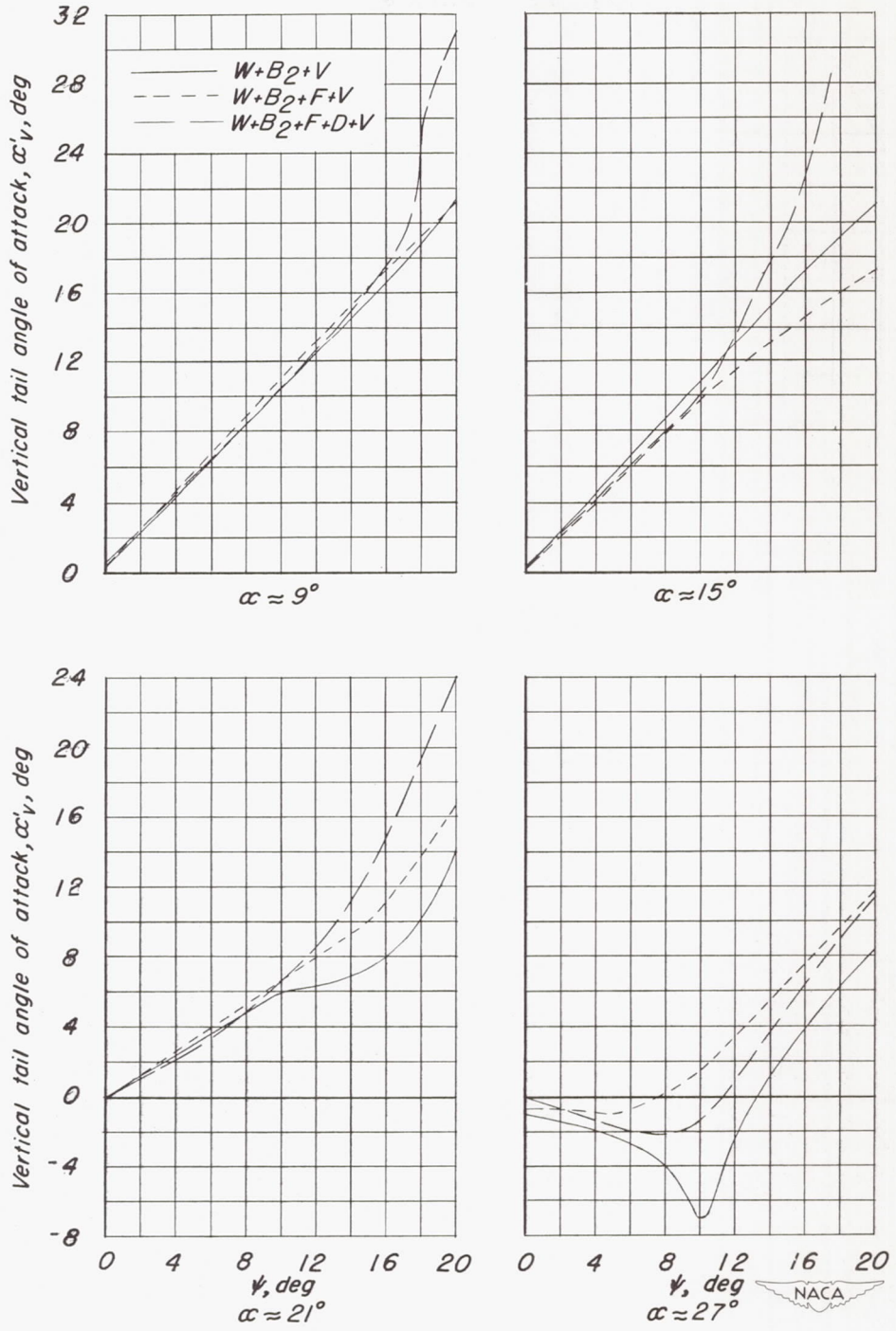

(a) Effect of flaps on the vertical-tail angle of attack.

Figure 36.- Effect of flaps on the angle of attack α'_V and the dynamic pressure ratio of the vertical tail with the wing-fuselage configurations in a yawed attitude. Data presented are based on experimental yawing moments at $R = 4.45 \times 10^6$. $l_V/b_W = 0.500$.

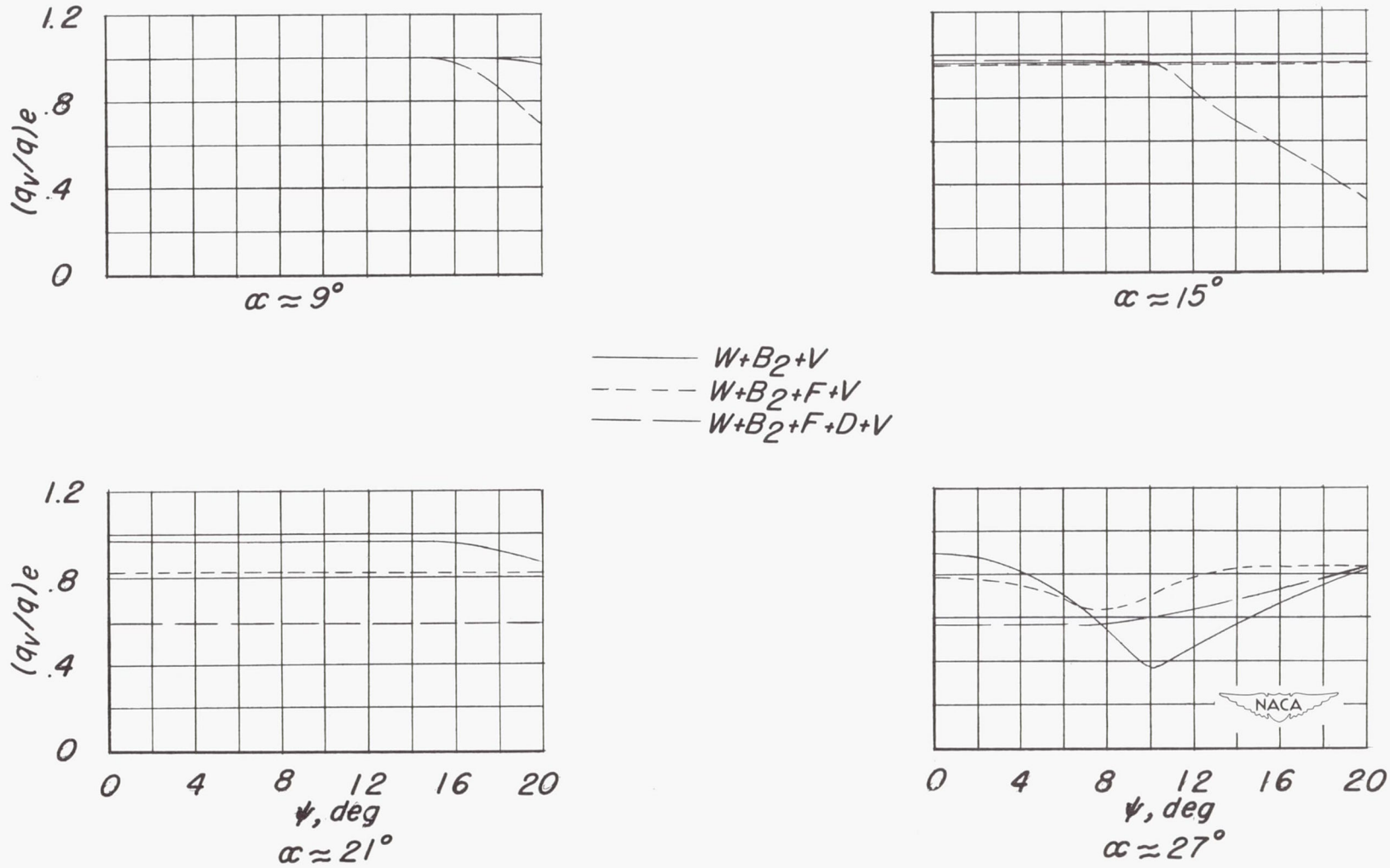

(b) Effect of flaps on dynamic pressure ratio.

Figure 36.- Concluded.

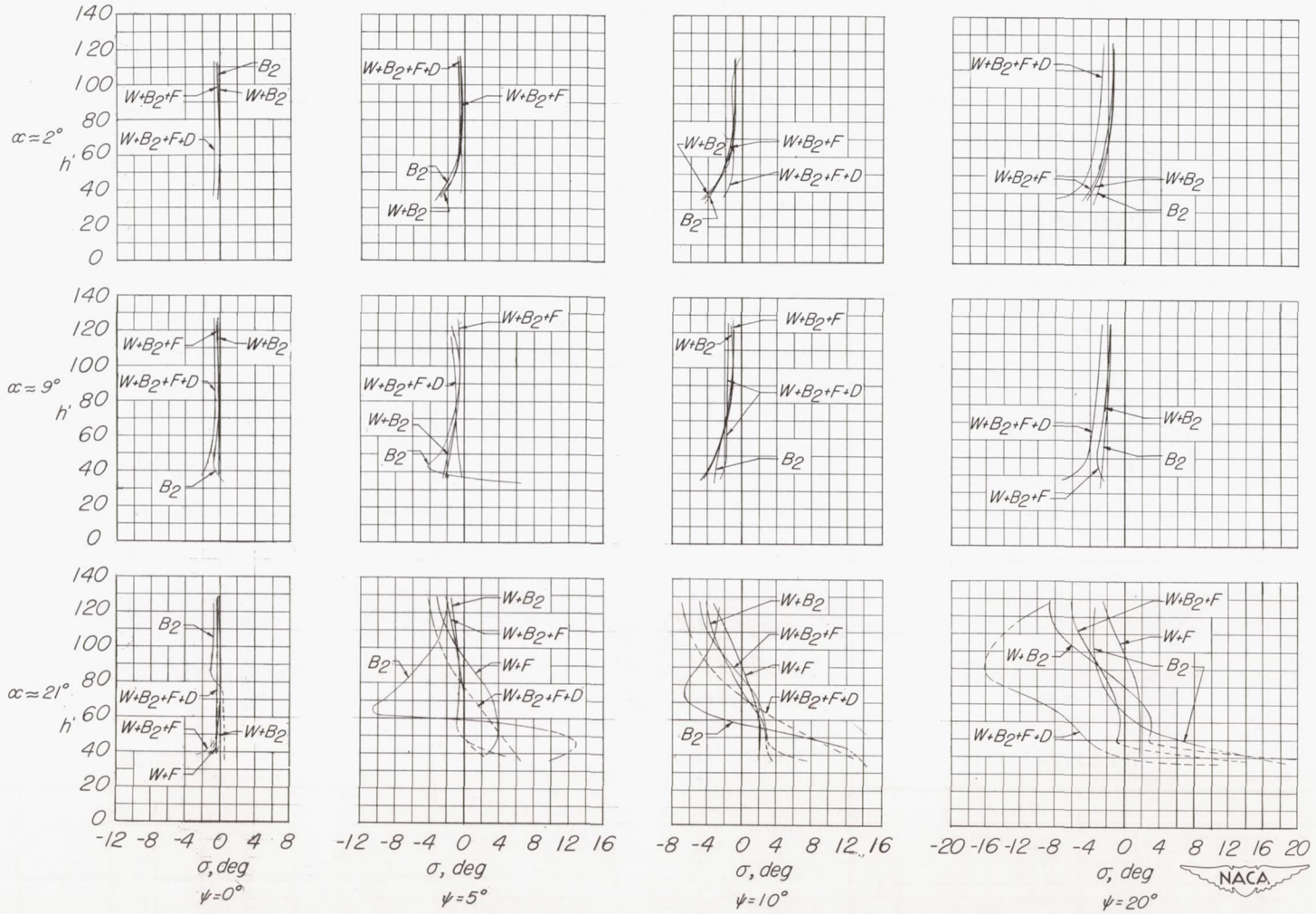

Figure 37.- Summary of the sidewash characteristics in the vicinity of vertical tail behind the component parts of the airplane model having a midwing swept back 47.7°. Extrapolated data are indicated by the broken lines. $R = 4.45 \times 10^6$.

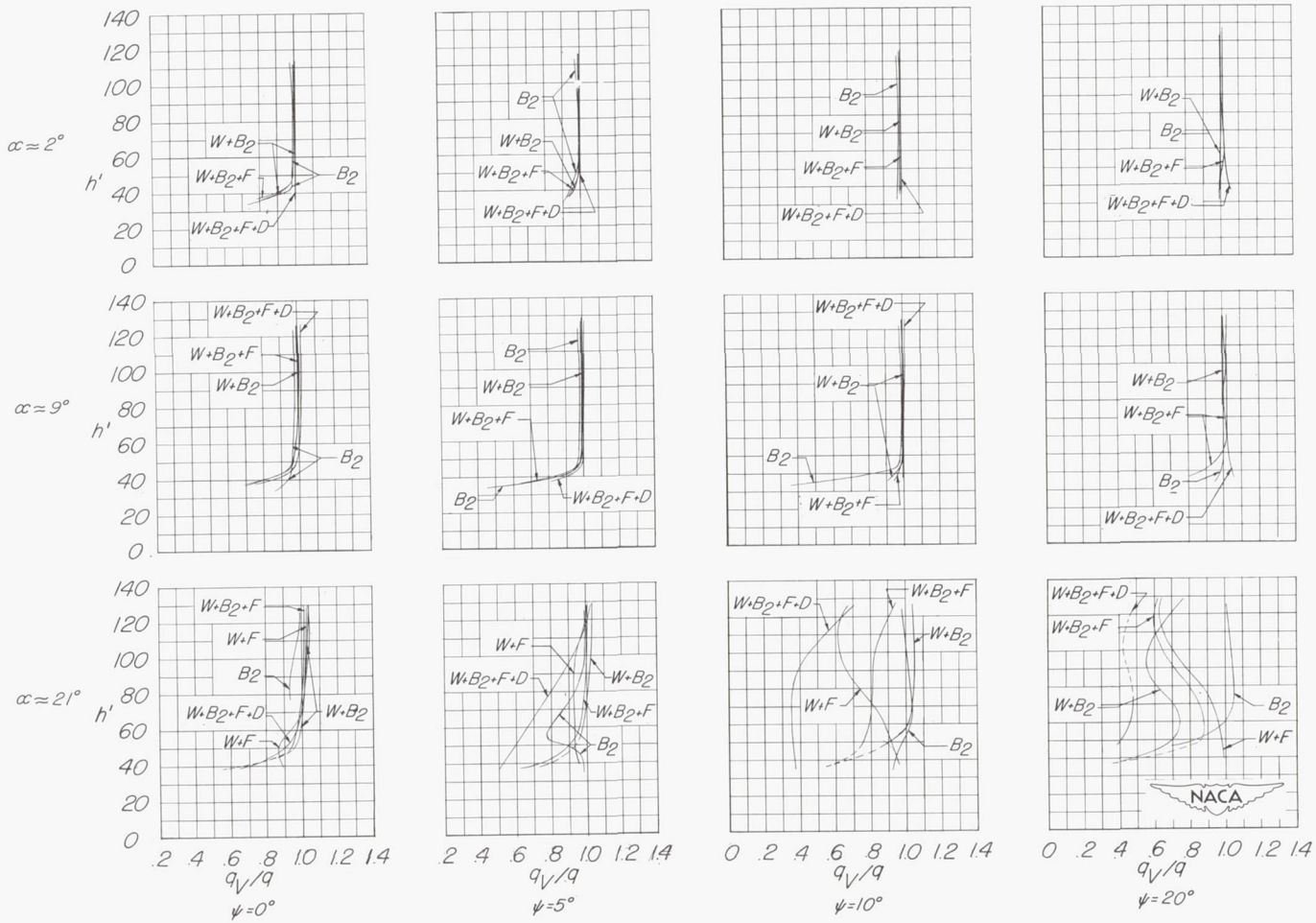

Figure 38.- Summary of the dynamic pressure ratio in the vicinity of the vertical tail if located behind the component parts of the airplane model having a midwing swept back 47.7°. Extrapolated data are indicated by the broken lines. $R = 4.45 \times 10^6$.

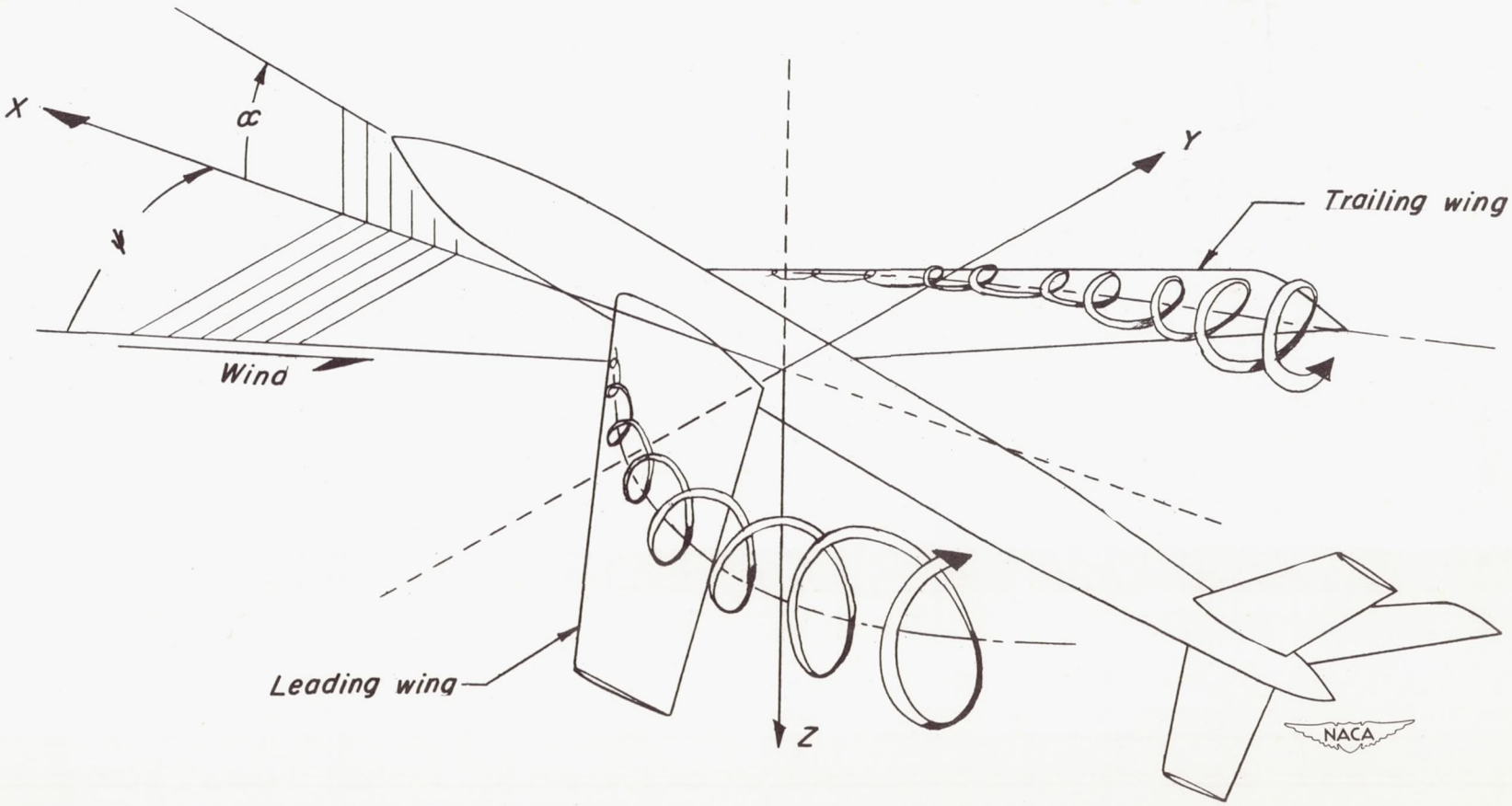

Figure 39.- Schematic drawing of the leading-edge vortex flow of the wing in a yawed attitude.

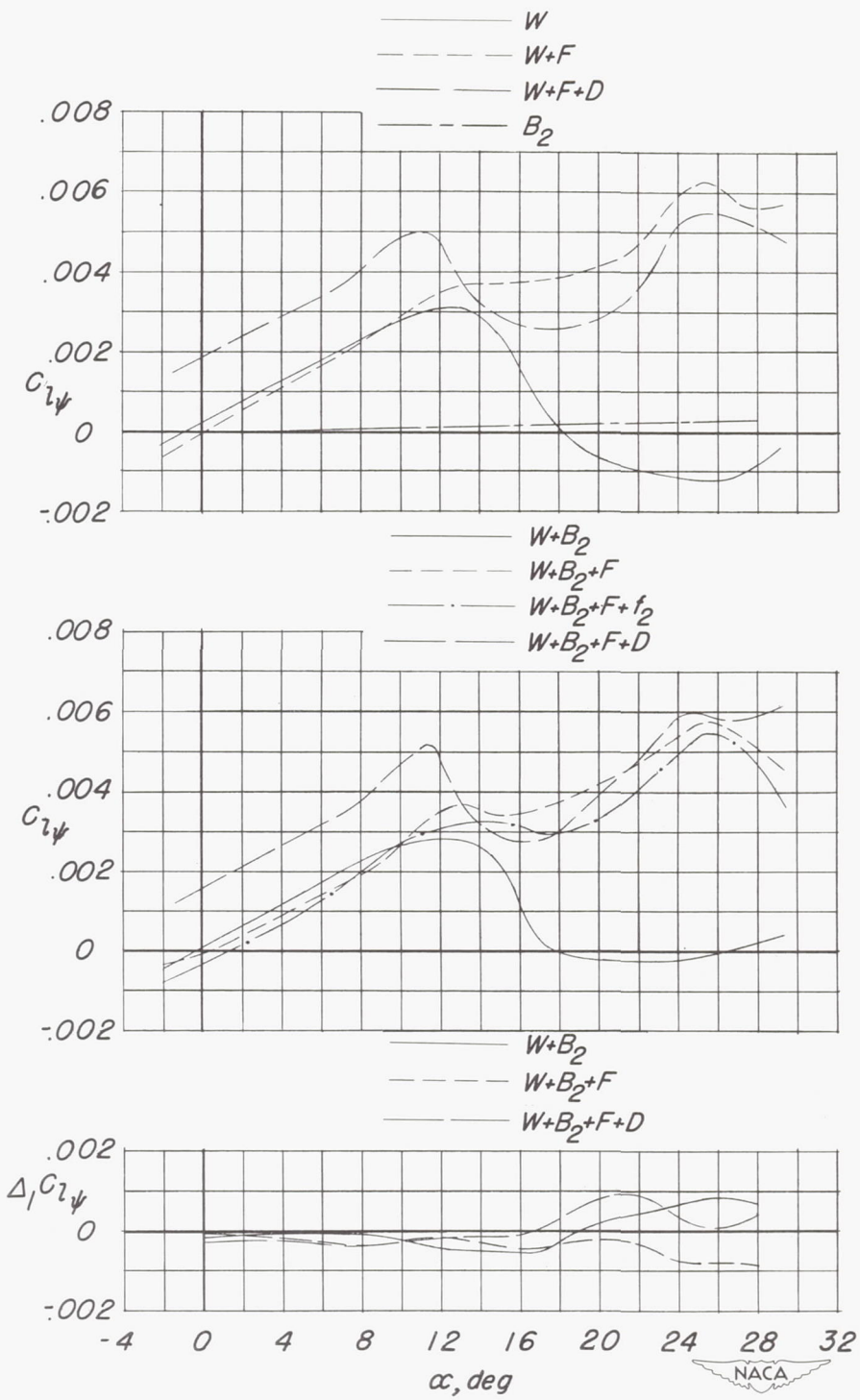

Figure 40.- Variations with angle of attack of the effective-dihedral parameter for the wing, fuselage, and wing-fuselage configuration and the increments caused by the wing-fuselage interference. $R = 4.45 \times 10^6$.

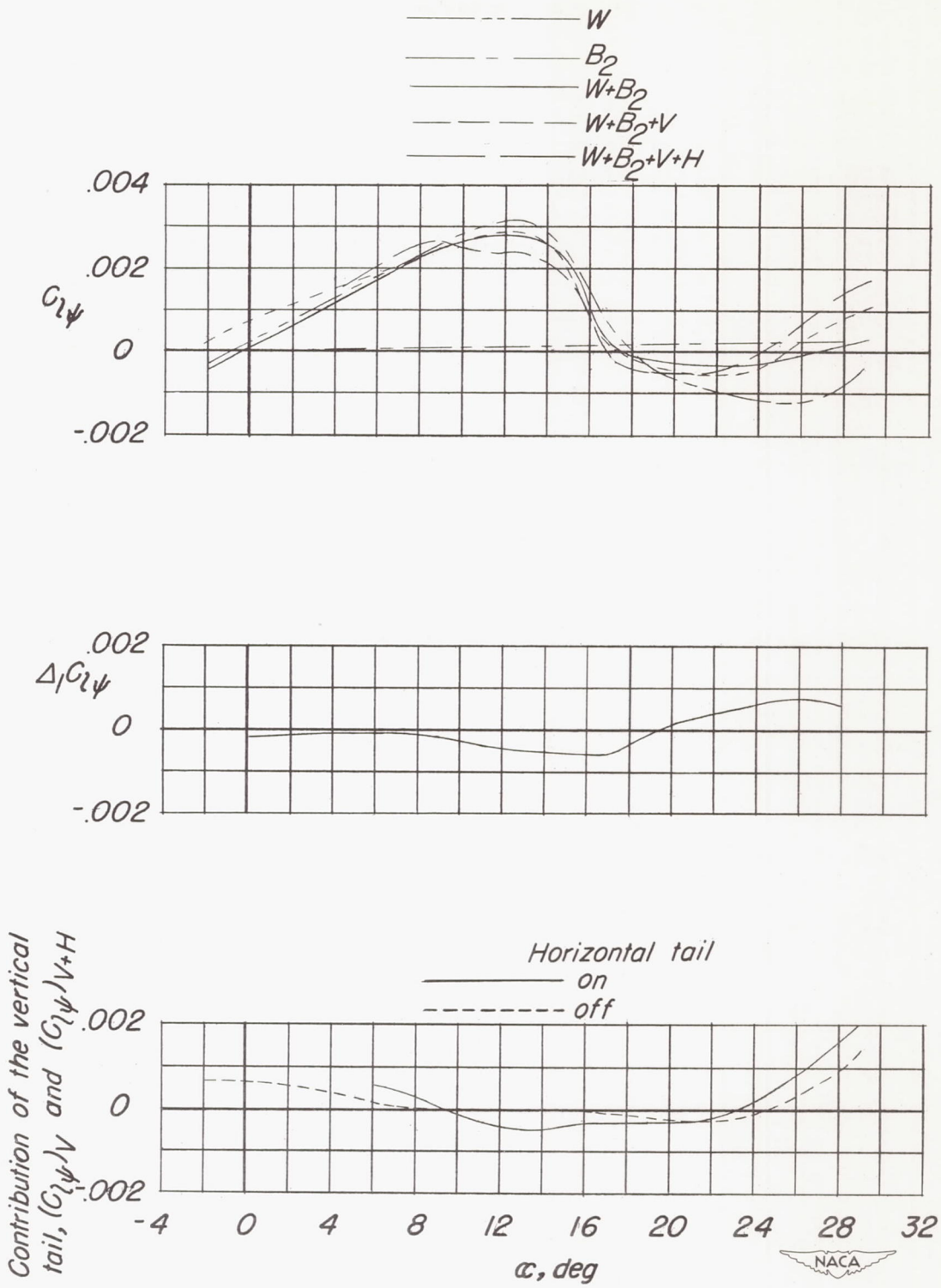

Figure 41.- Summary of the contributions of the main model components to the effective-dihedral parameter of the complete model. Vertical-tail length is $0.500b_W$ and $R = 4.45 \times 10^6$.

NACA-Langley - 9-1-53 - 325